

Doctoral thesis

Doctoral theses at NTNU, 2024:32

Magdalena Susanne Müller

Machinability of Low-Lead and Lead-Free Brass Alloys

NTNU
Norwegian University of Science and Technology
Thesis for the Degree of
Philosophiae Doctor
Faculty of Engineering
Department of Mechanical and Industrial
Engineering



Norwegian University of
Science and Technology

Magdalena Susanne Müller

Machinability of Low-Lead and Lead-Free Brass Alloys

Thesis for the Degree of Philosophiae Doctor

Trondheim, January 2024

Norwegian University of Science and Technology
Faculty of Engineering
Department of Mechanical and Industrial Engineering

NTNU

Norwegian University of Science and Technology

Thesis for the Degree of Philosophiae Doctor

Faculty of Engineering

Department of Mechanical and Industrial Engineering

© Magdalena Susanne Müller

ISBN 978-82-326-7666-8 (printed ver.)

ISBN 978-82-326-7665-1 (electronic ver.)

ISSN 1503-8181 (printed ver.)

ISSN 2703-8084 (online ver.)

Doctoral theses at NTNU, 2024:32

Printed by NTNU Grafisk senter

Preface

This PhD thesis is submitted to the Norwegian University of Science and Technology (NTNU) in partial fulfillment of the requirements of the degree of Philosophiae Doctor, under the supervision of Prof. Knut Sørby and co-supervision of Prof. Chao Gao. This doctoral work was carried out at the Department of Mechanical and Industrial Engineering at NTNU, Trondheim, between October 2020 and September 2023. This work was performed within the research project LOBUS - Low Lead Brass for Sustainable Community Development (RCN Project No. 296054), co-funded by the Research Council of Norway and owned by Isiflo AS. The consortium participants besides the already mentioned were SINTEF Manufacturing Raufoss, VP metall AS, and Nordic Brass Gusum AB.

Abstract

The machinability of traditional free-machining lead-alloyed brass alloys is excellent. Lead segregates as small globules around the grain boundaries of the brass, acting as an internal crack starter. This behavior of the lead leads to short chips, low cutting forces, and high tool life in leaded brass alloys.

New regulations regarding the use of lead restrict the amount allowed as an alloying element in brass. Likely, the use of lead will be prohibited completely in the future. The adaption of brass machining processes is therefore necessary. Lead-free and low-lead brass alloys generally show higher cutting forces, shorter tool life, and longer and tangled chips.

Cutting processes used nowadays need to be adapted to the new materials, aiming for lower cutting forces and good chip breakability. This thesis investigates and discusses the impact of different cutting parameters, tool geometries, temper conditions, and cutting fluid supply strategies on lead-free brass machinability.

All investigations in this thesis were performed using a radial turning process using grooving tools and extruded brass rods. Mainly the alloys CW511L (CuZn38As), CW724R (CuZn21Si3P), and, as a reference, CW625N (CuZn35Pb1.5AlAs) were used. Additionally, CW510L (CuZn42) and CW508L (CuZn37) were investigated in one study. A radial turning operation, in which thin disks were cut, was established for all investigations in this study. In the following tests, different parameters were varied. An increased positive rake angle was beneficial to reduce cutting forces in lead-free and low-lead brass alloys to various extents. The possible reduction in cutting forces was the highest for CW511L and lowest for low-lead CW625N. However, the chip breakability decreased with increasing the rake angle for all investigated materials. Chip-breaking geometries and high-pressure cutting fluid supply proved to be beneficial regarding chip breakability. Heat treatment of CW511L to increase the β -phase content did not improve the machinability. Additionally, the selected heat treatment decreased the alloy's dezincification resistance, and the strength and hardness were no longer within the values specified in the standard for CW511L alloy.

The machinability of lead-free brass alloys can be improved by adapting the process and the tool geometry to the new alloys. New tool geometries were investigated and discussed.

Acknowledgement

After finishing my studies, I dreamed of taking my PhD abroad. As a global pandemic, lockdowns, and closed borders arose when I applied for PhD positions, this dream seemed unrealistic. I am happy and grateful for my supervisor Prof. Knut Sørby, who employed me anyway and made it possible for me to take my PhD in Norway. He made my start as a PhD student in Trondheim smooth despite my quarantine during the first ten days. Later on, he kindly supported my scientific process through countless discussions, teaching me more about the basics of machining, proofreading my drafts, and encouraging me when I wanted to go abroad for a research stay. I thank Chao Gao for being my co-supervisor.

This project would not have been possible without the Department of Mechanical and Industrial Engineering at NTNU offering the research infrastructure and the Research Council of Norway funding this study through the LOBUS project.

I am grateful for the project partners of the LOBUS project, ISIFLO AS, SINTEF Manufacturing Raufoss, VP Metall AS, and Nordic Brass Gusum. Through regular discussions, each of them contributed to this project. Special thanks to Stanka Tomovic Petrovic from SINTEF Manufacturing, the project leader of the LOBUS project, who always had an open ear for me, read and commented on all paper drafts, and has been my co-author. Also, Per-Eric Persson from Nordic Brass Gusum took the time to always make useful comments on my publication drafts and taught me about the heat treatment of brass and how it influences the microstructure.

Most PhD projects in engineering rely on, at least to some extent, lab work. So did mine. First, I want to thank Marius Kvithyll and Espen Larsen, who reliably and decently helped me perform the machining tests by operating the different lathes. I want to thank Cristian Torres Rodriguez and Ingvild Runningen for taking the time to help me figure out how to grind and polish brass alloys in the best possible way. I thank Di Wan and Dong Wang for teaching me how to operate the SEM and for the fruitful discussions regarding my samples. Thanks to Christian Frugone and Børge Holen for helping with new ideas when my initial idea for a test setup did not work.

While pursuing my PhD, I was fortunate to spend four months at the Laboratory for Machine Tools and Production Engineering (WZL) at RWTH Aachen University. I am deeply grateful to the WZL for making this possible and for their hospitality during my stay. In particular, Kilian Brans and Stefan Baier contributed through numerous discussions with their knowledge of the machining of copper alloys.

Markus Meurer was a great department leader for the Cutting Technology Department. Tobias Kelliger was an excellent group leader for the Cutting Fundamentals Group, which I was part of during my stay. Since my first day there, both the department and the group have welcomed me as a member. Tobias Hilgers patiently and thoroughly discussed and performed all cutting tests at WZL Aachen with me. Dr. Marina Kemperle helped prepare all metallographic samples needed for the study in Aachen and extensively discussed preparation methods for brass samples with me. Additionally, I am thankful to the co-authors of the paper on the tests performed in Aachen; Kilian Brans, Markus Meurer, and Prof. Thomas Bergs. Many people believe that pursuing a PhD can be a solitary experience due to the intense focus on a specific topic and the limited opportunities for an in-depth discussion with others. Anyway, I was surrounded by people who shared the same experience. Although we couldn't always discuss our topics at length, we were all in the same situation. Through countless coffee breaks, great work lunches, chaotic pizza dinners, the traditional easter celebration, inspiring discussions, and wonderful weekends we became friends. I want to thank my office mates Chiara Zarna, Victor Marneval, Shaoquan Wang, Sondre Østre Rokvam, and Mohd Fadzil Bin Mohd Tahir, who were, despite all of them working with composites, always open to cheerful discussions. Besides my office mates, I had many more wonderful colleagues, probably too many to mention all of them. There are, for example, Saveria Spiller, Ambra Celotto, Anni Cao, and Maria Luisa Casasin Garcia, who all motivated me to work out together at different times, or Sara Esmaeilian and Javad Sadeghinia, who always had encouraging words for me. I had the pleasure of meeting numerous people and thoroughly enjoyed spending time with them. However, it is impossible to list all of their names here.

During a PhD it is important to do non-work related things to keep the mind open and generate new ideas. Strinda Ungdomskorps and Nidaros Roklubb helped me to achieve this. Thanks to all the wonderful members, thanks for countless rowing trips, coffees, rehearsals, convincing me to try playing the baritone saxophone, three entirely different 17th of May parades, and all the emotional support. Thanks to Ellen Værnes and Rikke Helbo, my flatmates during my first year. They made my arrival and all the required bureaucracy after moving to a new country half as hard, and they were wonderful Norwegian teachers by taking away my fear of just trying to speak in this new language. Thanks to the knitting club girls, they have been wonderful emotional support. Thanks to all my friends in Germany. Every time I visited them, they always made me feel at home despite the distance. I want to thank especially Lea Haus and Julia Heilemann. Lea also took a PhD so we could cheer each other up or complain about everything in endless phone calls. It was great emotional support. Julia started working at a brass rod mill during my PhD. In addition to providing reliable emotional support, she made valuable scientific contributions through numerous discussions via email, telephone, and Skype. Last but not least, I want to thank my family for their support. Despite it being not easy to see me moving 1500 km away, they always supported me.

Contents

Preface	ii
Abstract	iii
Acknowledgement	iv
Contents	vi
1 Introduction	1
1.1 Background and Motivation	2
1.2 State of the Art	5
1.2.1 Microstructure and Mechanical Properties of Brass Alloys	5
1.2.2 Machinability	9
1.2.3 The Orthogonal Cutting Model	10
1.2.4 Tool Geometries	11
1.2.5 Tool Materials and Coatings	12
1.2.6 High-pressure cutting fluid supply	12
1.3 Problem Statement	13
1.3.1 Problem Description	14
1.3.2 Scope of the PhD project	14
1.3.3 Research Objectives	16
1.3.4 Context of the appended papers	16
2 Research Methodology	19
2.1 Materials	19
2.1.1 Heat treatment	20
2.2 Material Characterization Methods	21
2.2.1 Microstructural analysis	21
2.2.2 Mechanical Properties	22
2.3 Machining Process	22
2.4 Analysis of Tools, Chips and Machined Parts	23
2.5 Tool Wear Tests	24
2.6 Summary of the research methods used	24
3 Results	28
3.1 I - Cutting Forces in Machining of Low-Lead and Lead-Free Brass Alloys	28
3.2 II - Investigation of heat treatment to improve the machinability of lead-free brass alloy CW511L	30

3.3	III - The Influence of the Rake Angle on the Cutting of Low-Lead and Lead-Free Brass Alloys	32
3.4	IV - The Effect of High-Pressure Cutting Fluid Supply on the Chip Breakability of Lead-Free Brass Alloys	34
3.5	V - Investigations on chip breakability in lead-free brass alloy CW511L using different chip breaking geometries	36
3.6	VI - Analysis of Chip Formation and Chip Morphology of Lead-Free Brass Alloy	38
3.7	Tool Wear	41
4	Discussion	45
4.1	Cutting force	46
4.2	Chip breakability	47
4.3	Tool wear	49
4.4	Recommendations for the implementation of the results	49
5	Conclusion	51
6	Suggestions for further Work	53
	Bibliography	55
	Paper I	65
	Paper II	75
	Paper III	81
	Paper IV	93
	Paper V	113
	Paper VI	121

Chapter 1

Introduction

Goal 6 of the sustainable development goals defined by the United Nations is clean water and sanitation (United Nations, 2015). To ensure the distribution of clean drinking water, it is crucial that no contamination, such as bacteria or heavy metals, occurs during transport.

Brass alloys are often used in fittings in drinking water systems because they have good machinability, excellent corrosion resistance, and an antibacterial effect (Hilbrans, 2013; Weißbach, 2012). Usually, free-machining brass alloys contain lead to improve the machinability (Hilbrans, 2013; Weißbach, 2012).

Due to the high machinability of lead-alloyed free-machining brass alloys, the manufacturing costs of brass components for drinking water supply systems are low (Schultheiss et al., 2018). Unfortunately, lead can be dissolved from the alloy and pollute the drinking water. Therefore, the EU and several authorities increasingly restrict the use of lead as alloying element (Estelle, 2016; European Parliament and Council of the European Union, 2006).

This PhD work is part of the LOBUS project (Low Lead Brass for Sustainable Community Development), owned by Isiflo AS and led by SINTEF Manufacturing Raufoss. The work aims to improve the machinability of lead-free brass alloys. New tool geometries and high-pressure cutting fluid supply in turning operations are investigated. The microstructure and mechanical properties of different alloys are analyzed. The main alloys studied in this thesis are CW511L (CuZn38As), CW724R (CuZn21Si3P), and CW625N (CuZn35Pb1,5AlAs). In addition, CW508L (CuZn37) and CW510L (CuZn42) are analyzed in one study.

The following sections describe the context, motivation, and scope of the PhD-project within the LOBUS project. State-of-the-art in machining low-lead and lead-free brass alloys is discussed. In addition, a brief overview of the basics of turning processes and tool design is given.

1.1 Background and Motivation

Copper and copper alloys are the third most consumed commercial metals, behind steel and aluminum (Davis et al., 2001). Due to the outstanding corrosion resistance of copper-zinc alloys, i.e., brasses are used in different applications such as pipes, valves, and fittings in drinking water supply systems. Plumbing and heating installations account for 15.1% of the copper consumption in the US (Davis et al., 2001). Furthermore, copper and copper alloys are recyclable, and alloying elements can be separated from copper. Recycling copper uses only 15 % of the energy needed to extract copper from a mine. That makes copper highly sustainable (Deutsches Kupferinstitut, 2019). Copper from scrap covered 32% of the annual copper consumption in 2022 in the USA (U.S. Geological Survey, 2023). Brasses retain the good corrosion resistance of copper, but the mechanical properties improve. In a pure α -brass, only the face-centered cubic α -phase is present, which is a solid solution. When the zinc content increases, in addition to the α -phase, the body-centered cubic β -phase is formed. It is stronger, has excellent hot workability, and improves machinability. On the other hand, it is prone to the corrosion mechanism dezincification (Davis et al., 2001).

Lead is added to brass in small quantities to improve machinability. Lead segregates as small globules around the grain boundaries. During the cutting process, the globules elongate and help the chip break. Therefore, lead-containing brass alloys usually produce shorter chips, and process forces are lower due to reduced tool-chip contact (J. Johansson, Alm, et al., 2022). Especially in highly automated cutting processes, short-breaking chips are crucial, as long chips could get tangled around the tool or workpiece and lead to premature tool breakage. Other studies additionally describe lead as an internal lubricant, which melts during the cutting process due to its comparatively low melting temperature (Nobel et al., 2014a). However, J. Johansson, Alm, et al. (2022) conclude that the temperature during the cutting of leaded-brass alloys is too low to melt the lead. Additionally, tool wear is usually lower in leaded brass alloys (Nobel et al., 2014a).

As lead is hazardous to the environment and human health (Needleman, 2004), the addition of lead is restricted and will most likely be restricted further in the future (Estelle, 2016). For example, the European Union restricts the amount of lead allowed in a brass product (European Parliament and Council of the European Union, 2006).

The lead reduction in brass alloys leads to higher cutting forces, higher tool wear, and longer chips when cutting with the same cutting parameters and inserts used in traditional brass alloys (Nobel et al., 2014a; Schultheiss et al., 2017).

Due to the new regulations, new low-lead and lead-free alloys were developed in past years. For example, silicon and bismuth are used in these new alloys to replace lead (Suksongkarm et al., 2017, 2018; Taha et al., 2012). However, the literature review shows that the cutting force and tool wear increase while chip breakage degrades. Thus, the motivation for this project is to find cutting parameters, different tools, or a cutting fluid supply strategy to improve the cutting process of

lead-free brass alloys.

The literature discusses a variety of different lead-free and low-lead alloys. Commercial and experimental alloys are studied.

Klocke et al. (2016) investigated the machinability of CW511L (CuZn38As), CW510L (CuZn42), and CW724R (CuZn21Si3P) in comparison to CW614N (CuZn39Pb3) using different tool materials and coatings. They focused on the cutting forces, workpiece quality, chip formation, and tool wear. All low-lead alloys had a higher cutting force than the lead-containing reference alloy. Out of the low-lead alloys, CW724R had the lowest cutting forces. A cemented carbide tool coated with TiAlN showed the lowermost tool wear of all tested cemented carbide tools, while the polycrystalline diamond (PCD) tool showed an overall better performance making it the most promising alternative (Klocke et al., 2016). Schultheiss et al. (2017) compared the machinability of CW724R and CW614N and the tool wear of two different tool coatings. Additionally, Schultheiss et al. (2018) studied CW724R and CW614N in comparison with a focus on surface integrity, chip geometry, cutting forces, tool deterioration, and a case study on the costs for using the lead-free alloy in the industry compared to the leaded alloy. Schultheiss, Lundström, Johansson, Bushlya, Zhou, Nilsson, and Ståhl (2014) investigated the tensile strength, hardness, abrasiveness, cutting forces, and tool wear of CW724R and CW614N. To evaluate and compare the potential machinability of an alloy, they use polar diagrams. Generally, these studies showed that using the lead-free alloy leads to higher cutting forces, longer lamellar chips, and more tool wear. For the lead-free alloy, the surface roughness depends mainly on the feed rate during cutting, while the chip breakage improves with increasing depth of cut and feed rate. A case study showed higher manufacturing costs for the lead-free alloy due to higher material costs, tool wear, and cutting forces. Using an experimental (Ti, V, Zr, Hf, Nb, Ta)N coated cemented carbide tool led to an extended tool life (Schultheiss, Lundström, Johansson, Bushlya, Zhou, Nilsson, & Ståhl, 2014; Schultheiss et al., 2017; Schultheiss et al., 2018).

Nobel et al. (2014b) investigated the chip formation, specific cutting forces, tool temperature, and tool wear of CW508L (CuZn37), CW511L (CuZn38As), CW510L (CuZn42), CW724R (CuZn21Si3P), and CW614N (CuZn39Pb3) in comparison while using cemented carbide tools with titanium aluminum nitride coating. According to their investigations, CW724R has the best machinability among the lead-free brass alloys in their study. However, the machinability of CW724R is still lower than the machinability of the studied leaded brass CW614N (Nobel et al., 2014b).

Toufatzis et al. (2018b) studied the lead-free brass alloys CW510L (CuZn42), CW511L (CuZn38As), and C27450 (CuZn36) in comparison to the lead-alloy brass CW614N (CuZn39Pb3). First, they did a material characterization, followed by machinability testing in turning operation, statistical analyses, and optimization. Their results were similar to the reviewed literature since they determined that CW614N showed the lowest cutting force. Additionally, Toufatzis et al. (2018a) studied the influence of final heat treatment on machinability. They investigated the

machinability of the alloys CW510L, CW511L, and C27450 while using uncoated cemented carbide tools. The final heat treatment improved the chip morphology. Moreover, the final heat treatment reduced cutting forces for CW510L and CW511L marginally while reducing the power consumption during cutting only for CW511L (Toufatzis et al., 2018a).

Taha et al. (2012) studied experimental alloys with varying silicon content and the influence of the silicon content on machinability. They focused on cutting force, tool wear, chip type, and surface roughness of the workpiece. For comparison, they used the leaded brass alloy C37700 (CuZn39Pb2). They measured the lowest cutting force for the leaded brass and the highest for the brass with 1% silicon content. The tool wear increased with the silicon content, and the chip breakage improved. The surface roughness was better for lower silicon-contents (Taha et al., 2012).

Chunlei et al. (2016) studied an experimental brass alloy with different magnesium contents by investigating the microstructure, hardness, and machinability while milling. The magnesium refines the grain size and forms brittle intermetallic particles. Therefore an increasing magnesium content leads to shorter chips, and the machinability improves by increasing magnesium content (Chunlei et al., 2016). Atsumi et al. (2011) studied Cu-40Zn-Cr-Fe-Sn and Cu40-Zn-Cr-Fe-Sn-Bi in drilling tests, comparing the drilling speed and mechanical properties. They concluded that the addition of bismuth improved the machinability. Nevertheless, the machinability of the Bi-alloyed brass was only 75% of the machinability of leaded brass alloys (Atsumi et al., 2011).

Suksongkarm et al. (2017) used experimental brass alloys with varying additions of recycled electrical solder. The recycled electrical solder contained bismuth and tin. First, they analyzed the microstructure and tensile properties, second, they did machining tests focusing on the cutting force and chip formation. The recycled electrical solder improved the chip breakage and the machinability. They gained the best results for adding 3% of recycled solder to the alloy (Suksongkarm et al., 2017). The German Copper Institute advises against using bismuth as an alloying element to improve the machinability of lead-free brass. Bismuth expands when solidifying, and thereby it can form stresses and cause stress corrosion and it is almost impossible to remove bismuth from the brass alloy during the nowadays used recycling processes for copper alloys (Deutsches Kupferinstitut, 2020).

The most studied lead-free brass alloys are CW511L (CuZn38As), CW510L (CuZn42), and CW724R (CuZn21Si3P). In conclusion, lead-free brass alloys show lower machinability than leaded brass alloys. Some elements or special heat treatments can change the microstructure of the alloys to improve machinability. Following the advice of the German Copper Institute, using bismuth to increase the machinability should be avoided these alloys were not investigated. The use of PCD tools can be an alternative to the use of commonly used cemented carbide tools. Additionally, an adapted cutting fluid supply strategy could improve the machinability of lead-free brass.

1.2 State of the Art

1.2.1 Microstructure and Mechanical Properties of Brass Alloys

The mechanical properties of an alloy are dependent on microstructure and chemical composition. Thus, both will influence machinability. Due to the high strain rates and elevated temperatures in the machining process, the properties and the microstructure might change. The machining process, as well as the product properties, will be influenced by that.

Brass alloys can consist of different phases. The α -phase is a solid solution of zinc in copper and shows a face-centered cubic structure. Single α -phase brasses show excellent cold workability and are ductile. The β -phase shows a body-centered cubic structure and forms at higher zinc contents. Below 460 °C it is of ordered type. This phase has higher strength and lower ductility. It is not suitable for cold working but shows good hot workability. At copper contents below 50%, the hard and brittle γ -phase forms. Most commercial brasses used for machining are α - or $\alpha + \beta$ -brasses (West, 1982).

Adineh et al. (2019) showed that both the phases present and their morphology influence machinability. They suggest using alloys with a more inhomogeneous structure like a fine-grained $\alpha + \beta$ -brass to get better chip breakability. García et al. (2010) concluded in a study of leaded brass CuZn39Pb3 that the morphology and distribution of lead have an impact on the machinability of leaded brasses. Smaller and equally distributed lead globules will lead to better machinability. To accomplish this, they recommend a high cooling rate after solidification (García et al., 2010).

The influence of alloying elements on the microstructure

The addition of different elements to the alloy can influence the microstructure. According to Rajabi et al. (2018), tin in brass will stabilize the β -phase and decrease the size of the α -grains. Additionally, the hardness of the brass will be decreased, and by increasing the tin addition, the α -phase will be eliminated, and γ -phase will appear. By adding tin, the force required to cut the brass and the surface roughness was decreased, and the chips became shorter (Rajabi et al., 2018).

Taha et al. (2012) investigated the influence of silicon added to a lead-free brass alloy. While up to 1% silicon increased the β -phase and thereby the ultimate tensile strength, the hardness and decreased the ductility, higher additions of up to 4% silicon decreased the β -phase, while the content of α -phase remained the same and brittle γ -, λ -, η - and χ -phase appeared, which decreased the strength and ductility. The silicon content influenced the cutting forces, tool wear, surface roughness, and the chips. Adding just 1% silicon gave the highest cutting forces, which decreased by adding up to 4% Si, but at the same time, the tool wear and surface roughness were increased with increasing silicon content. Additionally, the chip type seems to be influenced by the hard precipitants in the alloy but not that much by the

mechanical properties (Taha et al., 2012).

Puathawee et al. (2013) found that the addition of tin to a silicon alloyed brass resulted in increased hardness and a higher amount of β -phase and more uniformly distributed γ -phase. Overall, they conclude this might enhance machinability (Puathawee et al., 2013).

Vilarinho et al. (2005) investigated the influence of the chemical composition on the machinability of brasses by comparing 27 different alloys. According to their results, the surface roughness is independent of the chemical composition of the alloys, and there is no significant correlation between the cutting force and the copper content or the cutting force and the hardness of the alloy. In their study, the only alloying element with a significant influence on the cutting force was lead (Vilarinho et al., 2005).

Lead, as an alloying element in brass, influences the microstructure. Lead is not solvable in brass, so it segregates as small globules at the grain boundaries. The lead globules will help to break the chips. Usually, the addition of lead results in very short, loose chips while machining brass alloys. Additionally, compared to brass, lead has a lower melting point. One explanation for its favorable impact on the machinability of brass is that lead is melting during machining, and acting as an internal lubricant. Thereby, it reduces friction and forces in the cutting process (Hilbrans, 2013; Nobel et al., 2014a). J. Johansson, Alm, et al. (2022) measured cutting temperatures during the machining of leaded brass and concluded that the temperatures reached were not high enough to melt the lead. They drew the conclusion, that the brass globules elongate and act as a crack starter leading to shorter breaking chips. Therefore, tool-chip contact length is reduced, which reduces friction, cutting force, and cutting temperature (J. Johansson, Alm, et al., 2022). However, the aforementioned advantages made lead a frequently used alloying element in free-cutting brass alloys.

Amaral et al. (2018) discussed how lead content influences the machinability of brass. Therefore, they studied three different brass alloys with different lead contents and compared them. Two alloys had a higher lead content of 1% and 1.5%, the microstructure was biphasic, and lead appeared as globules in the grain boundaries. The third alloy, with a lower lead content of 0.1 – 0.2% showed a mixture of single phasic and biphasic brass. A lower lead content led to increased hardness and a decrease in ductility. During the machining of the alloy with the lowest lead content, the power consumption was significantly higher. Additionally, the chips were longer, and the surface roughness of the workpiece was increased. The results show that a change in the lead content influences microstructure and machinability. Small lead content of 0.1 – 0.2% seemed not to improve the machinability significantly (Amaral et al., 2018).

Toufatzis et al. (2011) investigated the mechanical, microstructural, and machinability properties of two leaded brass alloys, CW614N (CuZn39Pb3) and CW602N (CuZn36Pb2As). The lead content influences the microstructure. Thereby, the lead content significantly affects the mechanical and machinability properties. With an increasing lead content, the size and distribution of the Pb globules changed.

The β -phase content was significantly different in the two alloys. CW614N was the optimal alloy regarding machinability in their investigation (Toufatzis et al., 2011).

Due to the increasing restrictions on the use of lead, new low-lead and lead-free brass alloys were developed to replace the free-cutting brasses. Examples of these alloys are silicon-alloyed CW724R (CuZn21Si3P), lead-free CW508L (CuZn37), CW511L (CuZn38As), and CW510L (CuZn42).

CW724R (CuZn21Si3P) consists of α - and κ -phases (Bushlya et al., 2017; Schultheiss et al., 2018) and is corrosion resistant (Seuss et al., 2017). In cutting tests, CW724R shows higher cutting forces compared to lead-containing brass alloys (Bushlya et al., 2017; Schultheiss et al., 2017; Schultheiss et al., 2018), but lower cutting forces compared to other lead-free brass alloys (Klocke et al., 2016) and lamellar chips (Schultheiss et al., 2016; Schultheiss, Lundström, Johansson, Bushlya, Zhou, Nilsson, & Ståhl, 2014; Schultheiss et al., 2017; Schultheiss et al., 2018). The surface roughness seems to be influenced by the cutting speed (Schultheiss et al., 2016), the feed (Schultheiss et al., 2017), and the tool (Reddy et al., 2017). Compared to lead-containing CW614N, uncoated, cemented carbide inserts show higher tool wear (Bushlya et al., 2017; Schultheiss et al., 2017). Additionally, the costs of the alloy are higher, and due to the low machinability, the overall product costs will increase when changing from lead-containing alloy to CW724R (Schultheiss et al., 2016).

Lead-free brass CW508L (CuZn37) consists of almost pure α -phase with only trace amounts of β -phase. According to Brandl et al. (2009), it shows selective corrosion. Due to the microstructure, the alloy is highly ductile. The cutting forces are significantly higher than in lead-alloyed brasses and higher than in CW724R. At the same time, the chips are longer (Nobel et al., 2014a).

CW511L (CuZn38As), similar to CW508L consists of almost pure α -phase with only trace amounts of β -phase. Additionally, it contains arsenic as active addition to prevent dezincification (Stålnacke et al., 2020). Mechanical properties as well as machining behavior of CW511L are comparable to CW508L. Cutting forces are higher and chips are longer compared to leaded brass alloys and silicon-alloyed CW724R (Nobel et al., 2014a).

CW510L (CuZn42) consists of nearly 50% β -phase and is therefore a dual-phase lead-free brass. Due to the properties of the β -phase, such as higher hardness and lower ductility, CW510L has a higher hardness and tensile strength compared to CW511L and CW508L (Nobel et al., 2014a). Due to the increased amount of β -phase present in CW510L, chip breakage is better compared to single-phase brass alloys (Nobel et al., 2014a).

The Influence of the Processing on the Microstructure and Mechanical Properties

Not only the chemical composition but also the processing, like casting and thermo-mechanical process parameters, will influence the phase structure (Pantazopoulos et al., 2008). Kozana et al. (2019) studied the influence of casting conditions on the microstructure and mechanical properties of CW511L (CuZn38As). Even though the chemical composition was nearly identical for all casts, the resulting tensile strength and hardness varied by approximately 20% for the different processing methods. Semi-continuous casting thereby showed lower properties compared to gravity casting methods (Kozana et al., 2019). Iecks et al. (2018) found that thinner pieces of casted brass parts will exhibit a finer and homogeneously distributed β -phase than a thicker piece. This was attributed to the lower cooling rate (Iecks et al., 2018).

Reetz (2006) and Reetz et al. (2008) investigated the influence of hot extrusion parameters on the microstructure and mechanical properties of the four different brass alloys CW501L (CuZn10), CW503L (CuZn20), CW508L (CuZn37) and CW617N (CuZn40Pb2). The effect of temperature, degree of deformation, and deformation rate were analyzed. For the two brasses CW508L and CW617N a high temperature led to recrystallization of the alloy and transformation of highly deformed β -phase to α -phase. Grains became smaller at lower temperatures and high degrees of deformation, which led to increased hardness and strength. Overall, for the two alloys with the lower Zn-content, the grains were finer at a lower degree of deformation, while for CW617N the grains were finer at a higher degree of deformation (Reetz, 2006; Reetz et al., 2008).

Toufatzis et al. (2016) studied the impact of heat treatment on the microstructure and the mechanical properties of brass alloys. Alloys included in their study were CW510L (CuZn42), CW511L (CuZn38As), and C27450 (CuZn36) (Toufatzis et al., 2016). As β -phase is known to improve machinability (Davis et al., 2001), the goal of the heat treatment by Toufatzis et al. (2016) was to enhance the β -phase content by dynamic recrystallization and water quenching to suppress the β to α transformation when cooling down. For all three studied alloys the β -phase content was increased, which lead to alloy strengthening and a reduction in elongation. Not all temper conditions fulfilled the standard requirements (Toufatzis et al., 2016). In a further study, Toufatzis et al. (2018a) investigated the machinability for selected temper conditions of these materials. All alloys showed improved chip breakability in the heat-treated conditions with an enhanced β -phase content, while only for CW511L a reduction in power consumption during machining was noticed (Toufatzis et al., 2018a).

During machining brass alloys can be affected by thermal softening and strain hardening. Laakso et al. (2013) investigated these effects for CW511L (CuZn38As). The strain hardening effect decreased at elevated temperatures of 200 °C for CW511L

(CuZn38As), while the tensile strength did not change. At higher temperatures, both dropped significantly. This can be attributed to grain growth and recrystallization (Laakso et al., 2013).

1.2.2 Machinability

Machinability describes how easy or how difficult material can be machined with a cutting tool. It is challenging to measure machinability since there is no generally accepted parameter (Mills et al., 1983). Usually, the term focuses on one characteristic, which is essential for the observer, e.g., tool life or surface quality (Davis et al., 2001). Additionally, the number describing this characteristic might change, depending on the parameters or processes used for testing and machining. In general, machinability tests are either ranking tests or absolute-value tests. Both machinability tests with and without the use of a machining operation are possible. For example, machinability could be evaluated based on the chemical composition, the microstructure, classifying the chips of the cutting process, or using a tool life criterion (Mills et al., 1983).

There are different approaches to measuring machinability. One machinability index is defined by ASTM E 618. Here, the criteria are chip formation and tool wear. A reference material gets a machinability index of 100. In Europe, CuZn39Pb3 is the reference material for copper alloys. Usually, machinability indexes are not determined by tests but based on the experiences of the company while manufacturing. Identifying the machinability index by special tests is very time- and material-consuming (Klocke, 2018b).

A similar test method to ASTM E 618 for copper alloys is presented by Zachert et al. (2022). Here, cutting force, surface roughness, tool wear, and chip shape are evaluated. Each of these criteria gets a value between 0 and 100 assigned. The factors are weighted regarding the needs of the analysis to calculate the machinability index. As reference material, CuZn39Pb3 was used (Zachert et al., 2022). Since machinability is influenced by many different factors, such as the cutting parameters, the machine tool, the clamping situation, or the geometry and material of the tool, it is difficult to derive a uniform index from it. Often, for example, chip breaking can be improved by a different tool or a higher feed rate, but this is neglected in these indices. Therefore, they can only be used as a first impression and for rough comparison. Machinability indices are no longer widely used in industry.

Another method to evaluate machinability was introduced by Andersson et al. (2007). Here, polar diagrams were used to evaluate the machinability of a material based on its properties (Andersson et al., 2007). The properties used are abrasiveness, adhesion, strain hardening, hardness, and thermal conductivity since these parameters influence the process stability and tool wear. The method compares materials with reference materials. Based on the diagrams, suggestions are made on how to select cutting tools and cutting parameters.

J. Johansson et al. (2019) investigated different lead-free brass alloys and com-

pared them to a lead-containing alloy utilizing polar machinability diagrams and machining tests. They showed the suitability of polar machinability diagrams to evaluate brass alloys regarding their machinability (J. Johansson et al., 2019). Often, the machinability of copper alloys is rated by the chips formed during a turning process. In general, there are three categories of machinability or chips for copper-base alloys. Type I are free-cutting alloys with small fragmented chips, type II alloys are readily machinable and show short, curled, and brittle chips and type III alloys are difficult-to-machine alloys having long, continuous, and often curled chips. Lead-containing brasses are usually in category I, while multiphase alloys, like $\alpha + \beta$ -brasses, mostly are in category II, and single-phase materials usually fall in category III (Davis et al., 2001; Kuyucak et al., 1996; Mills et al., 1983).

1.2.3 The Orthogonal Cutting Model

Cutting is a process of shaping a part by removing excess material in a shearing process using a wedge-shaped tool. In orthogonal cutting, the cutting edge of the tool moves perpendicular to the direction of the relative work motion. This approach is widely used in theoretical and experimental investigations since it eliminates as many independent variables as possible. Orthogonal cutting is a two-dimensional rather than a three-dimensional process (Boothroyd et al., 1988). Therefore, when using the orthogonal cutting model, forces in a direction parallel to the tool cutting edge are neglected.

Figure 1.1 shows the orthogonal cutting model and the forces in orthogonal cutting. The cutting force F_c and the feed force or thrust force F_f are the forces acting on the tool and can be measured directly. The friction force F and the normal force to friction F_N or N can be calculated from the measured forces using the rake angle α . The quotient of F and F_N is frequently referred to as the coefficient of friction (Boothroyd et al., 1988; Groover, 2017). However, in other references, the quotient of F and F_N is described to be rather referred to as force ratio (Albrecht, 1960; Klocke et al., 2016). The force ratio will indicate the friction conditions in the cutting zone but is not exactly the coefficient of friction. Albrecht (1960) concluded, that when considering the tool edge geometry, the coefficient no longer increases when increasing the rake angle, and thus, such an approach will give a more accurate description of the coefficient of friction (Albrecht, 1960).

Based on the assumption of constant shear strength Merchant (1945) developed the equation to calculate the shear plane angle ϕ :

$$\phi = 45 + \frac{\alpha}{2} - \frac{\beta}{2} \quad (1.1)$$

where α is the rake angle and β is the friction angle or the inverse tangent of the force ratio (Groover, 2017; Merchant, 1945). The assumption of constant shear strength of the work material is violated in practical machining operations. Therefore, Merchant's equation is rather an approximate relation than a physically accurate equation. However, based on this relation between rake angle, force ratio,

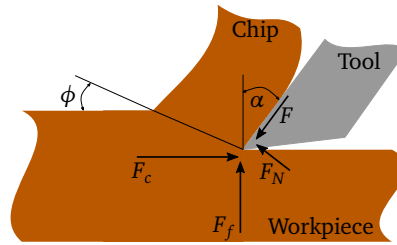


Figure 1.1: Schematic drawing of the orthogonal cutting model.

and shear plane angle, some conclusions can be drawn. The shear force required to cut the chip decreases when the area where it needs to be applied decreases. This area decreases when the shear plane angle increases. Based on equation 1.1 the shear plane angle increases when the rake angle is increased or the inverse tangent of the force ratio decreases. Hence, to decrease cutting forces and power requirements it should be tried to increase the rake angle and decrease the friction in the cutting zone and thereby increase the shear plane angle (Groover, 2017).

1.2.4 Tool Geometries

Several macro- and micro-geometrical factors define the tool geometry and influence the cutting process. The rake angle, for example, is one of the most impactful parameters on the tool-chip contact area. In a turning operation, the cutting forces will decrease, and the chip length will increase at an increased rake angle (Duan et al., 2013; Saglam et al., 2006). Using the right rake angle is crucial for achieving optimal results. When the rake angle is at its optimum value, the contact length between the tool and chip is minimal, resulting in lower cutting forces. Also, this can lead to better surface quality. However, if the rake angle is above the optimum value, tool wear will accelerate, cutting forces will increase, and the tool will be weaker (Saglam et al., 2006).

One option to prevent long, unbroken chips is to use chip-breaking geometries. When using groove-type chip breakers, it is important to ensure that the chip breaker land width is shorter than the natural tool-chip contact length because this allows the chip to flow into the groove and be deformed by the chip breaker. Additionally, the groove radius should be appropriately sized. If it is too small, the chip may not follow the curve of the chip-breaking geometry (Boothroyd et al., 1988).

Jawahir et al. (1995) conducted an experiment where they tested different tools with varying chip breaker land widths, groove styles, and nose radii on low, medium, and high carbon steels. They found that choosing the right chip-breaking geometry led to less power consumption. Regarding chip breakability, the best outcomes were achieved with shorter land widths, lower grooves, a raised back wall, and a sharp tool (Jawahir et al., 1995). Nobel, Hofmann, Klocke, and Veselovac (2015)

found in their study that lead-free brass alloy CW511L had no chip breakage when a carbide tool with a flat rake face and a positive rake angle was used in turning. Negative rake angles, on the other hand, improved the chip breakability slightly but also increased the cutting forces. As a result, they studied groove-type chip breakers. Nobel, Hofmann, Klocke, and Veselovac (2015) suggested using a high chip breaker land width and a lower back angle because of the high chip compression and upward chip curl radius.

By adapting the cutting edge radius to the process parameters and material, tool wear is reduced, and the tool life can be increased (Wegener et al., 2016). The chip formation, the cutting forces, and the workpiece quality can be affected by the cutting edge (Byrne et al., 2003). Zoghipour et al. (2022) found that an increased cutting edge radius improved the surface quality. On the other hand, it led to higher cutting forces, tool vibrations, and burr heights.

1.2.5 Tool Materials and Coatings

Besides the geometry, the tool coating and the tool material can have an impact on the cutting forces, the chip breakability, and the friction in the cutting zone. Amaral et al. (2018) used polycrystalline diamond tools and concluded these could be a good option to overcome the machinability challenges of lead-free brass alloys due to no visible tool wear. Nevertheless, chip-breaking geometries will be necessary which could be cut in the tools by laser machining (Amaral et al., 2018).

Schultheiss et al. (2017) showed that a (Ti, V, Zr, Hf, Nb, Ta)N tool coating could reduce the tool wear when cutting lead-free brass alloy CW724R. Therefore, they concluded, tool coatings can contribute to enhancing the machinability of lead-free brass (Schultheiss et al., 2017).

Klocke et al. (2016) concluded, that a polycrystalline diamond (PCD) tool has the best overall performance when cutting lead-free brass alloys. In the same study, a TiAlN-coated cemented carbide tool showed the lowest tool wear, and a multilayer chemical vapor deposition (CVD)-diamond-coated cemented carbide tool had the lowest adhesion tendency (Klocke et al., 2016). In a different study, the friction reduced slightly for cutting CW511L and CW724R when using a TiAlN-coated cemented carbide tool compared to an uncoated cemented carbide tool (Nobel, Hofmann, Klocke, Veselovac, & Puls, 2015).

1.2.6 High-pressure cutting fluid supply

High-pressure cutting fluid supply is one way of applying a cutting fluid in a cutting process. Here, the supply of the cutting fluid takes place directly at the cutting point. Therefore the cutting fluid is supplied through a hole in the cutting tool or a nozzle in the tool holder (Klocke, 2018a). The cutting fluid is supplied at a pressure of up to 300 MPa, but usually at a lower volume flow rate than in conventional cooling (Pusavec et al., 2010).

The focused jet of cutting fluid puts a force on the bottom side of the chip and thereby acts as a chip former and a chip discharger. Additionally, the cutting fluid

decreases the temperature and the friction at the cutting point. Thereby, the tool wear is declined, and the lifetime of the tool is increased. Hence, high-pressure cutting fluid supply can enhance productivity (Klocke, 2018a; Pusavec et al., 2010). Klocke et al. (2012) already applied this technique in the cutting of lead-free brass alloys. They used a pressure of 40 to 150 bar and a volume flow rate of 15 to 30 L/min. Even in finishing machining of lead-free brass alloys, they gained good chip breakability with the use of cemented carbide and PCD tools without chip-breaking geometry (Klocke et al., 2012).

Machining of lead-free brass alloys can lead to long and snarled chips (J. Johansson, Alm, et al., 2022; Nobel et al., 2014a). Additionally, tools with positive rake angles will help to reduce cutting forces but lead to longer chips (Duan et al., 2013; Saglam et al., 2006). High-pressure cutting fluid supply or chip-breaking geometries can counteract this (Puls et al., 2012).

Different studies using several workpiece materials achieved varying results regarding the cutting forces (Braham-Bouchnak et al., 2015; Courbon et al., 2009; Craford et al., 1999; Machado et al., 1994). High-pressure cutting fluid supply can decrease the length of the tool-chip contact on the rake face, and, thereby, contributing to lower cutting forces as well as impacting the grade of chip segmentation (Sharma et al., 2009). Additionally, a high-pressure cutting fluid supply promotes the efficient evacuation of the chip from the cutting zone (Klocke et al., 2011).

In the conventional cutting fluid supply, a jet of cutting fluid is directed onto the workpiece. The nozzle is usually located above the point of contact. This means that the cutting fluid jet normally hits the upper side of the chip. The cutting fluid can therefore hardly or not at all penetrate the actual cutting point or tool-chip contact, especially in continuous processes like drilling or turning (Sharman et al., 2008).

In high-pressure cutting fluid, the cutting fluid is supplied as a high-pressure jet forced into the tool-chip contact. Adapted tooling systems are necessary (Sørby et al., 2006). There is no general definition, of which pressure levels can be considered high-pressure.

1.3 Problem Statement

As discussed in the previous subsections, the use of leaded brass is not feasible in the long term. Even a reduction in lead content has resulted in a decline of machinability when the same machining parameters are used as for alloys with higher lead content (Nobel, Hofmann, Klocke, & Veselovac, 2015). There have been numerous attempts to replace lead with other elements, such as bismuth, silicon, or graphite (Bushlya et al., 2017; Taha et al., 2012; Zhang et al., 2020). However, these each come with different disadvantages. The graphite additions lead to weaker mechanical properties (Zhang et al., 2020). Silicon-containing brass swarf must usually be recycled separately from other brass swarf. Due to

the formation of the hard and abrasive κ -phase, adding silicon leads to increased tool wear (Bushlya et al., 2017; Schultheiss et al., 2018; Taha et al., 2012). Due to higher tool wear, worse chip breakability, and higher material costs, the overall manufacturing costs for lead-free brass alloys are higher than for lead-alloyed brasses (Schultheiss et al., 2018). These issues need to be addressed.

1.3.1 Problem Description

The overall problem addressed by this thesis is to improve the machinability of lead-free brass alloys to promote the change from lead-alloyed to lead-free brasses in the sanitary industry. Today, brass alloys with low quantities of lead are used, considering this is still allowed, and even small quantities can improve machinability. Nevertheless, the goal is to machine lead-free brass alloys as efficiently as lead-containing brass alloys and at the same or almost the same costs, as further restrictions are very likely to be placed. There are four major approaches to reaching this goal:

1. Finding adapted machining parameters.
2. Developing new tool geometries.
3. Implementing a cutting fluid supply strategy.
4. Changing the microstructure of the available alloys or designing new alloys.

The success of each of the aforementioned approaches can be measured based on a comparison to the cutting forces and chip forms produced in the currently used alloys and manufacturing processes. A visualization of the problem statement can be found in Figure 1.2. In the center of this graphic are the new lead-free brass alloys in a brown square. Different arrows connect it to the different parts of the visualization. The background of the problem, i.e. the restriction on the use of lead, is visualized in a turquoise color. Possible solutions to improve the machinability, are visualized in the orange squares. Additionally, the figure shows in the dark blue squares, that the mechanical and corrosion properties of the new alloys need to be analyzed. This thesis deals with a selection of the approaches written down in the orange boxes and connected by the continuous lines. The approaches in the orange boxes connected by the dashed lines were not investigated. Also, some of the properties mentioned in the blue boxes are investigated.

1.3.2 Scope of the PhD project

The scope of the PhD project is to identify parameters to machine new lead-free brass alloys efficiently. New tool geometries and different cutting fluid supply strategies were tested, and their effect was quantified. The corrosion properties of lead-free brass alloys were analyzed by the project partners in the LOBUS project. A short summary of the dezincification resistance of CW511L in different temper conditions is given in Paper II, and more detailed information can be found in papers published by the project partners (Tomovic Petrovic et al., 2022). It is out of scope to develop new brass alloys. Nevertheless, an alteration of the microstructure

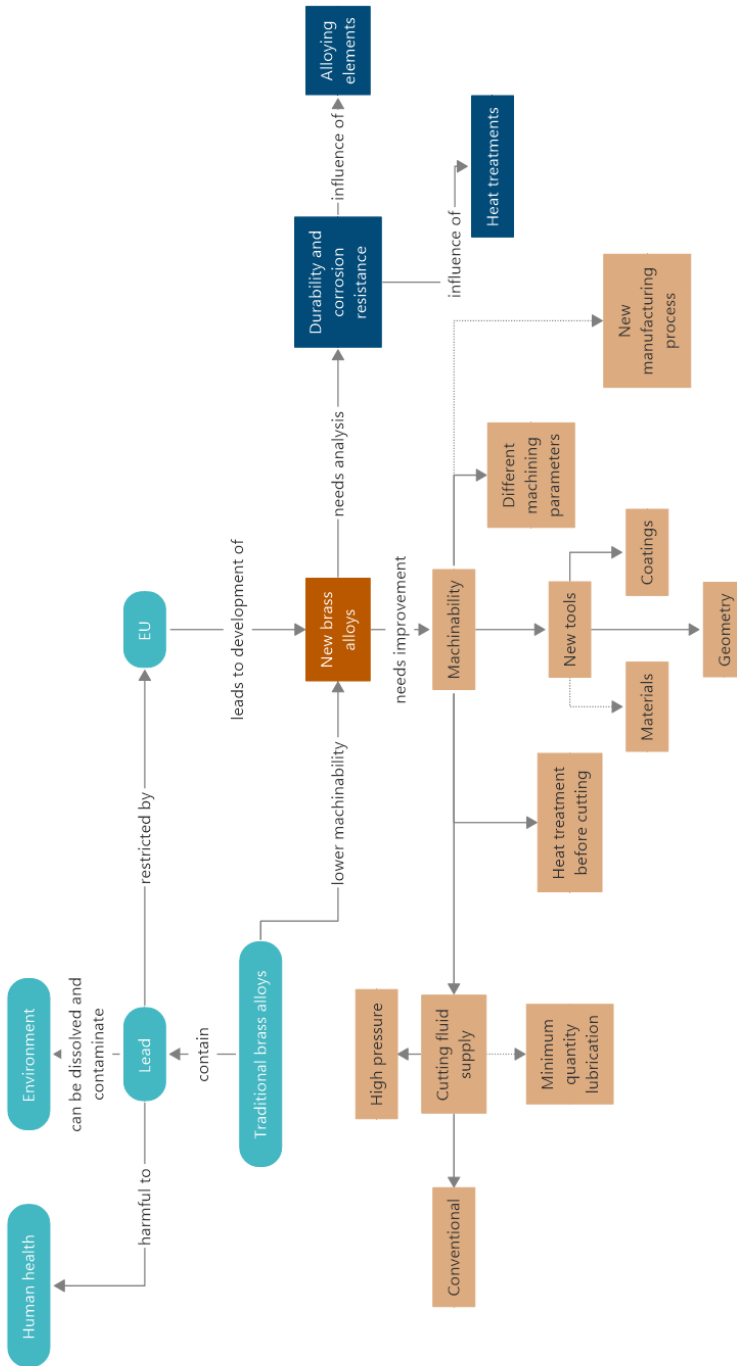


Figure 1.2: Visualization of the Problem Statement of the PhD Project.

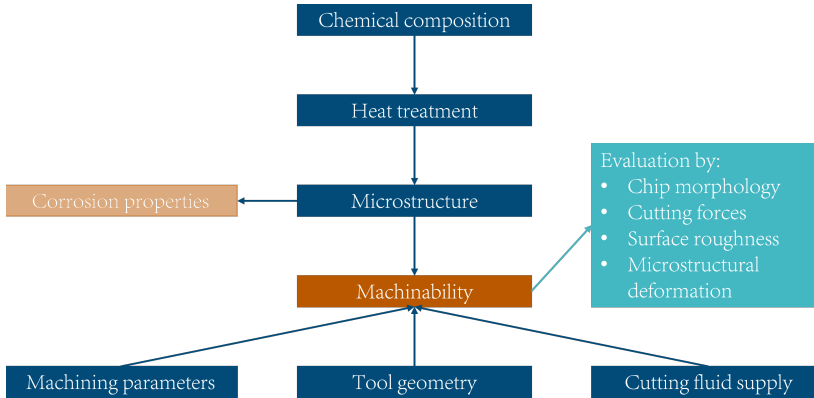


Figure 1.3: Context of the PhD Project.

was performed by heat treatment. Manufacturing methods other than turning were not tested or developed. Additionally, the used machining parameters were in the range of achievable values at the project partners' and laboratory facilities.

1.3.3 Research Objectives

The main objective of this PhD project is to quantify the effect of machining parameters, cooling strategy, tool coating, and tool geometry on the machining process. Therefore, the chip formation, the cutting forces, the surface texture, the microstructure, and briefly the corrosion properties should be analyzed. Different lead-free brass alloys will be considered.

Figure 1.3 shows the context of the PhD-project and some of the factors influencing machinability. The influencing parameters are pictured in dark blue, while parameters to evaluate machinability are pictured in turquoise. This project aims to quantify different impacts and to find optimal parameters within the boundaries defined in section 1.3.2.

1.3.4 Context of the appended papers

This thesis is based on a collection of articles written in the course of the PhD project. The papers are numbered chronologically in the sequence of publishing. All papers contribute to the overall aim of this PhD project, however, each of them is an individual entity and might have its own objectives.

Paper I

Müller, M. S., & Sørby, K. (2022). Cutting Forces in Machining of Low-Lead and Lead-Free Brass Alloys. In Y. Wang, K. Martinsen, T. Yu, & K. Wang (Eds.), *Advanced manufacturing and automation xi. iwama 2021. lecture notes in electrical engineering* (pp. 254–261). Springer, Singapore. https://doi.org/10.1007/978-981-19-0572-8_32

The first article proposes a method to analyze cutting forces and friction conditions during brass cutting. The proposed experimental procedure was established in all the following studies in this thesis. On the other hand, the proposed method to analyze friction in the cutting zone was found to be inaccurate. Besides, two different tool geometries were evaluated. A clear impact of the tool geometry was noticed.

Paper II

Müller, M. S., Tomovic Petrovic, S., & Sørby, K. (2022). Investigation of heat treatment to improve the machinability of lead-free brass alloy CW511L. *Copper Alloys 2022*, 42–45. <https://kupfer.de/wp-content/uploads/2022/12/Proceedings-Copper-Alloys-2022-2.pdf>

This article investigates a heat treatment procedure to impact the microstructure of CW511L alloy and increase the β -phase content. The influence of the heat treatment on the mechanical properties, the corrosion resistance, and the machinability were analyzed.

Paper III

Müller, M. S., & Sørby, K. (2023b). The Influence of the Rake Angle on the Cutting of Low-Lead and Lead-Free Brass Alloys. In H. Kohl, G. Seliger, & F. Dietrich (Eds.), *Manufacturing driving circular economy. proceedings of the 18th global conference on sustainable manufacturing, october 5-7, 2022, berlin. lecture notes in mechanical engineering* (pp. 219–227). Springer, Cham. https://doi.org/10.1007/978-3-031-28839-5_25

The third article compares different rake angles and different alloys. Uncoated cemented carbide tools as well as TiAlN-based cemented carbide tools are used. This article was an approach to decrease the cutting forces.

Paper IV

Müller, M. S., Brans, K., Meurer, M., Sørby, K., & Bergs, T. (2023). The effect of high-pressure cutting fluid supply on the chip breakability of lead-free brass alloys. *The International Journal of Advanced Manufacturing Technology*. <https://doi.org/10.1007/s00170-023-12440-8>

As chip breakability was considered a significant challenge, especially at increased rake angles, the fourth article investigates the influence of high-pressure cutting fluid supply in the machining of different lead-free brass alloys. A tool with a flat rake face and a tool with a chip-breaking geometry were utilized.

Paper V

Müller, M. S., & Sørby, K. (2023a). Investigation on chip breakability in lead-free brass alloy CW511L using different chip breaking geometries. *Intelligent Computation in Manufacturing Engineering-CIRP ICME'23 (in press) Procedia CIRP*

A different approach to enhancing chip breakability is the use of chip-breaking geometries. Paper V introduces four different chip-breaking geometries and one reference geometry using a rake angle of 20° . Chips and cutting forces are evaluated.

Paper VI

Müller, M. S., & Sørby, K. (2023c). The Effect of Tool Geometry on Chip Formation and Chip Morphology of Lead-Free Brass Alloy CW511L. *Submitted to: Advances in Manufacturing*. <https://doi.org/https://doi.org/10.21203/rs.3.rs-3423897/v1>

Paper VI deepens the analysis done in paper V by analyzing high-speed videos of the cutting process and chip morphology. Suggestions on future tool geometries in cutting CW511L are given.

Chapter 2

Research Methodology

The following chapter gives an overall overview of the research methods used to reach the expected results as described in section 1.3. The materials, processes, and methods used in this PhD project are described to provide a brief overview of the research work.

2.1 Materials

This thesis mainly studies the alloys CW625N (CuZn35Pb1,5AlAs), CW511L (CuZn38As), and CW724R (CuZn21Si3P). Additionally, CW510L (CuZn42) and CW508L (CuZn37) are investigated briefly. The chemical compositions of all alloys used in this project are shown in Table 2.1, and the mechanical properties are shown in Table 2.2. The microstructures are shown in Figure 2.1.

Brass alloys can consist of several phases. The commercial most relevant phases are α -phase and β -phase. The α -phase is a face-centered cubic (fcc) phase, which is a solid solution. The α -brass typically shows low hardness, high ductility, and cold workability. The β -phase is a body-centered cubic (bcc), which is harder and less formable at room temperature compared to α -phase. Single- α -phase brasses are known to be less machinable compared to dual-phase brasses or leaded brasses (Davis et al., 2001).

CW625N is a low-leaded α -brass alloy containing up to 1.5% lead. It is nowadays used in the project partner's production. In Figure 2.1 upper row to the left, the microstructure of CW625N is shown. The lead segregated around the grain boundaries is visible.

In CW508L and CW511L, Figure 2.1 upper row in the middle and lower row to the left, respectively, only trace amounts of β -phase are present around the grain boundaries of the α -grains. In contrast to CW508L, CW511L contains arsenic as active addition see table 2.1. Arsenic acts as a dezincification inhibitor protecting the α -phase (Stålnacke et al., 2020). Considering this, CW511L might be more suitable for drinking water supply systems than CW508L.

CW510L consists of approximately equal parts α - and β -phase. In Figure 2.1 upper row to the right, the microstructure of CW510L is shown. The bright elongated

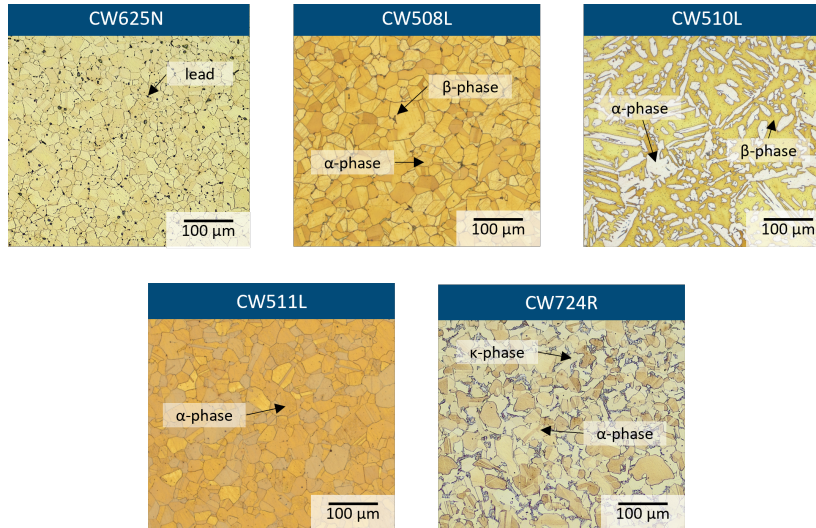


Figure 2.1: Microstructures of the brass alloys used.

grains are α -phase which are surrounded by the darker β -phase. Due to its duplex microstructure, CW510L can be expected to show better machinability (Davis et al., 2001). On the other hand, β -phase is more prone to dezincification (Moriarty et al., 2021), which makes this alloy less suitable for application in drinking water supply systems.

In the lower row to the right of Figure 2.1, the microstructure of CW724R is shown. CW724R is a silicon-alloyed brass, containing α - and κ -phase. The κ -phase forms due to the presence of silicon and is hard and abrasive. Therefore, it contributes to good chip breakability and increased tool wear (Bushlya et al., 2017; Nobel, Hofmann, Klocke, & Veselovac, 2015).

2.1.1 Heat treatment

Heat treatment can change the phase composition and grain size of an alloy and thereby the mechanical properties and machinability. Dual-phase brass alloys containing β -phase are known to show better machinability than pure α -brass (Davis et al., 2001). Depending on the temperature and zinc content the β -phase is stable. For example, at 800 °C β -phase is stable from 39% to 55% of zinc in brass, while at 500 °C β -phase is stable from 45% to 49% of zinc (Davis et al., 2001). Toulfatzis et al. (2016), Toulfatzis et al. (2018a) investigated heat treatment on different lead-free brass alloys to evaluate its potential to increase machinability. Heat treatment of CW511L at 850 °C with a holding time of 120 min followed by rapid water quenching showed to be successful in increasing the share of β -phase

in the microstructure (Toufatzis et al., 2016). Additionally cutting forces were slightly decreased and chips became shorter (Toufatzis et al., 2018a).

On the other hand, β -phase is known to be susceptible to dezincification, a corrosion mechanism of brass, where zinc is dissolved from brass and a porous copper sponge is left behind (Davis et al., 2001; Moriarty et al., 2021). To prevent this a pure α -brass microstructure is favorable. Therefore, after the procedure described above and the machining process, a second heat treatment would be necessary. In the second heat treatment, the workpiece must be heated to the recrystallization temperature (Davis et al., 2001). This was done by heating to 540 °C, holding for 180 min and slow cooling in still air. This is further described in Paper II.

2.2 Material Characterization Methods

To analyze the microstructure and properties of the different alloys different metallographic and mechanical testing methods were employed as described in the following.

2.2.1 Microstructural analysis

In order to analyze the microstructure, disc-shaped samples were first cut from the bars. These were then quartered and embedded in epoxy in a cold mounting process. All samples were wet ground with SiC-foil #320, followed by diamond and OP-S polishing.

For analysis of the microstructure in the light microscope the samples were prepared by etching. Most samples were etched with a solution of iron(III) chloride, hyperchloric acid, glycerol, and water. In contrast, the microstructure samples in Paper II were etched using a solution of ammonium peroxodisulfate, as these samples were prepared at one of the project partner's facilities. Both these techniques are grain boundary etching techniques.

Samples in Paper IV were etched using Klemm II solution which contains sodium thiosulfate, potassium metabisulfite, and water. Klemm II is a color etching technique, which is frequently used to analyze copper alloys. Therefore, Klemm II is the standard etching procedure at the metallography lab at WZL where the tests in Paper IV were performed. After these preparation steps, all samples were analyzed using a light microscope. Optical micrographs were generated, as shown in Figure 2.1.

As a further step of the analysis, some unetched samples were examined using a scanning electron microscope (SEM) and electron backscatter diffraction (EBSD). This was done in Paper II in order to be able to make a statement about the proportions of the phases and the grain sizes before and after the heat treatments.

2.2.2 Mechanical Properties

Mechanical properties in terms of tensile tests or hardness measurements are often performed by material suppliers to control and secure the quality of their products. Nevertheless, some mechanical properties were tested in the course of this project. In particular, in Paper II tensile properties and hardness were evaluated before and after the heat treatments performed.

The tensile tests were performed according to NS-EN-ISO 6892-1. The specimens had a diameter of 10 mm, as a test machine an Instron - Model 1342 - servo-hydraulic machine with a 100 kN load cell was used. The Brinell hardness measurements in Paper II were performed according to ISO 6506-1 at the project partner's facility by one of the project partners.

Additionally in Paper IV, hardness measurements according to ISO 6506-1 were performed using a Zwick hardness tester. The specimens were hot-mounted and polished to a mirror finish according to the procedure described in section 2.2.1 to remove subsurface deformations. Afterward, several indentations across the cross-section were made and analyzed. Average values of the hardness were calculated. It was noticed that the hardness varied slightly with the position of the indentation, as the materials presented a slightly lower hardness in the center of the cross-section.

2.3 Machining Process

As mentioned in section 1.2.3, in experimental investigations it is widely tried to generate cutting conditions as close to orthogonal cutting as possible. With this approach, the number of independent variables is decreased. Forces parallel to the cutting edge are reduced to a minimum and can be neglected.

In this project only extruded rods were used for investigations in turning processes. In the first step, all rods were prepared by turning them to a diameter of 31.5 mm. To get cutting conditions close to orthogonal cutting, these rods were prepared with radial grooves. Each disk was 2 to 3 mm wide, as indicated in the corresponding paper. Maximum three disks were prepared at a time as shown in Figure 2.2. Depending on the lathe, the rods were either clamped in a collet chuck or a three-jaw chuck.

All tests were performed as radial grooving operations where the tool is radially fed towards the center of the rod as indicated by f_n in Figure 2.2. The disks, as described above, were cut. Care has been taken to ensure that the insert hits the center of the disk while cutting to minimize the effects of the edges of the insert. Inserts were inserted into suitable tool holders, which were inserted into a force measurement platform. In this project, two different force measurement platforms were used depending on the lathe. In general, these two platforms work identically and utilize the piezoelectric effect to measure the cutting forces in three directions. As indicated in Figure 2.2, the three measured forces are the cutting force F_c , the feed force F_f , and the passive force F_p . In all tests, the cutting speed

v_c was kept constant, meaning the revolutions per minute increased when the tool approached the center of the rod. The feed rate was varied. Most of the tests were performed in dry-cutting conditions. Solely the tests in Paper IV were performed with conventional and high-pressure cutting fluid supply.

Different tools and tool geometries were investigated. Rake angles as well as chip-breaking geometries were varied. Additionally, uncoated cemented carbide tools were compared to AlTiN-coated tungsten carbide tools.

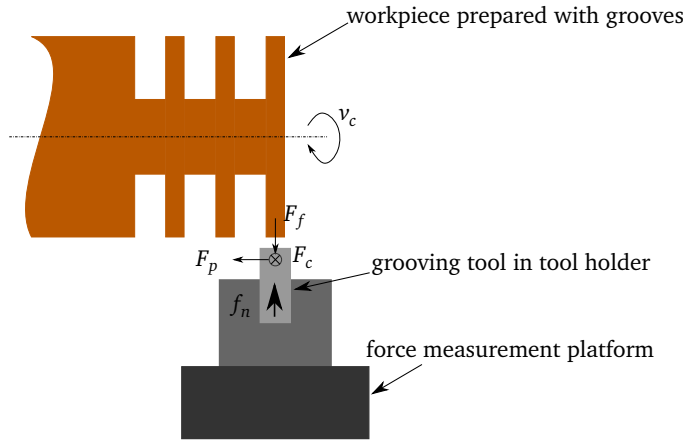


Figure 2.2: Schematic drawing of the machining test setup.

2.4 Analysis of Tools, Chips and Machined Parts

Besides the cutting process and process parameters, tool macro and micro geometries can impact the cutting forces, chip breakage, and surface integrity of the machined part. During this project, some tools were custom ground to evaluate the impact of their geometry on the cutting process. To gain a deeper knowledge about their actual geometry, it was evaluated using an Alicona Infinite Focus microscope. This microscope utilizes focus variation to scan a surface or part. The edge form, edge rounding, rake angle, clearance angle, and wedge angle of the cutting edge were evaluated, as well as the geometry of custom ground chip breaking geometries.

Low chip breakability is one of the significant drawbacks of lead-free brass alloys compared to leaded brass alloys. To evaluate the chip flow during the cutting process, the tests described in Paper VI were partly recorded with a high-speed camera. Thereby, the chip up-curl radius and the chip flow in the chip-breaking geometry could be evaluated. The chip thickness ratio was assessed by measuring the chip thickness after the cut in a digital microscope. For further analysis some chips were embedded, ground, polished, and etched and the microstructure was

analyzed, as described in Papers II, IV, and VI. Microstructural features and chip segmentation were revealed and evaluated.

The surface roughness of the parts machined in Paper IV was measured using a MarSurf LD 260 device by Mahr. However, considering the geometry and conditions of the cutting process used, the micro geometry of the cutting edge determined most likely the surface roughness, as the cutting tool was not moved across the surface. This was supported by the shape of the roughness profile which looked similar for different cuts using the same tool. Since all machining tests in this PhD project used grooving operations as the main evaluation method, no further roughness evaluations on machined parts were conducted.

2.5 Tool Wear Tests

Tool wear tests were conducted using the uncoated tools with 0° and 24° rake angle described in Paper III and the brass alloys CW511L, CW724R, and CW625N in a face-turning operation. For the tool life tests a CNC Okuma GENOS L200E-M lathe was used. The tests were performed in dry conditions with a prepared rod, which was turned to a diameter of 31 mm. The principle of the tool life tests is shown in Figure 2.3. The width of cut was $a_p = 1$ mm, the feed was $f_n = 0.1$ mm/r and the spindle speed was kept constant at 2000 r/min, leading to a varying cutting speed of 25 to 195 m/min. During one test 50 cuts were performed. As shown in Figure 2.3 the diameter of the core increased from 4 mm to 6 mm. This was done to prevent the tool from hitting the already machined surface. The machining time for a set of 50 cuts was 3.25 min. In total, tool wear tests were performed for 208 min in CW511L and CW724R and for 39 min in CW625N. For every 200 cuts, the tests were interrupted to check the tool wear in the microscope, measure cutting forces, and collect chips. A Weiler Commodor 230 VCD lathe and a Kistler dynamometer type 9257B were utilized for the force measurements. In contrast to most of the force measurements presented in this thesis, the force measurements in the tool wear tests were performed as regular face-turning operations to use the same process as in the wear test. For the force measurements the cutting speed was kept constant at 150 m/min, the width of cut was $a_p = 1$ mm and the feed was $f_n = 0.1$ mm/r.

2.6 Summary of the research methods used

To sum it up, the main research method in this project is machining tests using a modified radial turning process to bring the cutting conditions as close to orthogonal cutting as possible, and cutting force measurements. In the different publications, the focus was on different parameters, as shown in Table 2.3. Different machine tools were used due to availability in the labs and cutting fluid supply

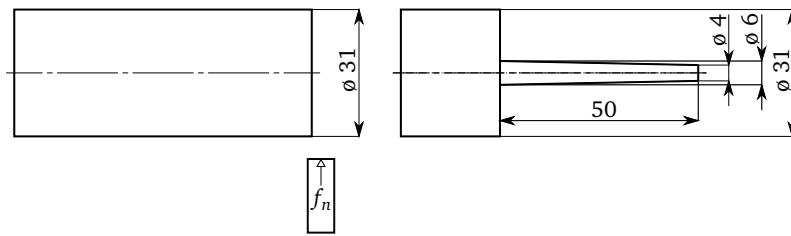


Figure 2.3: Schematic drawing of the tool life testing procedure.

options. Additional tests and analysis were performed to evaluate the cutting process further such as microstructural investigations, tool geometry evaluations, chip evaluations, and high-speed camera recordings.

Table 2.1: Overview of the chemical composition of the brass alloys used according to (European Standard, 2016; Nordic Brass Gustum AB, 2019).

Symbol	Number	Mass Fraction in [%]										Others
		Cu	As	Al	Fe	Mn	Ni	P	Pb	Si	Sn	
CuZn35Pb1,5AlAs	CW625N	63-64	0.02-0.08	0.5-0.6	≤ 0.1	≤ 0.1	≤ 0.2	-	1.2-1.5	-	≤ 0.3	Rem. ≤ 0.02
CuZn37	CW508L	62-64	-	≤ 0.05	≤ 0.1	-	≤ 0.3	-	≤ 0.1	-	≤ 0.1	Rem. ≤ 0.1
CuZn42	CW510L	57-59	-	≤ 0.05	≤ 0.3	-	≤ 0.3	-	≤ 0.2	-	≤ 0.3	Rem. ≤ 0.2
CuZn38As	CW511L	61.5-63.5	0.02-0.15	≤ 0.05	≤ 0.1	-	≤ 0.3	-	≤ 0.2	-	≤ 0.1	Rem. ≤ 0.2
CuZn21Si3P	CW724R	75-77	-	≤ 0.05	≤ 0.3	≤ 0.05	≤ 0.2	0.02-0.1	≤ 0.1	2.7-3.5	≤ 0.3	Rem. ≤ 0.2

Table 2.2: Overview of the mechanical properties of the brass alloys used.

Number	Symbol	Tensile Strength	Yield Strength	Elongation at Break	Hardness
		R _m [MPa]	R _{p0,2} [MPa]	A [%]	HBW
CW625N	CuZn35Pb1,5AlAs	400	300	30	110
CW508L	CuZn37	348	206	43	82
CW510L	CuZn42	506	406	34	110
CW511L	CuZn38As	354	296	56	91
CW724R	CuZn21Si3P	570	250	35	150

Table 2.3: Overview of the research methods used in the different publications.

Main Impact on Cutting Force	Machine Tool	Inserts	Cutting Speed v_c in [m/min]	Feed f_n in [mm/f]	Chip Breaker	Rake angle in [°]	Cooling Condition	Alloys	Other factors evaluated	Publication
Tool Geometry, Cutting conditions	Colechester V53250	N123H2-0520-0002-BG H13A; N123H2-0400-0004-TM H13A	200	0.1, 0.16, 0.2, 0.25	Yes; No	0 8	Dry	CW625N; CW511L; CW724R	Accuracy of the Merchant equation in brass alloys	Paper I
Microstructure	Weiler Commoodor 230 VDC	N123H2-0520-0002-BG H10F	150	0.05, 0.1, 0.16, 0.2	No	0	Dry	CW511L	Influence of microstructure on mechanical properties, chips and debrination resistance	Paper II
Tool coating, rake angle	Weiler Commoodor 230 VDC	IG123L1-0600-BG H13A; custom ground, partly coated with TiAlN-coating	150	0.05, 0.1, 0.16, 0.2	No	0 8 16 24	Dry	CW625N; CW511L; CW724R	Influence of the rake angle on the chip form	Paper III
High pressure cutting fluid supply; Chip breaking geometry	DMG Mori NX1 1500 ST13	GPA 4.00-0.40, grade (C20); partly ground to remove chip breaking geometry	150	0.1, 0.15, 0.2	Yes; No	16	conventional cooling and high-pressure cutting fluid using $p = 3, 24, 55, 72$ bar	CW508L CW510L CW511L	Microstructure and mechanical properties were evaluated	Paper IV
Chip-breaking geometry	Weiler Commoodor 230 VDC	N123H2-0520-0002-BG H13A; custom ground	150	0.05, 0.1, 0.16, 0.2	Yes, four different custom made geometries and one reference geometry without chip breaker	20 12	Dry	CW511L	Influence of the chip breaking geometry on the chip form	Paper V
Chip breaking geometry; rake angle	Weiler Commoodor 230 VDC	NH123H2-0520-0002-BG H13A; IG123L1-0600-BG H13A; custom ground, partly coated	150	0.05, 0.1, 0.16, 0.2	Yes; No	20; 0, 8, 16, 24	Dry	CW511L	Influence of rake angle and chip breaking geometry on chip formation process, chip analysis	Paper VI
Tool wear, rake angle	CNC Okuma GENOS L20ME-M; Weiler Commoodor 230 VDC	IG123L1-0600-BG H13A; custom ground	150	0.1	No	0, 24	Dry	CW511L	Influence of rake angle influence of different tool wear conditions	not published

Chapter 3

Results

In this chapter, the results of the different articles published during this PhD project are presented briefly. The full-length contributions are presented in Appendices I - VI. Additionally, the unpublished results from the tool wear tests are presented.

3.1 I - Cutting Forces in Machining of Low-Lead and Lead-Free Brass Alloys

Authors: Magdalena S. Müller and Knut Sørby

Journal: Lecture Notes in Electrical Engineering

This study investigates two uncoated tungsten carbide tools with different geometries cutting the three alloys CW511L, CW625N, and CW724R. Tool #1 had a rake angle of 0° and a flat rake face. Tool #2 had a rake angle of 8° and a chip-breaking geometry. Additionally, two different cutting methods were investigated. First, radial face-turning was performed as shown in Figure 3.1. After that, the rod was prepared with disks and grooves to bring the cutting conditions as close to the orthogonal cutting model as possible. During the investigations, the disks were cut in a radial cutting operation as shown in Figure 3.2. This method is described more deeply in section 2.3. For the force vector measured using this method, the passive force was close to 0N, and therefore, it was considered successful and used in all further studies.

The lead alloyed brass CW625N showed the lowest cutting force for both cutting methods. The cutting force measured in CW724R was slightly increased by around 15% in radial face-turning and by 1% in disk-turning while the cutting force in CW511L was around 42% and 43% higher when compared to CW625N. Comparing the two tools in this study, a lower cutting force was measured for all materials when using the tool #2. The results from the radial face-turning are shown in Figure 3.1, and the results from the disk-turning method are shown in Figure 3.2.

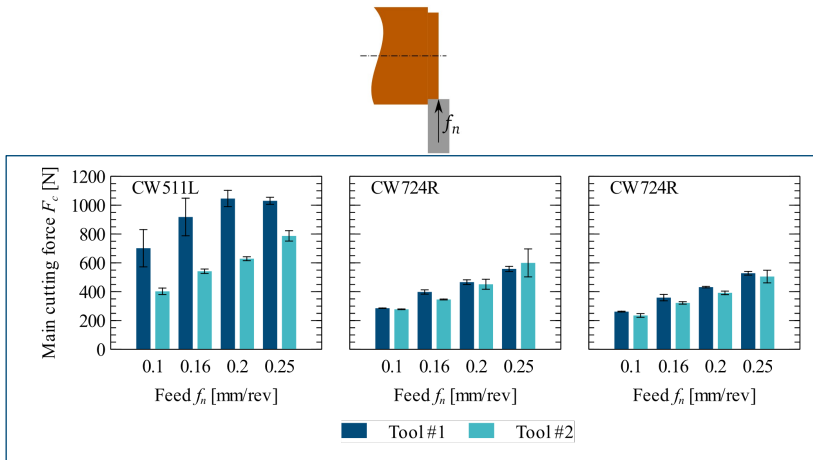


Figure 3.1: Results of the face-turning operation in the first paper.

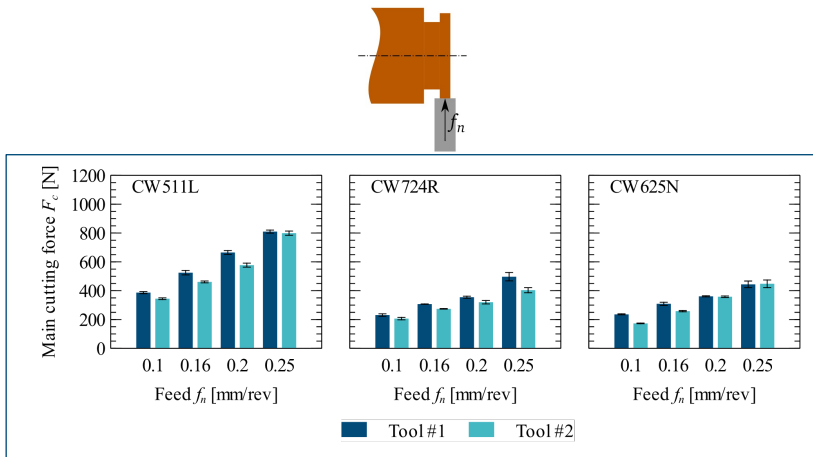


Figure 3.2: Results of the turning operation as close as possible to the orthogonal cutting model in the first paper.

3.2 II - Investigation of heat treatment to improve the machinability of lead-free brass alloy CW511L

Authors: Magdalena S. Müller, Stanka Tomovic Petrovic and Knut Sørby

Journal: Proceedings of Copper Alloys 2022

The β -phase is known to increase machinability. Therefore it was tried to increase the β -phase content of CW511L by heat treatment. On the other hand, the β -phase is more prone to dezincification. In this study CW511L was heated to 850 °C, held for 120 min and water quenched to increase the β -phase content. That was called the HT1 temper condition. To retain the dezincification resistance, a subsequent heat treatment was performed. Here, the alloy was heated to 540 °C, held for 180 min and slowly cooled in still air. That was called the HT2 temper condition. The second heat treatment is indicated to be performed after the machining process. The aim was to retain the pure α -microstructure and release any stresses that might have been induced during the machining process. Pictures of the microstructure in the three temper conditions are shown in Figure 3.3.

The β -phase content was at 3.5% in the as-received temper condition of CW511L, increased to 12.6% in HT1 temper condition, and decreased back to 4.8% in HT2 temper condition. The grain size increased for the HT1 temper condition in comparison to the as-received temper condition. Also, the HT2 temper condition had coarser grains compared to the as-received condition.

Even though β -phase content was increased in the HT1 condition compared to as received condition, the cutting force barely decreased by 4%. Overviews of the measured main cutting force F_c are given in Figure 3.3. Macroscopically the chips of both temper conditions showed similar sizes and form. On the microscale, the chips were observed to be slightly different. Chips in as received temper condition were non-homogeneous (serrated), while chips in the HT1 temper condition were discontinuous.

While HT2 and as-received temper conditions can be considered dezincification resistant according to ISO 6509, material in HT1 temper condition cannot be considered dezincification resistant. However, the depth of the dezincification attack in the HT2 temper condition was higher compared to the as-received condition. The hardness of HT1 and HT2 temper conditions decreased considerably compared to the as-received condition. Both temper conditions did not fulfill the hardness requirement of the NS-EN 12146 standard, while the as-received condition was within the standard. The tensile strength increased for the HT1 temper condition but decreased for the HT2 temper condition compared to the as-received condition. The HT2 temper condition did not meet the requirement for tensile strength given in NS-EN 12146 standard. An overview of the measured values is given in Figure 3.3.

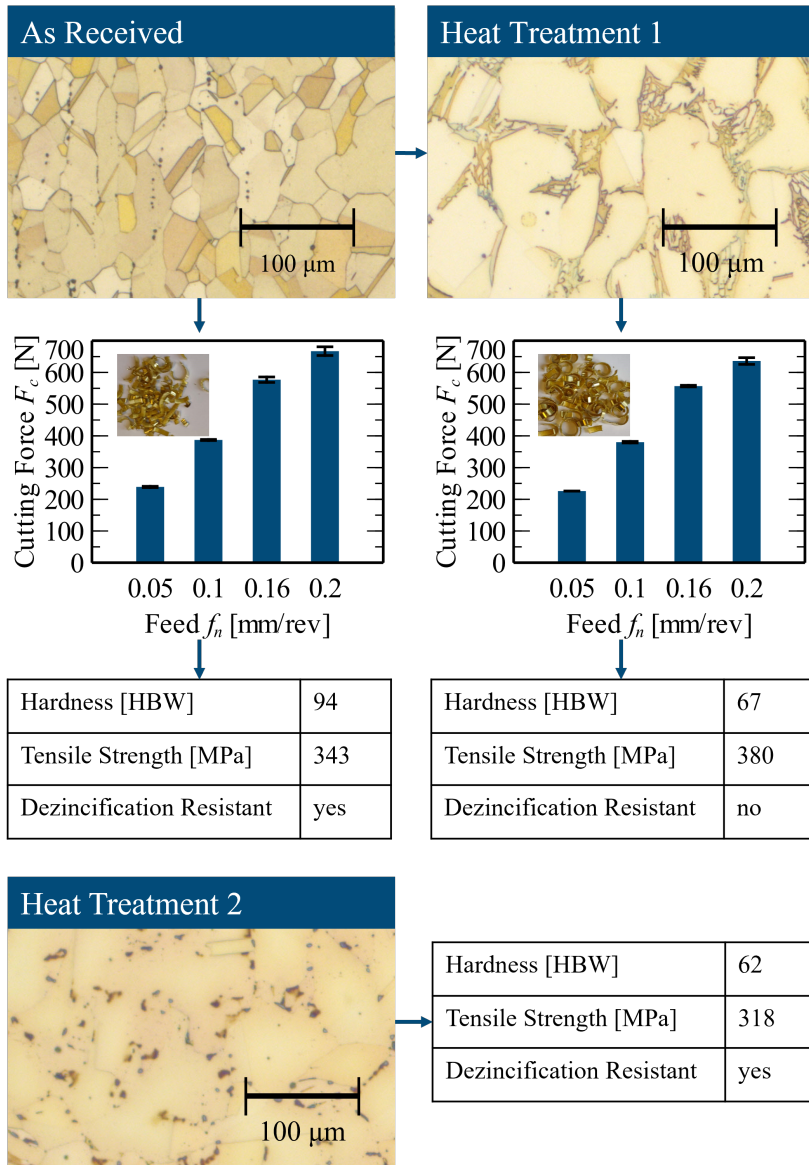


Figure 3.3: Overview of the microstructures, mechanical properties, chips and cutting force results of paper II.

3.3 III - The Influence of the Rake Angle on the Cutting of Low-Lead and Lead-Free Brass Alloys

Authors: Magdalena S. Müller and Knut Sørby

Journal: Lecture Notes in Mechanical Engineering

A method to reduce the cutting force is to increase the rake angle. Therefore, four different rake angles, 0° , 8° , 16° and 24° were compared at four different feed levels, $f_n = 0.05; 0.10; 0.16; 0.20\text{mm/r}$. The investigated tools were made of tungsten carbide. The tools were evaluated in uncoated condition and with a TiAlN tool coating. The two lead-free alloys CW511L and CW724R and the low-leaded alloy CW625N were investigated.

As expected the cutting force decreased when the rake angle increased for both coating conditions and all alloys. However, the effect was differently pronounced for the different alloys. For CW511L the cutting force reduced on average by 34% when changing from 0° rake angle to 24° , for CW724R this reduction was by around 17% and for CW625N it was by 22%. The AlTiN tool coating slightly increased the cutting force, which could be explained by the higher roughness of the coated tools compared to the uncoated tools. Similar to the results in Paper I, CW625N showed the overall lowest cutting force, while CW511L showed the overall highest cutting force. Regardless of the cutting tool, the cutting force in CW511L was the most sensitive to an increase in the feed. Figure 3.4 gives an overview of the cutting force measured for the uncoated tools.

Overall, the chip breakability decreased and the chips became longer with an increasing rake angle. This led to long and tangled chips, especially in CW511L. The chips for CW724R and CW625N became longer as well, but were, however, still acceptable regarding a potential automated cutting process. A schematic overview of the chip forms for the different rake angles is given in Figure 3.4.

Future investigations should focus on chip breakability when using tools with an increased rake angle, especially for ductile, single-phase alloys such as CW511L. Chip-breaking geometries or high-pressure cooling supply could be possible options. Additionally, the tool life of tools with higher rake angles should be investigated for brass alloys. When the rake angle is increased, the wedge angle decreases, leading to a potentially weaker cutting edge and more rapid tool wear. Remarkably lower cutting force might outperform slightly lower tool life, as lower cutting force most likely also leads to less surface deformation and residual stresses and, therefore, to less stress corrosion cracking.

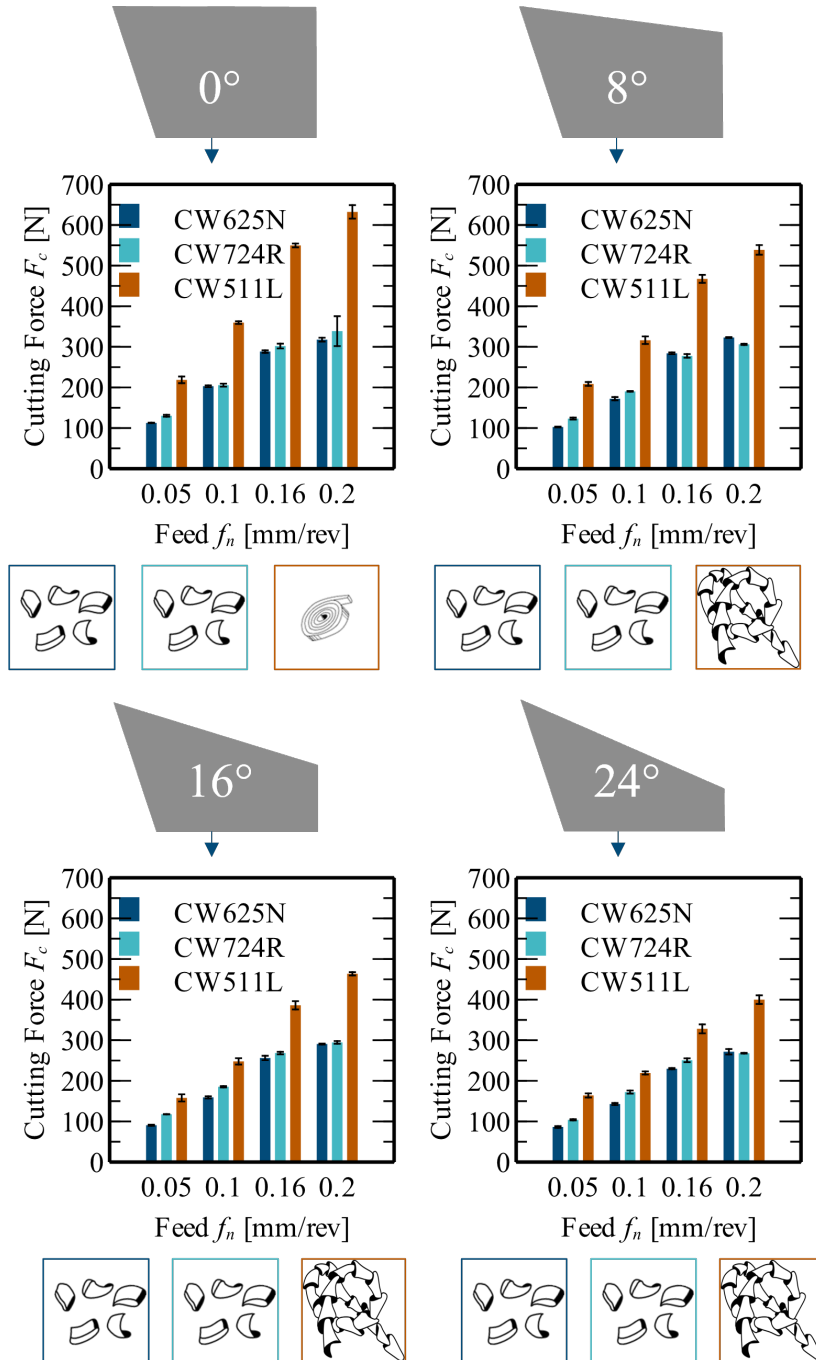


Figure 3.4: Overview of the results of paper III for cutting with the uncoated tools.

3.4 IV - The Effect of High-Pressure Cutting Fluid Supply on the Chip Breakability of Lead-Free Brass Alloys

Authors: Magdalena S. Müller, Kilian Brans, Markus Meurer, Knut Sørby and Thomas Bergs

Journal: The International Journal of Advanced Manufacturing Technology

The chip breakability in lead-free brass alloys is significantly lower compared to traditional lead-alloyed brasses. Lead-free brass alloys, especially single-phase alloys tend to form long and tangled chips, which can lead to challenges in automated cutting processes, as the chips can tangle around the tool or workpiece and lead to extended downtimes for example due to premature tool breakage. Possible solutions to improve chip breakability in terms of the cutting process are a high-pressure cutting fluid supply or a chip-breaking geometry. This paper investigated the influence of a high-pressure cutting fluid supply, as well as the influence of a chip-breaking geometry and the combined effect of both. The three lead-free brass alloys CW508, CW511L, and CW510L were studied at varying cutting fluid supply pressure levels and feed rates in a radial cutting operation. As a reference, conventional cooling was used. The chips produced during cutting and the cutting force were analyzed. The test setup is shown in of Figure 3.5.

There was only a marginal influence of the cutting fluid supply pressure visible on the cutting force. The average difference in cutting force between the highest and lowest cutting fluid levels was by only 3%. Solely in CW511L, this influence was slightly higher. Here the difference between the highest and lowest cutting force was 11%. The lowest force was measured at a pressure level of 24 bar with the tool with chip-breaking geometry. This was explained by a higher strain hardening effect due to more efficient cooling at higher pressure levels. The middle part of Figure 3.5 gives an overview of the measured cutting force for a feed of $f = 0.15 \text{ mm/r}$. The alloy used had a major impact on the chip forms produced during cutting. Overall, the chips became shorter at higher cutting fluid supply pressure levels, increased feed rates, and when using the tool with the chip breaking geometry. Figure 3.5 gives an overview of the chips produced at the highest and lowest pressure levels at a feed of $f = 0.15 \text{ mm/r}$ in the lower part.

While increased pressure levels seem to be the most beneficial when aiming for short chips, they also require more energy and cutting fluid to reach those. Additionally, it was visible in CW511L that the cutting force increased when the tool-chip contact was cooled more effectively at higher pressure levels. Based on the results of this study, a medium-high cutting fluid supply pressure at $p = 24 \text{ bar}$ with an adapted chip-breaking geometry for both high-pressure cutting fluid supply and brass alloys might be optimal. As only one chip-breaking geometry was evaluated in this study, further research is needed to optimize the geometry further.

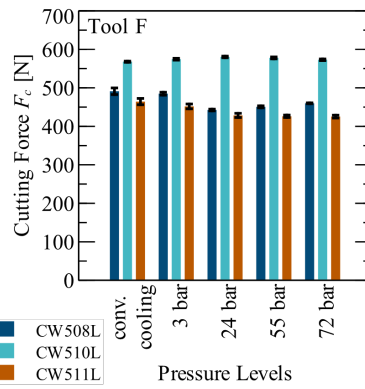
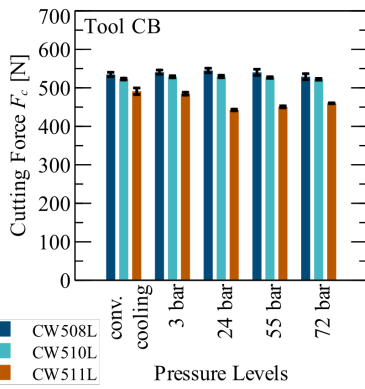
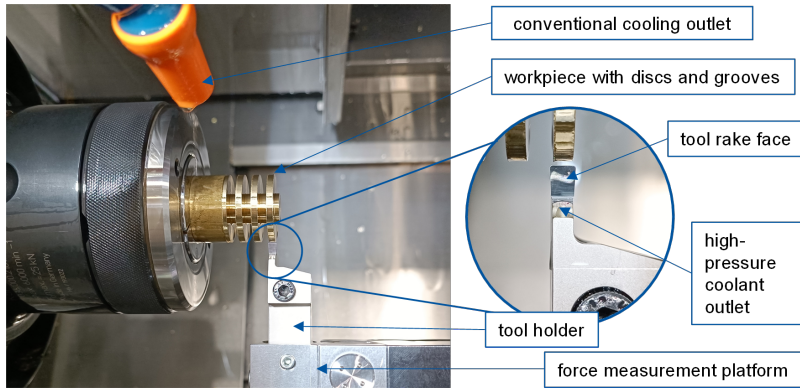


Figure 3.5: Overview of the test setup and the results of paper IV.

3.5 V - Investigations on chip breakability in lead-free brass alloy CW511L using different chip breaking geometries

Authors: Magdalena S. Müller and Knut Sørby

Journal: Procedia CIRP (in press)

This paper compares five different tool geometries in cutting lead-free brass alloy CW511L. All tools were manufactured from the same blank geometry. The groove radius r_G and the chip breaker land with l were varied. A schematic drawing of the tool geometries and a table with the measured values of the groove radius and the chip breaker land width are given in Figure 3.6. Four of the tools had a rake angle of 20° , while tool #4 despite the specification had a rake angle of 11.8° . Even though it was prepared with the smaller rake angle it was included in the study, to compare the influence of the rake angle to the influence of the chip-breaking geometry.

Overall, the chip-breaking geometry showed only a minor impact on the cutting force measured, while the tool with the smaller rake angle showed a significantly higher cutting force. An overview of the measured cutting force is given in Figure 3.6.

The feed has a visible impact on the chip breakability, as shown in Figure 3.6. The tool with the smaller rake angle showed overall the shortest chips, which can be attributed to a higher deformation induced into the chip by the lower rake angle. Out of the tools with a rake angle of 20° the tool with a groove radius of 3.5 mm and a chip-breaker land width of 0.7 mm showed the best results regarding chip breakability at the lowest feed tested, $f_n = 0.05$ mm/r. At higher feed rates differences in the chip length diminished, while differences in the chip curl radii became visible.

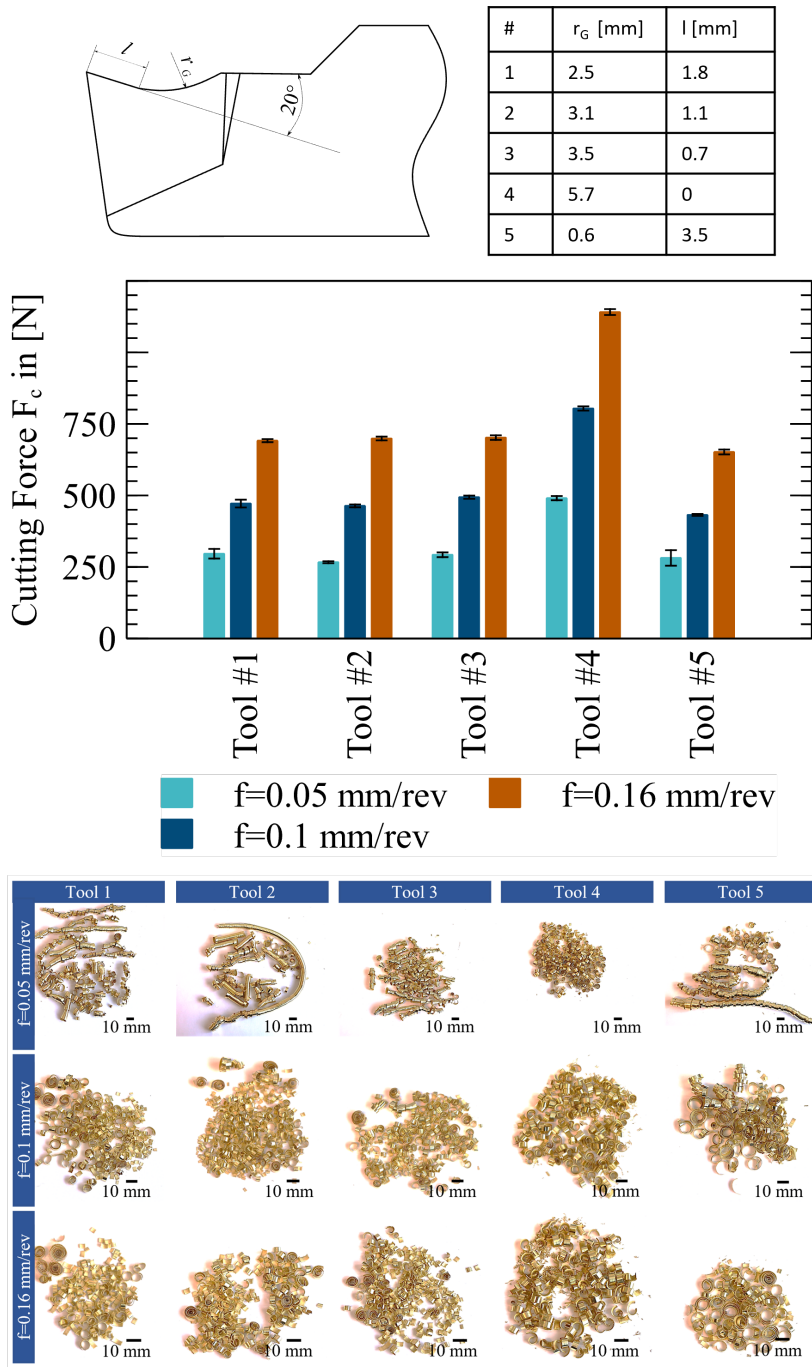


Figure 3.6: overview of the tool specifications chips and cutting force results of paper V.

3.6 VI - Analysis of Chip Formation and Chip Morphology of Lead-Free Brass Alloy

Authors: Magdalena S. Müller and Knut Sørby

Journal: submitted to *Advances in Manufacturing*

To deepen the understanding of the chip formation process in the cutting of the lead-free brass alloy CW511L, chips and cutting force produced with tools with different rake angles and groove-type chip-breaking geometries were analyzed in orthogonal cutting tests. The rake angles 0° , 8° , 16° , and 24° were investigated without a chip-breaking geometry. TO investigate different chip-breaking geometries, the rake angle was kept constant at 20° , while the chip-breaker land width was varied between 0.7 mm and 1.8 mm and the groove radius was varied from 2.5 mm to 3.5 mm. Furthermore, a reference tool geometry with a chip-breaker land width of 3.5 mm was used, leading to an unrestricted tool-chip contact and a natural chip flow. A high-speed camera recorded the cutting tests with the chip-breaking geometries to analyze the chip formation more in-depth.

The cutting force decreased with increasing rake angle. On the other hand, the chip length increased with increasing the rake angle, leading to long and snarled chips. The chip thickness ratio and the degree of chip segmentation decreased with an increased rake angle due to less deformation in the chip. Therefore, chip-breaking geometries are necessary to utilize the decreased cutting force at higher rake angles and, at the same time, secure a reliable process in automated continuous cutting. The chip-breaking geometries had no significant effect on the cutting force but influenced the chip formation. The chip formation was mainly influenced on a macroscopical scale, as chips broke more frequently and showed a lower up-curl radius. On the other hand, the chip thickness ratio was similar for all tools, and the degree of chip segmentation changed only marginally. The tool with a chip-breaker land width of 0.7 mm and a groove radius of 3.5 mm showed the lowest chip up-curl radii and overall the best chip breaking abilities. After measurements of the contact length, an even lower flank land width than 0.7 mm for use at lower feeds such as $f_n = 0.05 \text{ mm/r}$ in combination with a small groove radius of $r_G \leq 2.5 \text{ mm}$ could be recommended.

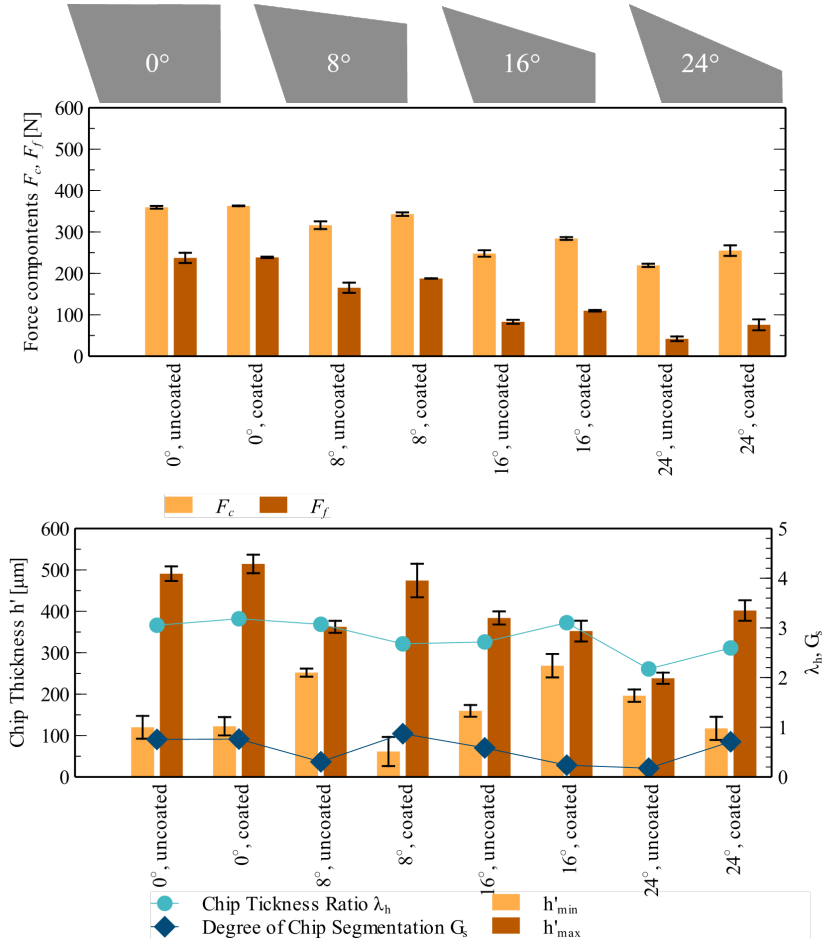


Figure 3.7: Results of cutting with the tools with varying rake angle in paper VI.

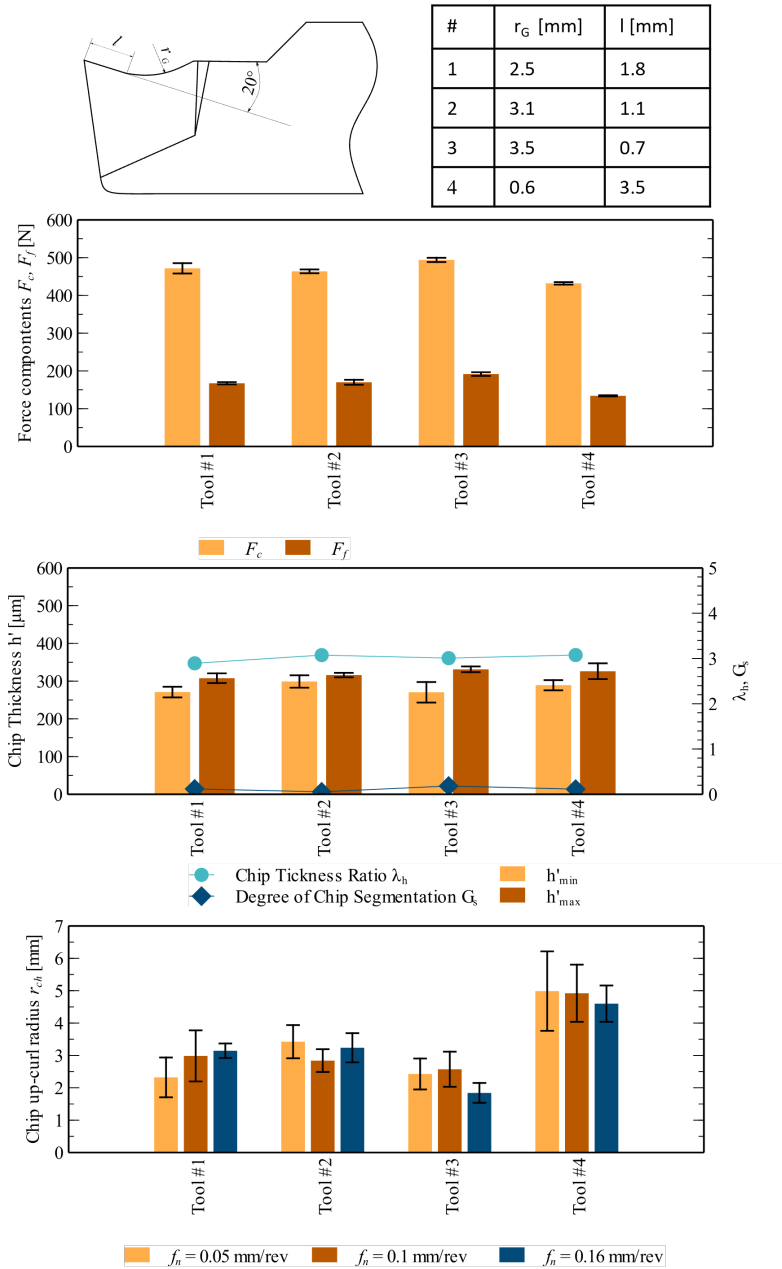


Figure 3.8: Results of cutting with the tools with chip breaking geometry in paper VI.

3.7 Tool Wear

The tool wear tests for CW724R and CW511L were performed for 208 min, while the test for CW625N was discontinued after 39 min. The main wear mechanism for all tools and materials was workpiece material adhesion. The adhesion seemed to be the most significant in CW511L.

Figure 3.9 shows pictures of the rake faces and clearance faces of the different tools for CW625N after 39 min taken with an optical microscope and a scanning electron microscope. No flank wear (VB) was measurable in CW625N after 39 min, as shown in Figure 3.9. No difference between the two tools was visible regarding the tool wear. The tests were discontinued, as no tool wear was noticeable and it was not expected to get flank wear in a reasonable time using a reasonable amount of material.

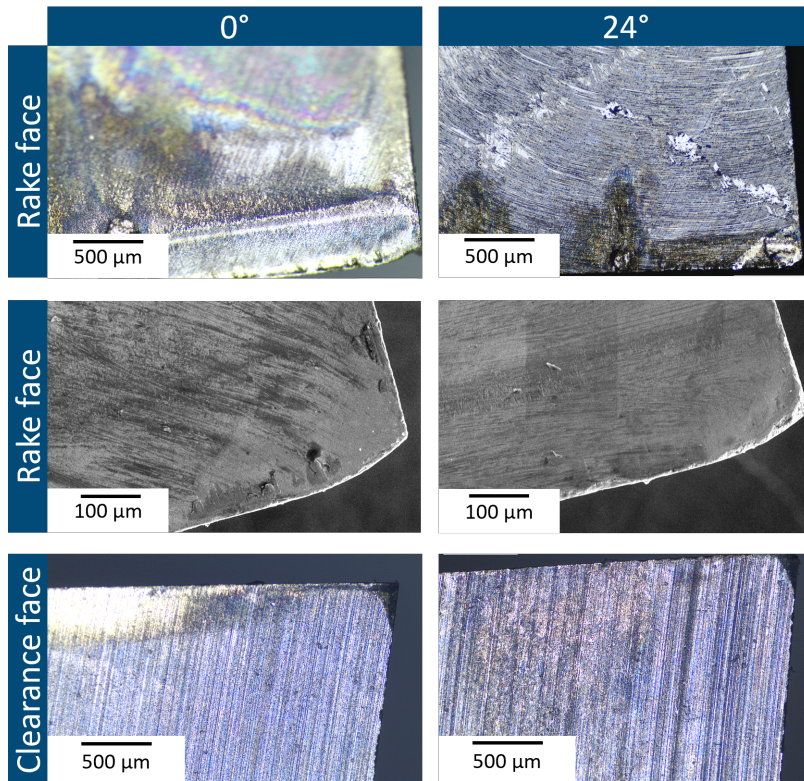


Figure 3.9: Microscopical pictures of the rake faces and the clearance faces of the tools in CW625N after 39 min.

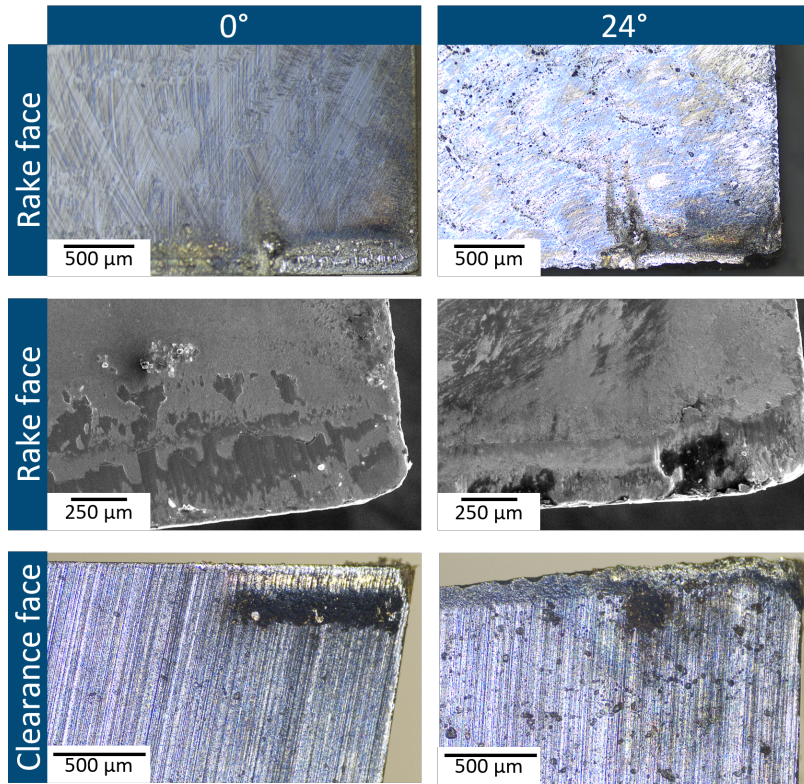


Figure 3.10: Microscopical pictures of the rake faces and clearance faces of the tools in CW724R after 208 min.

For the tools used in CW724R, mainly the material adhesions were noticed in the optical microscope after 208 min see Figure 3.10. There was very low flank wear visible, which was below $50\ \mu\text{m}$ for both tools. However, in the scanning electron microscope, some chipping was noticed on the 24° tool used for cutting CW724R, see Figure 3.10.

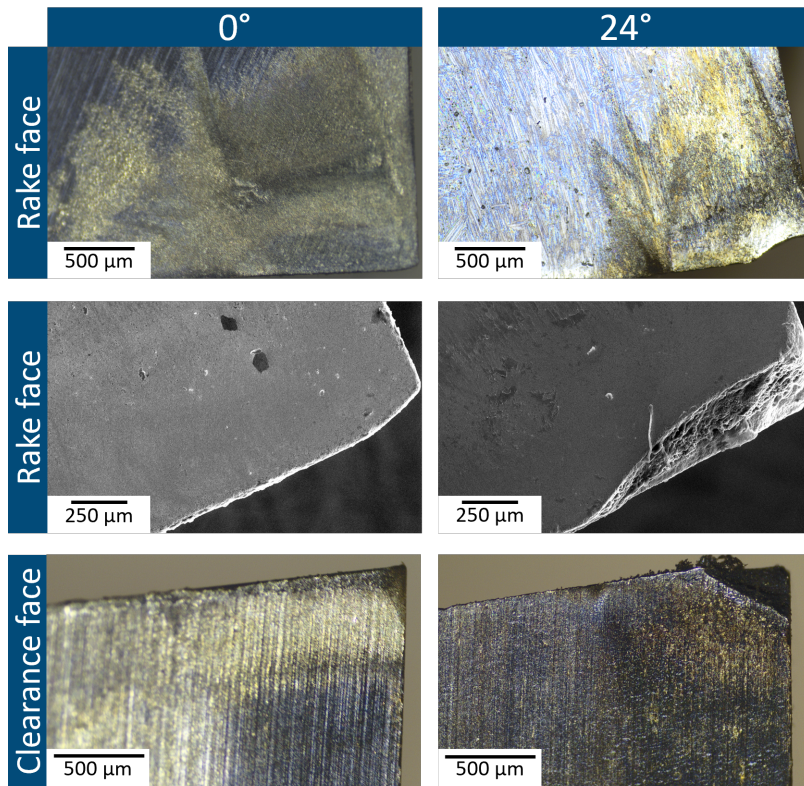


Figure 3.11: Microscopical pictures of the rake faces and clearance faces of the tools in CW511L after 208 min.

In the tests with CW511L, after 104 min the edge of the 24° was broken. This might be explained by the long chips tangling around the cutting tool and work-piece during the tests. For the 0° tool only material adhesions were present. The flank wear was below 50 μm for both tools. The broken edge was 350 μm high and 465 μm wide. In the scanning electron microscope the brittle fracture surface became visible, Figure 3.11.

The cutting force was measured after 0, 13, 26, 39, 104, 156, and 208 min. The results of this measurement are given in Figure 3.12. As seen in Paper III, the cutting force for CW511L is the highest, while CW625N shows the lowest cutting force and the cutting force for all materials is lower, when the material is cut with a higher rake angle. The cutting force for CW511L with the 0° tool varies, which might be explained by a varying build-up edge formation. Overall, the trend of

cutting force seems to increase, which might be explained by portions of the tool material chipping off together with the build-up edge. For cutting with the 24° tool, CW511L showed quite stable cutting force, which increases slightly after the breakage of the edge. CW724R shows a quite constant slope for both tools. The cutting force of the 24° tool increased after 156 min of machining noticeable and was above the level of the 0° tool at 208 min of tool wear testing. This is in good accordance with the slight tool wear visible in the 24° tool. In the CW625N tests were no major variations in the cutting force visible. Macroscopically the chips did not show variations during the cutting force measurements after different tool wear times.

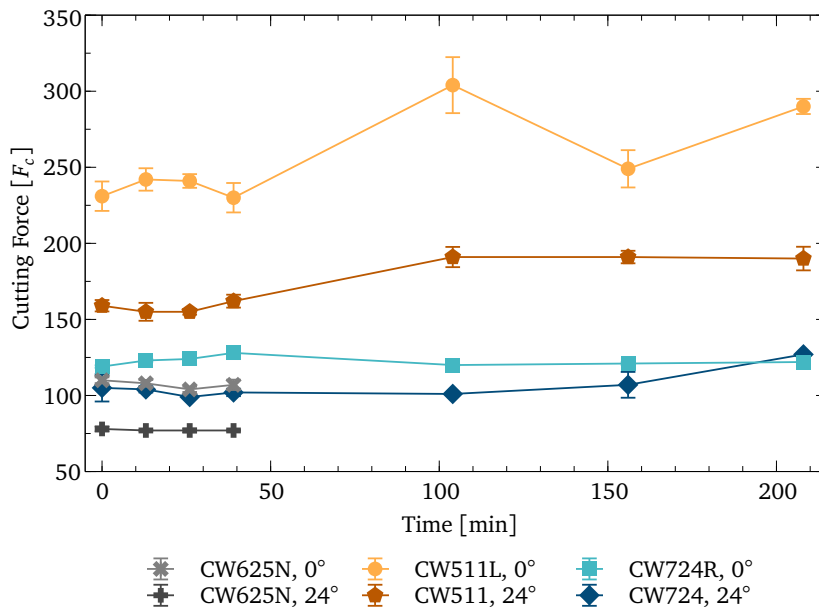


Figure 3.12: Cutting force measured after different durations of tool wear testing.

Chapter 4

Discussion

This chapter describes the decision-making to find machining parameters to increase the machinability of low-lead brass alloys by discussing the results given in Chapter 3. The decision-making process usually consists of planning the decision by defining the goals and objectives, identifying the stakeholder's needs, and putting the decision to be made in a context, which was done in Chapter 1, especially in Section 1.3. In the next step, data needs to be collected, the information needs to be processed and organized, and then the decision is made and implemented (Kossiakoff et al., 2020). In this thesis, merely a recommendation can be made on how to proceed in the machining of lead-free brass alloys based on the results, as the actual implementation was out of the scope of this thesis.

The main goals and objectives identified in the machining of lead-free brass alloys were

- lower the cutting force in lead-free brass alloys as close as possible to the cutting force in the cutting of lead-alloyed brass alloys,
- achieve good chip breakability, i.e., short, elemental chips, and
- find a method that is easy to implement and does not require too much additional equipment or energy.

The research methodology was established in the first paper (Paper I). It was decided to use a radial cutting operation, cutting prepared discs on the rod to get cutting conditions as close as possible to orthogonal cutting. Thereby, some independent variables could be eliminated to simplify the analysis. Additionally, the three brass alloys mainly used in this PhD project, CW511L, CW724R, and CW625N, were compared regarding the cutting force and the chip formation using two standard tool geometries by Sandvik Coromant. CW511L showed the highest cutting force and the lowest chip breakability. The cutting force in CW724R was closer to the lead-alloyed reference alloy CW625R but still slightly higher. The cutting force increased with an increasing feed. The impact of the tool geometry was visible in the cutting force. The tool with the increased rake angle showed a slightly decreased cutting force. It was noticed that chip side flow was present. Therefore, the process is not truly two-dimensional (Müller & Sørby, 2022). However, the

method of cutting discs in a radial cutting operation, as described in Chapter 2, was decided to be suitable for all further investigations.

4.1 Cutting force

The cutting force is influenced by the microstructure and chemical composition of the different alloys, the cutting parameters, such as feed, cutting speed and depth of cut, and the tool geometry.

The lead-containing alloy CW625N showed the lowest cutting force in all tests, followed by silicon-alloyed CW724R (Müller & Sørby, 2022; Müller, Brans, et al., 2023). Single-phase CW508L showed a higher cutting force than CW511L and dual-phase CW510L (Müller, Brans, et al., 2023). These results can be attributed to the different microstructures and chemical compositions. The lower cutting force in CW625N can be explained by the lead content (J. Johansson, Alm, et al., 2022). The silicon addition in CW724R formed the abrasive κ -phase, contributing to increased chip breakability and decreased cutting force compared to other lead-free brass alloys (Nobel et al., 2014b; Schultheiss et al., 2016). CW510L is a dual-phase alloy containing α - and β -phase. Hard and brittle β -phase can improve the chip breakability and decrease the cutting force. Single-phase alloys CW508L and CW511L are ductile and show the highest cutting force. A slightly higher residual lead content can explain the lower cutting force in CW511L.

To decrease the cutting force in CW511L and utilize the beneficial effects of the β -phase seen in alloy CW510L, a heat treatment was applied to increase the β -phase content. This approach was not considered beneficial, as the cutting force was only decreased by 4%. Additionally, subsequent heat treatment after the machining process would be necessary to restore the dezincification resistance and mechanical properties (Müller, Tomovic Petrovic, et al., 2022). This requires an additional processing step and additional energy. Therefore this approach was not investigated further.

The cutting force increases in general when the feed is increased. On the other hand, a lower feed leads to a lower material removal rate and a higher time required to shape the part. Therefore, lower feeds are usually only used for finishing processes but not for the whole cutting process. Further, the chip breakability decreases at lower feeds. The depth of cut, or in the chosen testing setup, the width of the discs, had an impact on the cutting force as a larger disc width led to an increased cutting force. This was not investigated further in the course of this PhD-project. The impact of the cutting speed was not directly studied in any of the attached papers, but when comparing the results in Paper I, II, and III, the higher cutting speed of 200 m/min (I) led to a higher cutting force than the cutting speed of 150 m/min (II, III). Nevertheless, a direct comparison of the measured cutting force is not reasonable due to the different cutting tools used in these studies. Literature comes to different conclusions regarding the cutting force-to-cutting speed relationship. Toulfatzis et al. (2018b) cut different lead-alloyed and lead-free

brass alloys in a transversal turning operation. An increase from 165 m/min to 192 m/min led to a slight increase in overall mean cutting force, while the mean cutting force decreased with a further increase in the cutting speed (Toufatzis et al., 2018b). Saglam et al. (2006) found a decrease in cutting force with an increase in cutting speed when turning hardened steel while Hou et al. (2014) found that the cutting force in milling of Ti-6Al-4V alloy was almost constant upon a certain speed and increased with a further increase in the speed. Şeker et al. (2004) also found a decrease in the cutting force when increasing the speed but an increase in cutting force when increasing the feed rate in the cutting of steel in a linear cutting operation. Mallesha et al. (2018) found cutting speed to be less influential on the cutting force in turning compared to the feed rate, which is in good accordance with Sivaraman et al. (2012). To sum it up, according to the literature and the results of this project had the feed the highest impact on the cutting force, followed by the depth of cut and the cutting speed. To quantify the impact of the depth of cut and the cutting speed in lead-free brass alloys further research is necessary.

A variety of tool geometries was investigated. The rake angle had the highest impact on the cutting force of all geometric parameters varied. With an increase in the rake angle from 0° to 24° the main cutting force was decreased by 22%, 19%, and 35% for CW625N, CW724R, and CW511L, respectively, see Paper III. As described in Paper V, the investigated chip-breaking geometries had little to no effect on the main cutting force. High-pressure cutting fluid supply, as described in Paper V did only have a small influence on the cutting force as well. In the literature, the impact of the tool geometry is discussed further. Zoghipour et al. (2022) describe an increase in the cutting force and tool vibrations in the cutting of brass alloys when the tool edge radius increases. Additionally, an increase in the cutting force was noticed during the tool wear tests. The increase can be attributed to changes in the tool geometry due to the tool wear. Further investigations should take the micro and macro geometry of the tool into consideration.

4.2 Chip breakability

Similar to the cutting force, the chip breakability is influenced by the microstructure and chemical composition of the alloy, the cutting parameters, and the tool geometry.

Many lead-free brass alloys tend to form long and snarled chips while lead-alloyed brasses usually show sufficient chip breakability. J. Johansson, Alm, et al. (2022) explain this by the elongation of the lead globules acting as a crack starter during the chip formation process. Out of the studied lead-free brasses silicon-alloyed CW724R showed the best chip breakability, which can be explained by the hard κ -phase formed due to the presence of silicon. Dual-phase CW510L had shorter chips compared to single-phase CW511L and CW508. The higher amount of β -phase present in CW510L improved the chip breakability of this alloy compared to CW508L and CW511L.

A higher feed usually led to shorter chips. This can be explained by a higher chip thickness, making the chip stiffer. Increased chip stiffness increases chip breakability, as the chip is less deformable and breaks more easily. An increase in the depth of the cut will lead to an increased chip width. Similar to increased chip thickness leads an increased chip width to a stiffer but more breakable chip. During this PhD project, the influence of the cutting speed on the chip formation was not investigated. From comparisons between Paper I and Paper II and III, no conclusion regarding the influence of the cutting speed on the chip breakability could be drawn.

An increased rake angle contributed to increased chip length. A lower rake angle led to higher chip deformation and an earlier chip breakage. To utilize the reduction in the cutting force achieved by increasing the rake angle as discussed above, a chip-breaking geometry or a high-pressure cutting fluid supply is necessary. Groove-shaped chip-breaking geometries were discussed in Paper V and VI.

Two important parameters are the chip-breaker land width and the groove radius. The chip-breaker land width needs to be small enough to restrict the contact length between tool and chip and thereby utilize the groove (Jawahir et al., 1995). In the tests conducted, the tool with a chip breaker land width of $l = 0.7$ mm performed best. According to measurements of the natural tool-chip contact length, at lower feeds, an even smaller chip breaker land width might be beneficial. The groove radius deforms the chip as it flows along its contour. A smaller groove radius will accordingly deform the chip more, while the chip might not follow the contour of the groove if the radius becomes too small. In the tests the tool with the groove radius $r_G = 3.5$ mm performed best. This is mainly attributed to the combination with the chip-breaker land width of 0.7 mm. For further research, a smaller radius is recommended. Additionally, an increased back wall could help chip break. The chip-breaking geometry improved the chip formation macroscopically mainly by a reduction of the chip up-curl radius while the microscopical chip formation was not influenced.

High-pressure cutting fluid supply improved the chip breakability macroscopically while the chips were not influenced by it microscopically similar to the chip-breaking geometries. Already pressure levels of 24 bar were beneficial regarding the chip breakability. Overall, a combination of chip-breaking geometry and high-pressure cutting fluid worked best.

Regarding the ease of implementation, chip-breaking geometries should be favorably implemented in comparison to the high-pressure cutting fluid supply. High-pressure cutting fluid supply might be beneficial when especially small tools are used and the fabrication of chip-breaking geometries is not possible or where the chip evacuation is important, for example in plunge milling (Baier et al., 2022).

4.3 Tool wear

The main source of tool wear noticed in the machining of brass was material adhesions resulting in build-up edges and chipping of the cutting edge. Long tangled chips caused additional tool breakage in cutting CW511L using a high rake angle. This problem might be eliminated by using a chip-breaking geometry to efficiently control the chip breakage and prevent chips from tangling around the tool and workpiece. After 208 min the cutting force measured in cutting CW724R with the 24° tool increased above the level of the cutting force measured with the 0° tool after the same time. This might be explained by the chipping of the cutting edge, visible in the pictures of the cutting edge taken with the scanning electron microscope. The wedge of the 24° tool was smaller, leading to an overall weaker tool. That might have accelerated the tool wear. However, based on these results a direct comparison between the tool wear in CW511L and CW724R is difficult, due to the premature tool breakage of the 24° tool in CW511L. This breakage was most likely caused by chips tangled around the tool.

J. Johansson, Bushlya, et al. (2022) evaluated the impact of tool wear on the subsurface deformation of the machined component in CW724R and CW511L. The work hardening increased with the worn tool, especially for CW511L. Overall, the tool condition had a bigger impact on the work hardening than the feed. On the other hand, a higher work hardening led to increased stress corrosion cracking. Therefore, the monitoring of the tool condition during the manufacturing process is important. Further investigations are necessary to evaluate the tool wear and the impact of the tool geometry on the tool wear.

4.4 Recommendations for the implementation of the results

CW625N alloy contains lead. It is considered low-lead but will most likely be prohibited in the future. Therefore, the use of CW511L or CW724R is more relevant in the future. CW511L and CW724R are both considered dezincification resistant (Seuss et al., 2017; Stålnacke et al., 2020). CW511L consists mainly of pure α -phase. The abrasive tool wear using this alloy is expected to be low, while on the other hand, strong material adhesions to the tool will be present (Klocke et al., 2016). The abrasive κ -phase will lead to high abrasive tool wear when cutting CW724R. Overall higher tool wear is expected when cutting CW724R (Klocke et al., 2016). Cutting of CW724R leads to a decreased cutting force and shorter more favorable chip forms in automated cutting compared to CW511L. The dual-phase brass alloy CW510L contains α and β -phase. This leads to a lower dezincification resistance, lower cutting force, and shorter chips compared to CW511L, while the tool wear is lower than in CW724R and higher than in CW511L (Klocke et al., 2016). However, the decreased dezincification resistance makes CW510L less suitable for application in drinking water supply systems. Here, a tradeoff needs to be made.

While a higher feed and a higher depth of cut improve the chip breakability and lead to a higher material-removal rate they increase the cutting force. Rather than giving one optimal value for feed and depth of cut, these should be varied according to the requirements of the finished product. As usual, first a roughing process with a higher feed and depth of cut should be performed to get the part as close as possible to the desired shape. In the next step, a finishing operation should be performed using a low feed and depth of cut to reach the desired surface quality. For both steps, different tool geometries might be useful. The first step might be best performed using a tool with a highly positive rake angle and a chip-breaking geometry with a slightly longer chip-breaker land width and a small to medium groove radius. The highly positive rake angle will decrease the cutting force and thereby minimize the energy required, while the chip-breaking geometry prevents the formation of long and snarled chips. As the cutting force decreases with a decreasing feed rate a slightly lower positive rake angle might be sufficient for the finishing operation to prevent the formation of long continuous chips. An additional chip-breaking geometry with a shorter chip-breaker land width and a medium to small groove radius might be beneficial as well. The high-pressure cutting fluid supply is an additional option to increase chip breakability. As it requires additional energy to run the high-pressure aggregate and most likely additional equipment, chip-breaking geometries should be preferred.

Chapter 5

Conclusion

The two main challenges regarding the machinability addressed in this thesis were the increased cutting force and the lower chip breakability of low-lad and lead-free brass alloys. The focus was put on the alloys CW625N, CW511L, and CW724R, but CW510L and CW508L were investigated in a part of the project. Emphasis was placed on the chip breakability of CW511L.

The different alloys exhibited different mechanical and microstructural properties. CW625N is a low-lead brass alloy. The cutting force was overall the lowest of all tested alloys, and the chip breakability was acceptable, especially at high feeds, depth of cut, and lower rake angles. However, due to further legislative restrictions, this alloy might not be allowed for use in drinking water applications in the future. Lead-free silicon-alloyed CW724R exhibits the lowest cutting force and the best chip breakability of the lead-free alloys investigated. It is known to be dezincification resistant, which makes it suitable as a material used in direct contact with drinking water (Seuss et al., 2017). However, considerably higher abrasive tool wear is expected due to the hard and abrasive κ -phase present in the alloy (Bushlya et al., 2017; Klocke et al., 2016). Increased rake angles lead to a lower cutting force, while the chip breakability was acceptable regardless of the rake angles.

Lead-free CW511L consists almost purely of ductile α -phase. The alloy is considered dezincification resistant (Stålnacke et al., 2020), and therefore suitable for drinking water-bearing applications. CW511L exhibits a higher cutting force and worse chip breakability in comparison to CW724R and CW625N. An increase in the rake angle led to a lower cutting force, but chip breakability decreased even further. Chip-breaking geometries and high-pressure cooling fluid supply were investigated to counteract the increased chip lengths while not changing the cutting force. As many tools are custom-made for companies producing couplings, specialized chip-breaking geometries are an easily implementable measure. In tests with different chip-breaking geometries, a geometry with a chip-breaker land width of 0.7 mm and a groove radius of 3.5 mm was the most beneficial for the tested cutting parameters. The chip-breaking geometry should, however, always be adapted to the applied cutting parameters. High-pressure cutting fluid supply also increased the chip breakability from pressures of $p = 24$ bar and above. The

application of a high-pressure cutting fluid supply requires additional equipment and energy. Therefore, custom-made tools with adapted chip-breaking geometries should be preferred over a high-pressure cutting fluid supply. Both methods, however, influenced the chip macroscopically by changing the chip length and chip up-curl radii. The chip formation mechanism and chip microstructural features remained almost unchanged.

CW510L and CW508L were investigated in one study regarding the influence of high-pressure cutting fluid supply on chip breakability. CW508L consists of an almost pure α -phase similar to CW511L. It showed comparable behavior during the tests while the cutting force was elevated. CW510L consists almost equally of α - and β -phase. This led to better chip breakability and a slightly lower cutting force compared to CW508L. However, the β -phase is prone to dezincification. Therefore, CW510L might be less suitable for drinking water applications than CW511L and CW508L.

Cutting parameters should be selected carefully. Higher feeds and depths of cut will increase the material removal rate and the chip breakability leading to a faster and most likely more stable process. On the other hand, higher feeds and depths of cut will increase the cutting force. Therefore the energy requirement and the requirements for the machine tool will increase. Here, a tradeoff needs to be made. For a roughing process, a highly positive rake angle, a chip-breaking geometry, high feeds, and a high depth of cut should be considered. For finishing processes, lower feeds, depth of cut, rake angles, and an adapted chip-breaking geometry will probably lead to the best results. The tool wear needs to be investigated further. Here, probably industrial-scale tests would be best to perform.

In summary, various lead-free brass alloys and methods to improve their machinability have been tested. To successfully machine the new lead-free brass alloys, the methods used today for machining leaded brass alloys must be adapted. Increased rake angles are a simple way to reduce the cutting force. Chip-breaking geometries should be used to improve chip breakability. Each set of cutting parameters may require individual chip breaker geometry features.

Chapter 6

Suggestions for further Work

This thesis mainly addressed the cutting force and the chip breakability of a selection of lead-free brass alloys.

The tool wear of the adapted tool geometries was not investigated in depth. An increased rake angle leads to a smaller wedge angle and a weaker cutting edge. This impacts the tool life negatively. In comparisons between a tool with a rake angle of 24° and 0° the tool with the higher rake angle showed more chipping when cutting CW724R. After 208 min this tool showed even higher cutting force than the 0° tool after machining for the same time. Unfortunately, in the same tests for CW511L, the 24° tool showed a premature breakage due to chips tangled around it. This made further comparisons regarding the tool wear almost impossible. More research, especially regarding the adapted geometries is necessary. Since such investigations are time and material-consuming, it would be best to conduct these at a production site by evaluating a tool with an adapted geometry in defined time intervals.

This thesis focused on cemented carbide as a tool material, as it is currently primarily used in the machining of leaded brass alloys. An AlTiN-based tool coating was briefly investigated regarding its influence on cutting force and chip breakability, but knowledge regarding tool life is lacking. Due to various mechanical and chemical properties, different tool materials and coatings might impact the cutting force, the chip breakability, and the tool life. Further research is needed.

Different rake angles and chip-breaking geometries have been investigated in this thesis. Further investigations regarding the optimal combination of a chip groove radius and chip breaker land width for different sets of cutting parameters are necessary. A variation of the back wall height could help increase the chip breakability.

Companies manufacturing couplings for drinking water supply often use custom-made profile and step drills. In this thesis, only radial turning processes were investigated. It should be examined to what extent these results are transferable to profile and step drills.

Simulations could be advantageous to save time and material when examining new tool geometries. On the other hand, little research was done regarding the

simulation of the machining of lead-free brass alloys. Parameters for each alloy need to be found to model the material.

The machining process and, primarily, the tool geometry will impact the surface and subsurface features of the brass. The surface roughness is influenced by the tool geometry and the machining parameters. Residual stresses might impact the component's corrosion resistance as brass alloys are prone to stress corrosion cracking. The relations between tool geometry, machining parameters, and surface and subsurface properties should be investigated.

New lead-free brass alloys might be developed. An adapted microstructure might positively influence machinability. The microstructure can be influenced by extrusion or heat treatment. New chemical compositions can be investigated, as well as the addition of hard or soft particles to act as a chip breaker and improve machinability. The development of new alloys was out of scope for this thesis but might be an influential variable to investigate in the future.

Bibliography

- Adineh, M., Doostmohammadi, H., & Raiszadeh, R. (2019). Effect of SI and AL on the Microstructure, Mechanical Properties and Machinability of 65CU-35ZN Brass. *Iranian Journal of Materials Science and Engineering*, 16(2), 21–32. <https://doi.org/10.22068/IJMSE.16.2.21> (cit. on p. 5)
- Albrecht, P. (1960). New Developments in the Theory of the Metal-Cutting Process: Part I. The Ploughing Process in Metal Cutting. *Journal of Engineering for Industry*, 82(4), 348–357. <https://doi.org/10.1115/1.3664242> (cit. on p. 10)
- Amaral, L., Quinta, R., Silva, T. E., Soares, R. M., Castellanos, S. D., & de Jesus, A. M. (2018). Effect of lead on the machinability of brass alloys using polycrystalline diamond cutting tools. *The Journal of Strain Analysis for Engineering Design*, 53(8), 602–615. <https://doi.org/10.1177/0309324718796384> (cit. on pp. 6, 12)
- Andersson, M., & Ståhl, J.-E. (2007). POLAR MACHINABILITY DIAGRAMS- A MODEL TO PREDICT THE MACHINABILITY OF A WORK MATERIAL. *Proceedings of the 1st International Swedish Production Symposium 2007, 28-30 Augusti, Gothenburg, Sweden*. <https://portal.research.lu.se/en/publications/polar-machinability-diagrams-a-model-to-predict-the-machinability> (cit. on p. 9)
- Atsumi, H., Imai, H., Li, S., Kondoh, K., Kousaka, Y., & Kojima, A. (2011). High-strength, lead-free machinable α - β duplex phase brass Cu-40Zn-Cr-Fe-Sn-Bi alloys. *Materials Science and Engineering: A*, 529(1), 275–281. <https://doi.org/10.1016/j.msea.2011.09.029> (cit. on p. 4)
- Baier, S., Brans, K., Schraknepper, D., & Bergs, T. (2022). Experimental optimization of tool geometry and lubricoolant supply in plunge milling of lead-free Brass. *Copper Alloys 2022*, 4–7. https://kupfer.de/wp-content/uploads/2022/11/Proceedings-Copper-Alloys-2022_.pdf (cit. on p. 48)
- Boothroyd, G., & Knight, W. A. (1988). *Fundamentals of Machining and Machine Tools* (G. Boothroyd & W. A. Knight, Eds.; Second Edition, Vol. 28). mdi Dekker. (Cit. on pp. 10, 11).
- Braham-Bouchnak, T., Germain, G., Morel, A., & Furet, B. (2015). Influence of High-Pressure Coolant Assistance on the Machinability of the Titanium Alloy Ti555-3. *Machining Science and Technology*, 19(1), 134–151. <https://doi.org/10.1080/10910344.2014.991029> (cit. on p. 13)

- Brandl, E., Malke, R., Beck, T., Wanner, A., & Hack, T. (2009). Stress corrosion cracking and selective corrosion of copper-zinc alloys for the drinking water installation. *Materials and Corrosion*, 60(4), 251–258. <https://doi.org/10.1002/maco.200805079> (cit. on p. 7)
- Bushlya, V., Johansson, D., Lenrick, F., Ståhl, J. E., & Schultheiss, F. (2017). Wear mechanisms of uncoated and coated cemented carbide tools in machining lead-free silicon brass. *Wear*, 376-377, 143–151. <https://doi.org/10.1016/J.WEAR.2017.01.039> (cit. on pp. 7, 13, 14, 20, 51)
- Byrne, G., Dornfeld, D., & Denkena, B. (2003). Advancing Cutting Technology. *CIRP Annals*, 52(2), 483–507. [https://doi.org/10.1016/S0007-8506\(07\)60200-5](https://doi.org/10.1016/S0007-8506(07)60200-5) (cit. on p. 12)
- Chunlei, G., Kaihong, Z., Haiyan, W., & Nan, Z. (2016). Effect of magnesium content on machinability of Cu-Zn-Bi-Sb alloy. *Materials Science Forum*, 850, 544–548. <https://doi.org/10.4028/www.scientific.net/MSF.850.544> (cit. on p. 4)
- Courbon, C., Kramar, D., Krajnik, P., Pusavec, F., Rech, J., & Kopac, J. (2009). Investigation of machining performance in high-pressure jet assisted turning of Inconel 718: An experimental study. *International Journal of Machine Tools and Manufacture*, 49(14), 1114–1125. <https://doi.org/10.1016/j.ijmachtools.2009.07.010> (cit. on p. 13)
- Crafoord, R., Kaminski, J., Lagerberg, S., Ljungkrona, O., & Wretland, A. (1999). Chip control in tube turning using a high-pressure water jet. *Proceedings of the Institution of Mechanical Engineers, Part B: Journal of Engineering Manufacture*, 213(8), 761–767. <https://doi.org/10.1243/0954405991517191> (cit. on p. 13)
- Davis, J. R., & ASM International Handbook Committee. (2001). *ASM Specialty Handbook @ Copper and Copper Alloys* (J. R. Davis & prepared under the direction of the ASM International Handbook Committee, Eds.; VII). ASM International. (Cit. on pp. 2, 8–10, 19–21).
- Deutsches Kupferinstitut. (2019). *Kupfer-die beste Wahl* (tech. rep.). Deutsches Kupfer Institut. Düsseldorf. https://kupfer.de/wp-content/uploads/2019/06/Kupfer_die_beste_Wahl_final.pdf. (Cit. on p. 2)
- Deutsches Kupferinstitut. (2020). *The effects of using bismuth as lead replacement* (tech. rep.). Deutsches Kupferinstitut. Düsseldorf. https://kupfer.de/wp-content/uploads/2020/04/Factsheet_Bismut-als-Bleiersatz_English.pdf. (Cit. on p. 4)
- Duan, C., & Zhang, L. (2013). A reliable method for predicting serrated chip formation in high-speed cutting: analysis and experimental verification. *The International Journal of Advanced Manufacturing Technology*, 64(9-12), 1587–1597. <https://doi.org/10.1007/s00170-012-4125-0> (cit. on pp. 11, 13)
- Estelle, A. A. (2016). Drinking water lead regulations: impact on the brass value chain. *Materials Science and Technology*, 32(17), 1763–1770. <https://doi.org/10.1080/02670836.2016.1220906> (cit. on pp. 1, 2)

- European Parliament and Council of the European Union. (2006). REGULATION (EC) No 1907/2006 OF THE EUROPEAN PARLIAMENT AND OF THE COUNCIL of 18 December 2006 concerning the Registration, Evaluation and Restriction of Chemicals (REACH). <https://eur-lex.europa.eu/legal-content/EN/TXT/?uri=OJ:L:2006:396:TOC>. (Cit. on pp. 1, 2)
- European Standard. (2016). EN12163 - Copper and copper alloys - Rod for general purposes. (Cit. on p. 26).
- García, P., Rivera, S., Palacios, M., & Belzunce, J. (2010). Comparative study of the parameters influencing the machinability of leaded brasses. *Engineering Failure Analysis*, 17(4), 771–776. <https://doi.org/10.1016/J.ENGFAILANAL.2009.08.012> (cit. on p. 5)
- Groover, M. P. (2017). *Groover's principles of modern manufacturing : materials, processes, and systems* (6th edition, Vol. SI version). John Wiley & Sons. (Cit. on pp. 10, 11).
- Hilbrans, H. (2013). Nichteisenmetalle. In H.-J. Bargel & G. Schulze (Eds.), *Werkstoffkunde* (11th ed., pp. 309–355). Springer. https://doi.org/10.1007/978-3-642-17717-0_5. (Cit. on pp. 1, 6)
- Hou, J., Zhou, W., Duan, H., Yang, G., Xu, H., & Zhao, N. (2014). Influence of cutting speed on cutting force, flank temperature, and tool wear in end milling of Ti-6Al-4V alloy. *The International Journal of Advanced Manufacturing Technology*, 70(9-12), 1835–1845. <https://doi.org/10.1007/s00170-013-5433-8> (cit. on p. 47)
- Iecks, G., Aram Maiolo, L. M., Bortolozzo, A. D., & Osório, W. R. (2018). Designing a microstructural array associated with hardness of dual-phase Cu-Zn alloy using investment casting. *Materials Research*, 21(4). <https://doi.org/10.1590/1980-5373-MR-2017-1059> (cit. on p. 8)
- Jawahir, I. S., & Fang, X. D. (1995). A knowledge-based approach for designing effective grooved chip breakers ? 2D and 3D chip flow, chip curl and chip breaking. *The International Journal of Advanced Manufacturing Technology*, 10(4), 225–239. <https://doi.org/10.1007/BF01186875> (cit. on pp. 11, 48)
- Johansson, J., Persson, H., Ståhl, J. E., Zhou, J. M., Bushlya, V., & Schultheiss, F. (2019). Machinability Evaluation of Low-Lead Brass Alloys. *Procedia Manufacturing*, 38, 1723–1730. <https://doi.org/10.1016/J.PROMFG.2020.01.102> (cit. on pp. 9, 10)
- Johansson, J., Alm, P., M'Saoubi, R., Malmberg, P., Ståhl, J.-E., & Bushlya, V. (2022). On the function of lead (Pb) in machining brass alloys. *The International Journal of Advanced Manufacturing Technology*. <https://doi.org/10.1007/s00170-022-09205-0> (cit. on pp. 2, 6, 13, 46, 47)
- Johansson, J., Bushlya, V., Obitz, C., M'Saoubi, R., Hagström, J., & Lenrick, F. (2022). Influence of sub-surface deformation induced by machining on stress corrosion cracking in lead-free brass. *The International Journal of Advanced Manufacturing Technology*, 122(7-8), 3171–3181. <https://doi.org/10.1007/s00170-022-10081-x> (cit. on p. 49)

- Klocke, F., Sangermann, H., Krämer, A., & Lung, D. (2011). Influence of a High-Pressure Lubricoolant Supply on Thermo-Mechanical Tool Load and Tool Wear Behaviour in the Turning of Aerospace Materials. *Proceedings of the Institution of Mechanical Engineers, Part B: Journal of Engineering Manufacture*, 225(1), 52–61. <https://doi.org/10.1177/09544054JEM2082> (cit. on p. 13)
- Klocke, F., Lung, D., & Nobel, C. (2012). Ansätze zur Hochleistungserspannung bleifreier Kupferwerkstoffe. https://www.kupferinstitut.de/wp-content/uploads/2020/01/496_KS_Nobel_2012.pdf. (Cit. on p. 13)
- Klocke, F. (2018a). Kühlschmierstoffe (KSS). *Fertigungsverfahren 1* (9th ed., pp. 251–279). Springer Vieweg. https://doi.org/10.1007/978-3-662-54207-1_6. (Cit. on pp. 12, 13)
- Klocke, F. (2018b). Standvermögen. *Fertigungsverfahren 1* (9th ed., pp. 281–405). Springer Vieweg, Berlin, Heidelberg. https://doi.org/10.1007/978-3-662-54207-1_7. (Cit. on p. 9)
- Klocke, F., Nobel, C., & Veselovac, D. (2016). Influence of Tool Coating, Tool Material, and Cutting Speed on the Machinability of Low-Leaded Brass Alloys in Turning. *Materials and Manufacturing Processes*, 31(14), 1895–1903. <https://doi.org/10.1080/10426914.2015.1127944> (cit. on pp. 3, 7, 10, 12, 49, 51)
- Kossiakoff, A., Seymour, S. J., Flanigan, D. A., & Biemer, S. M. (2020). DECISION ANALYSIS AND SUPPORT. *Systems engineering principles and practice* (pp. 275–325). Wiley. <https://doi.org/10.1002/9781119516699.ch11>. (Cit. on p. 45)
- Kozana, J., Garbacz-Klempka, A., & Piękoś, M. (2019). Lead-free casting brasses. Investigations of the corrosion resistance and shaping of microstructure and properties. *Archives of Foundry Engineering*, 19(2), 113–118. <https://doi.org/10.24425/afe.2019.127126> (cit. on p. 8)
- Kuyucak, S., & Sahoo, M. (1996). A review of the machinability of copper-base alloys. *Canadian Metallurgical Quarterly*, 35(1), 1–15. [https://doi.org/10.1016/0008-4433\(95\)00023-2](https://doi.org/10.1016/0008-4433(95)00023-2) (cit. on p. 10)
- Laakso, S. V., Hokka, M., Niemi, E., & Kuokkala, V.-T. (2013). Investigation of the effect of different cutting parameters on chip formation of low-lead brass with experiments and simulations. *Proceedings of the Institution of Mechanical Engineers, Part B: Journal of Engineering Manufacture*, 227(11), 1620–1634. <https://doi.org/10.1177/0954405413492732> (cit. on pp. 8, 9)
- Machado, A. R., & Wallbank, J. (1994). The Effects of a High-Pressure Coolant Jet on Machining. *Proceedings of the Institution of Mechanical Engineers, Part B: Journal of Engineering Manufacture*, 208(1), 29–38. https://doi.org/10.1243/PIME_PROC_1994_208_057_02 (cit. on p. 13)

- Mallesha, V., & Shivananda Nayaka, H. (2018). Investigation of machinability characteristics on EN47 steel for cutting force and tool wear using optimization technique. *Materials Research Express*, 5(6), 066501. <https://doi.org/10.1088/2053-1591/aac67f> (cit. on p. 47)
- Merchant, M. E. (1945). Mechanics of the Metal Cutting Process. II. Plasticity Conditions in Orthogonal Cutting. *Journal of Applied Physics*, 16(6), 318–324. <https://doi.org/10.1063/1.1707596> (cit. on p. 10)
- Mills, B., & Redford, A. H. (1983). *Machinability of Engineering Materials* (1st ed.). Springer Netherlands. <https://doi.org/10.1007/978-94-009-6631-4>. (Cit. on pp. 9, 10)
- Moriarty, M., Wu, Y., Murray, T., & Hutchinson, C. (2021). The effect of phase fraction, size and shape on the dezincification of duplex brasses. *Corrosion Science*, 184, 109366. <https://doi.org/10.1016/j.corsci.2021.109366> (cit. on pp. 20, 21)
- Müller, M. S., & Sørby, K. (2022). Cutting Forces in Machining of Low-Lead and Lead-Free Brass Alloys. In Y. Wang, K. Martinsen, T. Yu, & K. Wang (Eds.), *Advanced manufacturing and automation xi. iwama 2021. lecture notes in electrical engineering* (pp. 254–261). Springer, Singapore. https://doi.org/10.1007/978-981-19-0572-8_32. (Cit. on pp. 17, 45, 46, 65)
- Müller, M. S., & Sørby, K. (2023a). Investigation on chip breakability in lead-free brass alloy CW511L using different chip breaking geometries. *Intelligent Computation in Manufacturing Engineering-CIRP ICME'23 (in press) Procedia CIRP* (cit. on pp. 18, 113).
- Müller, M. S., & Sørby, K. (2023b). The Influence of the Rake Angle on the Cutting of Low-Lead and Lead-Free Brass Alloys. In H. Kohl, G. Seliger, & F. Dietrich (Eds.), *Manufacturing driving circular economy. proceedings of the 18th global conference on sustainable manufacturing, october 5-7, 2022, berlin. lecture notes in mechanical engineering* (pp. 219–227). Springer, Cham. https://doi.org/10.1007/978-3-031-28839-5_25. (Cit. on pp. 17, 81)
- Müller, M. S., Tomovic Petrovic, S., & Sørby, K. (2022). Investigation of heat treatment to improve the machinability of lead-free brass alloy CW511L. *Copper Alloys 2022*, 42–45. <https://kupfer.de/wp-content/uploads/2022/12/Proceedings-Copper-Alloys-2022-2.pdf> (cit. on pp. 17, 46, 75)
- Müller, M. S., Brans, K., Meurer, M., Sørby, K., & Bergs, T. (2023). The effect of high-pressure cutting fluid supply on the chip breakability of lead-free brass alloys. *The International Journal of Advanced Manufacturing Technology*. <https://doi.org/10.1007/s00170-023-12440-8> (cit. on pp. 18, 46, 93)
- Müller, M. S., & Sørby, K. (2023c). The Effect of Tool Geometry on Chip Formation and Chip Morphology of Lead-Free Brass Alloy CW511L. *Submitted to: Advances in Manufacturing*. <https://doi.org/https://doi.org/10.21203/rs.3.rs-3423897/v1> (cit. on pp. 18, 121)
- Needleman, H. (2004). Lead Poisoning. *Annual Review of Medicine*, 55(1), 209–222. <https://doi.org/10.1146/annurev.med.55.091902.103653> (cit. on p. 2)

- Nobel, C., Hofmann, U., Klocke, F., & Veselovac, D. (2015). Experimental investigation of chip formation, flow, and breakage in free orthogonal cutting of copper-zinc alloys. *The International Journal of Advanced Manufacturing Technology*, 84(5), 1127–1140. <https://doi.org/10.1007/s00170-015-7749-z> (cit. on pp. 11–13, 20)
- Nobel, C., Hofmann, U., Klocke, F., Veselovac, D., & Puls, H. (2015). Application of a new, severe-condition friction test method to understand the machining characteristics of Cu–Zn alloys using coated cutting tools. *Wear*, 344-345, 58–68. <https://doi.org/10.1016/j.wear.2015.10.016> (cit. on p. 12)
- Nobel, C., Klocke, F., Lung, D., & Wolf, S. (2014a). Machinability Enhancement of Lead-free Brass Alloys. *Procedia CIRP*, 14, 95–100. <https://doi.org/10.1016/j.procir.2014.03.018> (cit. on pp. 2, 6, 7, 13)
- Nobel, C., Klocke, F., Lung, D., & Wolf, S. (2014b). Machinability Enhancement of Lead-free Brass Alloys. *Procedia CIRP*, 14, 95–100. <https://doi.org/10.1016/j.procir.2014.03.018> (cit. on pp. 3, 46)
- Nordic Brass Gusum AB. (2019). Rod CW625N. <https://www.nordicbrass.se/en/products/rod-cw625n>. (Cit. on p. 26)
- Pantazopoulos, G., & Vazdirvanidis, A. (2008). Characterization of the Microstructural Aspects of Machinable a-b Phase Brass. *Microscopy and Analysis*, 22(5), 13–16. <https://analyticalscience.wiley.com/doi/10.1002/micro.469/full/ic931eac859ccf20ea30cd4a63fe6bd8f.pdf> (cit. on p. 8)
- Puathawee, S., Rojananan, S., & Rojananan, S. (2013). Lead-free Cu-Si-Zn brass with tin addition. *Advanced Materials Research*, 802, 169–173. <https://doi.org/10.4028/www.scientific.net/AMR.802.169> (cit. on p. 6)
- Puls, H., Klocke, F., & Lung, D. (2012). A new experimental methodology to analyse the friction behaviour at the tool-chip interface in metal cutting. *Production Engineering*, 6(4-5), 349–354. <https://doi.org/10.1007/s11740-012-0386-6> (cit. on p. 13)
- Pusavec, F., Kramar, D., Krajnik, P., & Kopac, J. (2010). Transitioning to sustainable production - Part II: Evaluation of sustainable machining technologies. *Journal of Cleaner Production*, 18(12), 1211–1221. <https://doi.org/10.1016/j.jclepro.2010.01.015> (cit. on pp. 12, 13)
- Rajabi, Z., & Doostmohammadi, H. (2018). Effect of addition of tin on the microstructure and machinability of α -brass. *Materials Science and Technology*, 34(10), 1218–1227. <https://doi.org/10.1080/02670836.2018.1435484> (cit. on p. 5)
- Reddy, V. V., Krishna, A. V., Schultheiss, F., & Rosén, B. G. (2017). Surface topography characterization of brass alloys: Lead brass (CuZn39Pb3) and lead free brass (CuZn21Si3P). *Surface Topography: Metrology and Properties*, 5(2), 000000. <https://doi.org/10.1088/2051-672X/aa612b> (cit. on p. 7)
- Reetz, B. (2006). *Mikrostruktur und Eigenschaften stranggepresster sowie kaltverformter Messinglegierungen* (Doctoral dissertation). TU Berlin. Berlin. <https://doi.org/https://doi.org/10.14279/depositonce-1430>. (Cit. on p. 8)

- Reetz, B., & Reimers, W. (2008). Hot extrusion of α and α/β -brass alloys. *International Journal of Materials Research*, 99(7), 787–794. <https://doi.org/10.3139/146.101694> (cit. on p. 8)
- Saglam, H., Unsacar, F., & Yaldiz, S. (2006). Investigation of the effect of rake angle and approaching angle on main cutting force and tool tip temperature. *International Journal of Machine Tools and Manufacture*, 46(2), 132–141. <https://doi.org/10.1016/J.IJMACHTOOLS.2005.05.002> (cit. on pp. 11, 13, 47)
- Schultheiss, F., Lundström, E., Johansson, D., Bushlya, V., Zhou, J., Nilsson, K., & Ståhl, J. (2014). Machinability of Lead-Free Brass – A comparative study. *The 6th Swedish Production Symposium*. <http://conferences.chalmers.se/index.php/SPS/SPS14/paper/view/1697.html> (cit. on p. 3)
- Schultheiss, F., Johansson, D., Linde, M., Tam, P. L., Bushlya, V., Zhou, J., Nyborg, L., & Ståhl, J. E. (2016). Machinability of CuZn21Si3P brass. *Materials Science and Technology (United Kingdom)*, 32(17), 1744–1750. <https://doi.org/10.1080/02670836.2016.1189199> (cit. on pp. 7, 46)
- Schultheiss, F., Lundström, E., Johansson, D., Bushlya, V., Zhou, J., Nilsson, K., & Ståhl, J.-E. (2014). MACHINABILITY OF LEAD-FREE BRASS-A COMPARATIVE STUDY. <https://doi.org/10.1.1.982.4730> (cit. on p. 7)
- Schultheiss, F., Johansson, D., Bushlya, V., Zhou, J., Nilsson, K., & Ståhl, J. E. (2017). Comparative study on the machinability of lead-free brass. *Journal of Cleaner Production*, 149, 366–377. <https://doi.org/10.1016/j.jclepro.2017.02.098> (cit. on pp. 2, 3, 7, 12)
- Schultheiss, F., Windmark, C., Sjöstrand, S., Rasmusson, M., & Ståhl, J.-E. (2018). Machinability and manufacturing cost in low-lead brass. *The International Journal of Advanced Manufacturing Technology*, 99(9-12), 2101–2110. <https://doi.org/10.1007/s00170-018-1866-4> (cit. on pp. 1, 3, 7, 14)
- Şeker, U., Kurt, A., & Çiftçi, I. (2004). The effect of feed rate on the cutting forces when machining with linear motion. *Journal of Materials Processing Technology*, 146(3), 403–407. <https://doi.org/10.1016/j.jmatprotec.2003.12.001> (cit. on p. 47)
- Seuss, F., Gaag, N., & Virtanen, S. (2017). Corrosion mechanism of CuZn21Si3P in aggressive tap water. *Materials and Corrosion*, 68(1), 42–49. <https://doi.org/10.1002/maco.201609018> (cit. on pp. 7, 49, 51)
- Sharma, V. S., Dogra, M., & Suri, N. (2009). Cooling techniques for improved productivity in turning. *International Journal of Machine Tools and Manufacture*, 49(6), 435–453. <https://doi.org/10.1016/j.ijmachtools.2008.12.010> (cit. on p. 13)
- Sharman, A. R., Hughes, J. I., & Ridgway, K. (2008). Surface integrity and tool life when turning Inconel 718 using ultra-high pressure and flood coolant systems. *Proceedings of the Institution of Mechanical Engineers, Part B: Journal of Engineering Manufacture*, 222(6), 653–664. <https://doi.org/10.1243/09544054JEM936> (cit. on p. 13)

- Sivaraman, V., Sankaran, S., & Vijayaraghavan, L. (2012). The Effect of Cutting Parameters on Cutting Force During Turning Multiphase Microalloyed Steel. *Procedia CIRP*, 4, 157–160. <https://doi.org/10.1016/j.procir.2012.10.028> (cit. on p. 47)
- Sørby, K., & Tønnessen, K. (2006). High-pressure cooling of face-grooving operations in Ti6Al4V. *Proceedings of the Institution of Mechanical Engineers, Part B: Journal of Engineering Manufacture*, 220(10), 1621–1627. <https://doi.org/10.1243/09544054JEM474> (cit. on p. 13)
- Stålnacke, E., Claesson, E., Obitz, C., Lilja, M., Odqvist, J., Hagström, J., & Rod, O. (2020). Corrosion–microstructure interrelations in new low-lead and lead-free brass alloys. *Materials Science and Technology*, 36(8), 917–924. <https://doi.org/10.1080/02670836.2018.1489619> (cit. on pp. 7, 19, 49, 51)
- Suksongkarm, P., Rojananan, S., & Rojananan, S. (2017). Using Recycled Bismuth-Tin Solder in Novel Machinable Lead-Free Brass. *MATERIALS TRANSACTIONS*, 58(12), 1754–1760. <https://doi.org/10.2320/matertrans.M2017227> (cit. on pp. 2, 4)
- Suksongkarm, P., Rojananan, S., & Rojananan, S. (2018). Bismuth Formation in Lead-Free Cu–Zn–Si Yellow Brass with Various Bismuth–Tin Alloy Additions. *MATERIALS TRANSACTIONS*, 59(11), 1747–1752. <https://doi.org/10.2320/matertrans.M2018081> (cit. on p. 2)
- Taha, M. A., El-Mahallawy, N. A., Hammouda, R. M., Moussa, T. M., & Gheith, M. H. (2012). Machinability characteristics of lead free-silicon brass alloys as correlated with microstructure and mechanical properties. *Ain Shams Engineering Journal*, 3(4), 383–392. <https://doi.org/10.1016/J.ASEJ.2012.05.004> (cit. on pp. 2, 4–6, 13, 14)
- Tomovic Petrovic, S., Gulbrandsen-Dahl, S., & Wenner, S. (2022). Corrosion susceptibility of the CuZn35Pb1,5AlAs (CW625N) brass alloy in various environments. *Copper Alloys 2022 - Conference Proceedings*, 52–55. <https://kupfer.de/wp-content/uploads/2022/12/Proceedings-Copper-Alloys-2022-2.pdf> (cit. on p. 14)
- Toufatzis, A. I., Besseris, G. J., Pantazopoulos, G. A., & Stergiou, C. (2011). Characterization and comparative machinability investigation of extruded and drawn copper alloys using non-parametric multi-response optimization and orthogonal arrays. *The International Journal of Advanced Manufacturing Technology*, 57(5-8), 811–826. <https://doi.org/10.1007/s00170-011-3319-1> (cit. on pp. 6, 7)
- Toufatzis, A. I., Pantazopoulos, G. A., & Paipetis, A. S. (2016). Microstructure and properties of lead-free brasses using post-processing heat treatment cycles. *Materials Science and Technology (United Kingdom)*, 32(17), 1771–1781. <https://doi.org/10.1080/02670836.2016.1221493> (cit. on pp. 8, 20, 21)

- Toufatzis, A. I., Pantazopoulos, G., David, C., Sagris, D., & Paipetis, A. (2018a). Final Heat Treatment as a Possible Solution for the Improvement of Machinability of Pb-Free Brass Alloys. *Metals*, 8(8), 575. <https://doi.org/10.3390/met8080575> (cit. on pp. 3, 4, 8, 20, 21)
- Toufatzis, A. I., Pantazopoulos, G., David, C., Sagris, D., & Paipetis, A. (2018b). Machinability of Eco-Friendly Lead-Free Brass Alloys: Cutting-Force and Surface-Roughness Optimization. *Metals*, 8(4), 250. <https://doi.org/10.3390/met8040250> (cit. on pp. 3, 46, 47)
- United Nations. (2015). THE 17 GOALS | Sustainable Development. <https://sdgs.un.org/goals>. (Cit. on p. 1)
- U.S. Geological Survey. (2023). *Mineral commodity summaries 2023* (tech. rep.). U.S. Geological Survey. <https://doi.org/10.3133/mcs2023>. (Cit. on p. 2)
- Vilarinho, C., Davim, J. P., Soares, D., Castro, F., & Barbosa, J. (2005). Influence of the chemical composition on the machinability of brasses. *Journal of Materials Processing Technology*, 170(1-2), 441–447. <https://doi.org/10.1016/J.JMATPROTEC.2005.05.035> (cit. on p. 6)
- Wegener, K., Kuster, F., Weikert, S., Weiss, L., & Stirnimann, J. (2016). Success Story Cutting. *Procedia CIRP*, 46, 512–524. <https://doi.org/10.1016/j.procir.2016.04.110> (cit. on p. 12)
- Weißbach, W. (2012). Nichteisenmetalle. *Werkstoffkunde* (18th ed., pp. 191–227). Vieweg+Teubner Verlag. https://doi.org/10.1007/978-3-8348-8318-6_7. (Cit. on p. 1)
- West, E. G. (1982). *Copper and its alloys*. Ellis Horwood. (Cit. on p. 5).
- Zachert, C., Brans, K., Scharknepper, D., & Bergs, T. (2022). Assessment and Comparison of the Machinability of Innovative Copper Alloys. *Copper Alloys 2022*, 56–59. <https://kupfer.de/wp-content/uploads/2022/12/Proceedings-Copper-Alloys-2022-2.pdf> (cit. on p. 9)
- Zhang, X., Ma, C., Li, S., Pan, D., & Zheng, F. (2020). Interface design of lead-free free-cutting titanium reinforced graphite brass composites and its effect on mechanical properties and cutting performance. *Materials Science and Engineering: A*, 774, 138909. <https://doi.org/10.1016/j.msea.2020.138909> (cit. on p. 13)
- Zoghipour, N., Tascioglu, E., Celik, F., & Kaynak, Y. (2022). The influence of edge radius and lead content on machining performance of brass alloys. *Procedia CIRP*, 112, 274–279. <https://doi.org/10.1016/j.procir.2022.09.084> (cit. on pp. 12, 47)

Paper I

Müller, M. S., & Sørby, K. (2022). Cutting Forces in Machining of Low-Lead and Lead-Free Brass Alloys. In Y. Wang, K. Martinsen, T. Yu, & K. Wang (Eds.), *Advanced manufacturing and automation xi. iwama 2021. lecture notes in electrical engineering* (pp. 254–261). Springer, Singapore. https://doi.org/10.1007/978-981-19-0572-8_32

This paper was presented at the 11th International Workshop of Advanced Manufacturing and Automation (IWAMA2021) in Henan, China. Due to the ongoing COVID19-pandemic, it was held online.

Knowledge of cutting forces and the influence of the tool geometry on lead-free brass is necessary due to the increasing restrictions on the use of lead. Today, research on the cutting of lead-free brass has mainly focused on comparing different cutting conditions and different alloys. This study aims to explain the differences in cutting forces using the orthogonal cutting model and Merchant equation. A turning method aiming for cutting conditions as close as possible to the orthogonal cutting model was used in the tests. In summary, the findings in this study suggest that the Merchant equation is not applicable in the cutting of brass, even though the cutting force decreased when increasing the rake angle. Measurements of the chip thickness give a good indication of the size of the shear plane angle.

This paper is not included in NTNU Open due to copyright restrictions

Paper II

Müller, M. S., Tomovic Petrovic, S., & Sørby, K. (2022). Investigation of heat treatment to improve the machinability of lead-free brass alloy CW511L. *Copper Alloys 2022*, 42–45. <https://kupfer.de/wp-content/uploads/2022/12/Proceedings-Copper-Alloys-2022-2.pdf>

This article was presented at Copper Alloys 2022 in Dusseldorf, Germany.

The machinability of brass is important in the manufacturing of couplings for drinking water supply systems. The reduction or elimination of lead in brass alloys affects both the cutting forces and the chip formation. Lead-free brasses that consist only of α -phase tend to form snarled and unbroken chips and show increased cutting forces. There are studies showing that the machinability of single α -phase alloys could be improved by modification of the microstructure by means of heat treatment conducted prior to machining, aiming to induce a certain amount of β -phase. In this study, lead-free CW511L alloy was heat treated and water quenched to induce β -phase prior to machining. Subsequent heat treatment with slow cooling was applied to change the microstructure back to α -phase.

Investigation of heat treatment to improve the machinability of lead-free brass alloy CW511L

Müller, M. S. (1); Tomovic Petrovic, S. (2); Sørby, K. (1)

Machinability of brass is important in the manufacturing of couplings for drinking water supply systems. The reduction or elimination of lead in brass alloys affects both the cutting forces and the chip formation. Lead-free brasses that consist only of α -phase tend to form snarled and unbroken chips and show increased cutting forces. There are studies showing that the machinability of single α -phase alloys could be improved by modification of the microstructure by means of heat treatment conducted prior to machining, aiming to induce a certain amount of β -phase. In this study, lead-free CW511L alloy was heat treated and water quenched to induce β -phase prior to machining. A subsequent heat treatment with slow cooling was applied to change the microstructure back to α -phase.

Lead-free brass alloys can be single α -phase or duplex α/β -phase materials. Both phases are associated with different properties. The α -phase is known for being soft and ductile, while the β -phase is known to be more brittle and harder [1]. The alloy CW511L consists mainly of α -phase. According to the literature, more brittle β -phase improves machinability, and a duplex structure exhibits better chip breakage than a pure α -structure [1], [2]. The amount of β -phase can be increased by appropriate heat treatment. However, a higher β -content also increases the sensitivity of the alloy to dezincification [3]. Therefore, it is advisable to perform another heat treatment after the machining process to reduce the amount of β -phase.

In this paper, the effect of a heat treatment process, which led to an increase in β -phase content, on machining properties of CW511L alloy, has been investigated. This heat treatment process was based on a study by Toulfatzis et al. [2]. In addition to cutting forces, the shape of the chips, the microstructure,

tensile properties, and dezincification properties have been determined. Furthermore, the influence of subsequent β -annealing on the microstructure, tensile properties, and dezincification has been investigated.

Materials and Methods

In this study, the machining behavior during turning of as-received and heat treated CW511L alloy is compared. In addition, the microstructure, mechanical properties, and the dezincification behavior after different heat treatments were analyzed. The applied heat treatments are listed in Table 1. The material was supplied as an extruded and β -annealed rod with a diameter of 32 mm.

The first heat treatment was performed according to Toulfatzis et al. [2] and Toulfatzis et al. [4] aiming to increase the amount of β -phase and thereby to improve the machinability of CW511L compared to the as-received (AR) condition. The brass was heat-treated at 850°C for 120 min in a preheated Nabtherm N 41/H

chamber furnace and rapidly water quenched. This step was called HT1. HT1 was followed by the subsequent heat treatment (HT2), at 540°C for 180 min followed by slow cooling in air. HT2 was performed to gain back the mainly α -phase microstructure.

For all three conditions, AR, HT1 and HT2 microstructural analysis was performed. Samples were wet ground with SiC foil #320, followed by diamond and OP-S polishing. To perform analysis in a light microscope the samples were etched with a solution of ammonium peroxydisulfate. Additionally, samples were analyzed by means of a scanning electron microscope (SEM) with electron backscatter diffraction (EBSD) techniques to measure the amount of the β -phase.

Tensile tests were performed for all three temper conditions according to NS EN ISO 6892 1. The hardness was measured using a Brinell hardness tester according to ISO 6506-1. Dezincification resistance was investigated according to NS EN ISO 6509.

In the AR and HT1 temper conditions, machining tests were performed. The tests were performed using a Weiler Commodor 230 VDC lathe and a N123H2-0520-0002-BG H10F cutting insert by Sandvik Coromant. Disk-shaped, 2 mm thick specimen were cut by a face-turning operation at a constant cutting speed of $v = 150$ m/min and at different feeds of $f = 0.05; 0.10; 0.16; 0.20$ m/min in dry conditions. The chips were collected after each cut and the cutting forces were measured with a Kistler 9257B dynamometer.

Results and Discussion

The microstructure of the alloy in the three temper conditions is shown in Figure 1, upper row. An overview of alteration in grain size is given in Fig-

Heat treatment	Temperature	Duration	Cooling
HT1	850°C	120 min	Water quenching
HT2	540°C	180 min	Slow cooling in air

Table 1: Heat treatments performed on CW511L

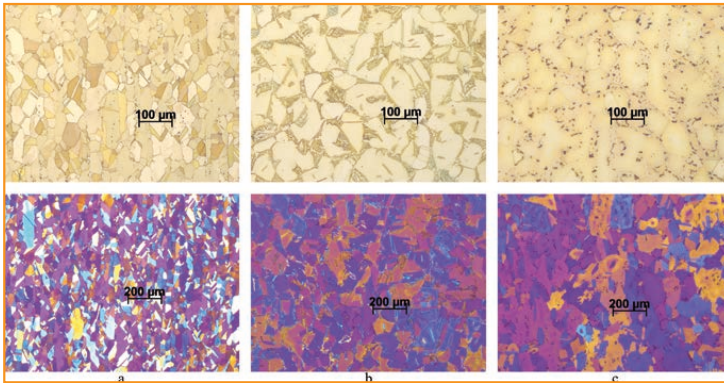


Fig. 1: Microstructure of CW511L in as-received condition (a), after heat treatment HT1 (b), and after heat treatment HT2 (c). Upper row: bright field, bottom row: polarized field pictures.

ure 1, bottom row. The grains in the AR condition are the smallest of all three temper conditions and 3.5% was pre-

hardness of HBW96, the Brinell hardness decreased to HBW67 and HBW62 after heat treatments HT1 and HT2,

Material's temper condition	HBW/2,5/62,5/11			
	1	2	3	Average
AR	96	92	95	94
HT1	66	68	68	67
HT2	61	63	63	62

Table 2: Brinell-hardness measurements of the different conditions

	As-Received AR	Heat Treatment HT1	Heat Treatment HT2
Tensile strength Rm [MPa]	343	380	318
0,2% proof strength R _{p0.2} [MPa]	315	317	243
Elongation A [%]	47	59	68

Table 3: Tensile test results for the different temper conditions

sent as β-phase in the alloy, see Figure 1a. After heat treatment HT1, 12.6% of the microstructure was presented as β-phase and the grain size increased. After heat treatment HT2, the proportion of β-phase was decreased to 4.8%, while the grains were still larger than in AR condition. Toulfatzis et al. [2] reported an increase in β-phase content, in CW511L alloy, from 5% measured in the as received condition to 35% measured after a heat treatment similar to HT1, while grain growth in the α-phase was also noticed. Changes in grain size and phase-composition influenced the measured hardness, see Table 2. While the material in AR condition shows a

respectively. This can be explained by a larger grain size. The HT1-condition shows a slightly higher hardness due to the presence of a higher amount of β-phase. The minimum value for the Brinell hardness given in NS-EN12164 standard is HBW70, which was not met by HT1 and HT2.

Results of the tensile testing in the three temper conditions are presented in Table 3. While for HT1 the tensile strength and the proof strength were increased compared to the AR condition, they were decreased for HT2. The increased values for HT1 can be explained by the presence of stronger β-phase, while the decreased values for HT2 can be explained by the coarser and mainly α-phase grain structure and thereby more ductile material behavior. The NS-EN12164 standard gives a minimum value of 320 MPa for tensile strength, which is not met by HT2 condition. The fracture elongation increased for HT1 and HT2 compared to the AR condition. This might be caused by the coarser grains. All three conditions showed ductile fracture and necking during the testing, which was most pronounced for the AR condition. The fracture surfaces are shown in Figure 2. All three temper conditions show similar fracture mechanisms with pronounced ductile dimple fracture.

The main cutting force in CW511L in AR and HT1 conditions is almost equal. In HT1 condition, the main cutting force was decreased by 4% compared to the AR condition, see Figure 3. Also, the force ratio, which

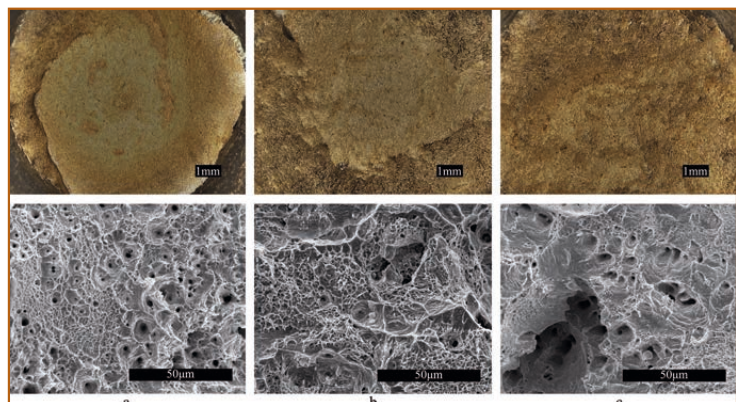


Fig. 2: Fracture surfaces on tensile test bars captured with digital microscope (upper row) and scanning electron microscope (bottom row). a - as extruded, b - heat treatment HT1, c - heat treatment HT2.

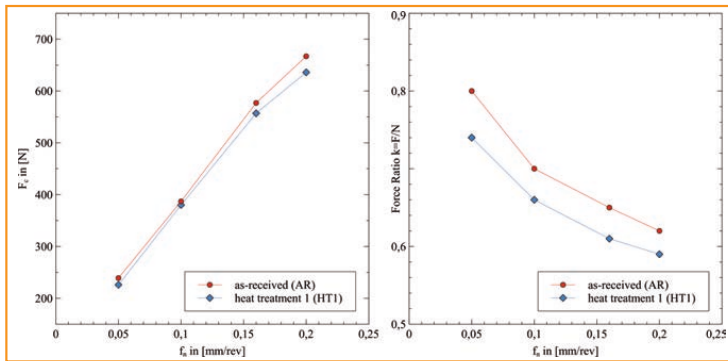


Fig. 3: Main cutting force and force ratio plotted over the feed for CW511L in as-received condition and after heat treatment HT1.

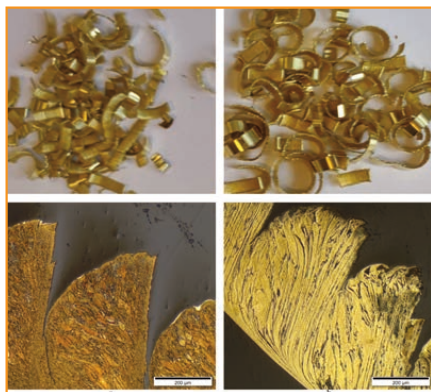


Fig. 4: Comparison between the chips in AR and HT1 condition on macro (top row) and micro scale (bottom row). Chips used in these pictures were produced while cutting with a feed of 0.16 mm/min.

is an indicator of the friction in the cutting zone [4], was decreased by 6%. Toulfatzis et al. [5] measured a force reduction of around 3% in a dry turning process using different cutting parameters. Although the β -content was lower compared to Toulfatzis et al. [5] the reduction in cutting forces was slightly higher. This might be due to measurement insecurities or the different cutting conditions, but also to the variance in β content. Toulfatzis et al. [5] additionally measured the power consumption and detected a decrease by 11,25%. Power consumption was not measured in this study, but similar values can be expected. The chip shape and length were equal at macroscopic scale in both conditions. Differences are visible at the microscale, see Figure 4. While the AR condition shows small grains inside

the chips as it is typical for nonhomogeneous chips, the HT1 condition shows elongated grains almost forming lamella, which is typical for discontinuous chips. These changes are similar to those reported by Toulfatzis et al. [5], who additionally noticed a change in chip length on macroscopic scale, where chips were shorter in the heat-treated condition. This difference

increased average dezincification depth in transversal direction the alloy is not dezincification resistant after HT1 according to ISO 6509-2, so HT2 is necessary to gain dezincification resistance back. Yet, the dezincification attack was on average twice as deep after HT2 as compared to the AR condition, but it is still considered dezincification resistant according to ISO 6509, see Table 4. This might be due to the increased grain size as discussed by Moriarty et al. [3]. Figure 5 shows micrographs of randomly chosen dezincification attacks in the three different conditions. It is visible, that in the HT1-condition the β -phase is attacked almost exclusively.

Conclusion

Regarding the main cutting force, the heat treatment was not very beneficial, since compared to AR condition only a reduction by 4% was achieved. When evaluating the microstructure of the chips it was visible, that after

Sample ID	No. of Measurements					Average	Max
	1	2	3	4	5		
AR_L*	9	-	-	-	-	<9	
AR_T*	9	-	-	-	-	<9	
HT1_L	132	114	152	144	142	137	152
HT1_T	176	164	116	118	77	130	176
HT2_L	Less than 20					<20	
HT2_T	44	26	29	9	9	23	44

Table 4: Depth of the dezincification attack in the three different conditions of alloy CW511L [μ m]

might be caused by different machining parameters used in the study. The dezincification tests showed, the alloy is dezincification resistant in the AR condition and after HT2, see Figure 5 and Table 4. Due to the

HT1 the chips turned from nonhomogeneous chips into discontinuous chips. On the macroscopic scale the length of the chips was not affected. With HT2 the dezincification resistance according to ISO 6509 was

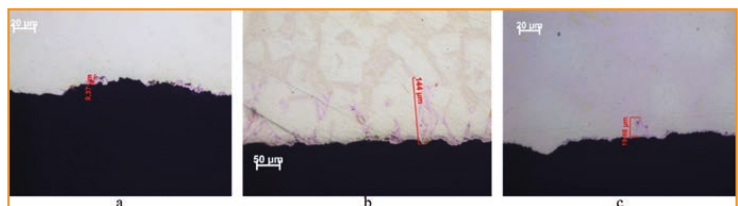


Fig. 5: Dezincification attack in CW511L in the three conditions (a) as-received, (b) after heat treatment HT1, (c) after heat treatment HT2.

retained, but the corrosion attack was slightly deeper compared to the AR condition. Neither HT1 nor HT2 fulfilled the hardness requirement given by NS-EN 12164 standard. HT2 additionally failed to fulfill the tensile strength requirement. A shorter heat treatment before cutting might be more beneficial to both machining, mechanical properties, and dezincification if grain growth would be less significant.

Acknowledgement

The authors thank the Research Council of Norway for supporting this work through the research project LOBUS – Low Lead Brass for Sustainable Com-

munity Development, (RCN Project No. 296054).

References

- [1] J. R. Davis and ASM International Handbook Committee, *Copper and copper alloys*. ASM International, 2001.
- [2] A. I. Toulfatzis, G. A. Pantazopoulos, and A. S. Paipetis, "Microstructure and properties of lead-free brasses using post-processing heat treatment cycles," *Mater. Sci. Technol.* (United Kingdom), vol. 32, no. 17, pp. 1771–1781, Nov. 2016, doi: 10.1080/02670836.2016.1221493.
- [3] M. Moriarty, Y. Wu, T. Murray, and C. Hutchinson, "The effect of phase fraction, size and shape on the dezincification of duplex brasses," *Corros. Sci.*, vol. 184, p. 109366, May 2021, doi: 10.1016/j.corsci.2021.109366.
- [4] P. Albrecht, "New developments in the theory of the metal-cutting process: Part I. the ploughing process in metal cutting," *J. Manuf. Sci. Eng. Trans. ASME*, vol. 82, no. 4, pp. 348–356, Nov. 1960, doi: 10.1115/1.3664242.
- [5] A. Toulfatzis, G. Pantazopoulos, C. David, D. Sagris, and A. Paipetis, "Final Heat Treatment as a Possible Solution for the Improvement of Machinability of Pb-Free Brass Alloys," *Metals (Basel)*, vol. 8, no. 8, p. 575, Jul. 2018, doi: 10.3390/met8080575.

- (1) *Magdalena S. Müller, Knut Sørby, Department of Mechanical and Industrial Engineering, Norwegian University of Science and Technology, 7491 Trondheim, Norway*
- (2) *Stanka Tomovic Petrovic, Department of Materials Technology, SINTEF Manufacturing AS, 2831 Raufoss, Norway*

Paper III



Müller, M. S., & Sørby, K. (2023b). The Influence of the Rake Angle on the Cutting of Low-Lead and Lead-Free Brass Alloys. In H. Kohl, G. Seliger, & F. Dietrich (Eds.), *Manufacturing driving circular economy. proceedings of the 18th global conference on sustainable manufacturing, october 5-7, 2022, berlin. lecture notes in mechanical engineering* (pp. 219–227). Springer, Cham. https://doi.org/10.1007/978-3-031-28839-5_25

This paper was presented at the 18th Global Conference of Sustainable Manufacturing 2022 in Berlin, Germany.

Components manufactured from brass alloys are widely used in plumbing systems. Traditionally, lead is added to the alloy to improve the machinability. In recent years, the use of lead has been restricted due to health and environmental concerns. New lead-free and low-lead alloys were developed. These alloys usually show a higher cutting force compared to traditional lead-containing brasses. This paper investigates the influence of different rake angles and tool coating on cutting force and chip formation. The two lead-free brass alloys, CW511L and CW724R, are compared to the low-lead brass CW625N.



The Influence of the Rake Angle on the Cutting of Low-Lead and Lead-Free Brass Alloys

Magdalena S. Müller^()  and Knut Sørby 

Department of Mechanical and Industrial Engineering, Norwegian University
of Science and Technology, 7491 Trondheim, Norway
`magdalena.s.muller@ntnu.no`

Abstract. Components manufactured from brass alloys are widely used in plumbing systems. Traditionally, lead is added to the alloy to improve the machinability. In recent years, the use of lead has been restricted due to health and environmental concerns. New lead-free and low-lead alloys were developed. These alloys usually show a higher cutting force compared to traditional lead-containing brasses. This paper investigates the influence of different rake angles and tool coating on cutting force and chip formation. The two lead-free brass alloys, CW511L and CW724R, are compared to the low-lead brass CW625N.

Keywords: Lead-Free Brass · Cutting Tool · Machinability

1 Introduction

Due to its favorable properties, brass is widely used in different applications, for example in couplings for drinking water supply systems. Brass is electric-conductive, antibacterial, and nonmagnetic. Different elements added to brass can change the properties of the alloy. In general, lead is known to enhance chip breakability and reduce cutting forces. This is commonly explained by the non-solubility of lead in brass, which causes the precipitation of lead particles around the grain boundaries, and the low melting point of lead compared to brass. Johansson et al. compared a lead-containing and a lead-free brass alloy. The tool-chip contact length was significantly shorter, and the friction coefficient was lower when machining lead-containing brass. By studying chip roots, it was found that lead in brass acts as a crack initiation point, contributing to discontinuous chips. However, no evidence was found for lead melting during the machining process [5]. However, lead can be toxic to humans and the environment. For this reason, many countries restrict the use of lead, such as the EU, the United States, Japan, and Canada. The restrictions are likely to tighten in the future [4]. As a result of this, new low-lead and lead-free brass alloys were developed. To compensate for the missing lead and its favorable effects, different elements were added. A widely studied lead-free brass is the silicon-alloyed special brass CW724R. CW724R shows increased cutting forces compared to lead-alloyed brass, but lower cutting forces than other lead-free alloys [10]. These are probably caused

by the brittle κ -phase, which is precipitated during solidification and as a result of silicon. In addition to the different alloying elements, the cutting forces can also be influenced by the tool geometry, the tool coating and the cutting conditions. Nobel et al. investigated the influence of tool geometry on chip breaking in the cutting of brass. In general, the rake angle had a lower influence compared to the chip-breaking geometry. A negative rake angle leads to increased cutting forces and average chip breakability in cutting CW511L [8]. In another study, Nobel et al. concluded that a TiAlN-coated carbide tool showed the lowest tool wear, a multilayer chemical vapor deposition (CVD)-diamond-coated carbide tool showed the lowest adhesion of carbide tools, and a polycrystalline diamond (PCD) tool had the best overall performance for the cutting of brass [6]. In general, for the more ductile copper-base alloys without lead addition, tools with a higher rake angle between 10° and 20° are recommended [3]. A higher rake angle will lead to a higher shear angle and thereby to lower cutting forces. On the other hand, a higher rake angle gives a smaller wedge angle. Thus, the tool is weakened and might wear out more quickly. Therefore, high rake angles are usually only used in difficult to machine high-ductility materials [7].

The goal of this paper is to investigate the influence of the rake angle and a AlTiN tool coating on the cutting forces and the tool wear in cutting of low-lead and lead-free brass. The alloys investigated are CW724R, CW511L, and CW625N. In the next section, the methods used in this paper are described, followed by the results and a discussion of the results, and a conclusion.

2 Materials and Methods

This study investigates and compares the cutting forces in the lead-free brass alloys CW511L and CW724R with the low-lead brass alloy CW625N. All alloys were supplied as extruded rods. LG123L1-0600-BG H13A carbide inserts from Sandvik Coromant were used. In preparation, the inserts were ground by the toolmaker company DanSpecial, and half of the inserts were coated. Four different rake angles 0° , 8° , 16° , and 24° and clearance angles of 6° to 8° were prepared. As a coating, the AlTiN-based FerroCon coating by CemeCon was applied by high-power impulse magnetron sputtering. According to Klocke et al. this coating gave slightly reduced cutting forces compared to uncoated tungsten carbide [6]. Investigations on a tribometer by Nobel et al. showed also lower friction for this coating compared to uncoated tungsten carbide with brass as counter body [9]. To minimize the influence of the tool nose in the cutting tests, in preparation, 5 mm wide grooves were cut in the rods, resulting in 2 mm wide disks. Cutting tests were performed on a Weiler Commodor 230 VCD open lathe under dry cutting conditions to measure cutting forces. A Kistler dynamometer was used to measure the cutting forces, and a LabView application was utilized. A constant cutting speed of 150 m/min was used, the width of cut was 2 mm as the disks. The feed was varied in four levels: 0.05, 0.1, 0.16, and 0.2 m/min. All tests were repeated three times. The chips were collected after each cut.

The geometry of the tool edge was analyzed on an Alicona InfiniteFocus microscope using focus variation prior to the cutting tests. The shape of the tool

edge was analyzed using a 10x magnification and the integrated edge measurement software tool. Measurements were taken at three different positions, and the average was calculated. According to the results, all the tools had a form factor K of 1, and the cutting edge segments were symmetric. The edge rounding r varied from 7 to 18 μm depending on the tool, and the profile flattening Δr of the tools varied from 4 to 23 μm , for detailed information, see Table 1.

Furthermore, the surface roughness of the coated and uncoated 0° rake angle tool was measured on the rake face and the clearance face in both the radial and transverse directions. A Mahr Perthometer M2 was used with a sampling length of 0.25 mm. The average results of the five repetitive measurements can be found in Table 2.

Table 1. Measurements of the tool geometry.

Rake angle γ [°]	Condition	Wedge angle β [°]	Edge rounding r [μm]	Cutting edge segment on flank face S_α [μm]	Cutting edge segment on rake face S_γ [μm]	Profile flattening Δr [μm]
0	Uncoated	84	7	9	9	4
0	Coated	84	16	19	19	8
8	Uncoated	75	16	23	23	13
8	Coated	76	13	21	21	12
16	Uncoated	66	14	23	23	13
16	Coated	68	17	28	28	15
24	Uncoated	60	18	36	36	23
24	Coated	60	17	31	31	18

Table 2. Surface roughness measurements of the rake face and clearance face.

Tool	Ra rake face, radial [μm]	Ra rake face, transversal [μm]	Ra clearance face, radial [μm]	Ra clearance face, transversal [μm]
0° , uncoated	0.013	0.011	0.103	0.206
0° , coated	0.049	0.05	0.237	0.238

3 Results and Discussion

From the three repetitive force measurements, the average was calculated. Figure 1 shows the calculated average main cutting force F_c plotted over the feed values f_n used for the different tools and workpiece materials. The main cutting force was the highest in the CW511L alloy, on average around 70% higher than in the CW625N alloy. This difference was higher for lower rake angles and decreased with increasing the rake angle. Also, it was slightly lower for the coated tools. The main cutting force in the CW724R alloy was approximately

10% higher than in CW625N. Here, the difference was slightly higher for the coated tools. Furthermore, the difference increased with increasing rake angle and was the highest for the tool with a rake angle of 16° but decreased slightly for the rake angle of 24° for coated and uncoated tools.

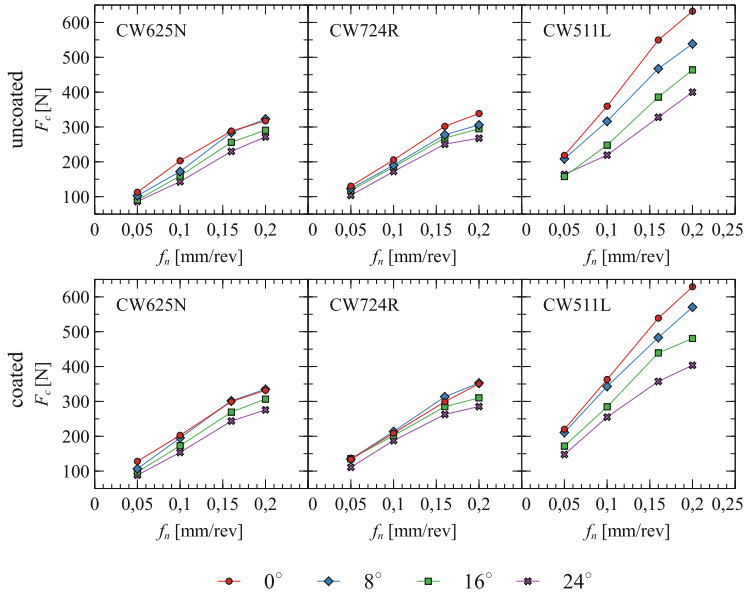


Fig. 1. Average main cutting force against feed for different tools and alloys.

Furthermore, it is visible in Fig. 1 that the main cutting force increases with increasing feed. From the comparison of the linear trend line, it is visible that this effect is the strongest for CW511L but decreases with increasing rake angle. For CW724R and CW625N, the slopes are relatively similar and slightly decreasing with increasing rake angle. When comparing the different rake angles with the 0° rake angle tool, overall, the cutting force decreased more for the uncoated tools than for the coated tools. The decrease in cutting forces increased with increasing rake angle for both coated and uncoated tools and all materials. The achievable reduction was the highest for CW511L and the lowest for CW724R, but even the minimum cutting forces for a particular feed in CW511L are still higher than the highest cutting forces for the same feed in CW724R or CW625N. Overall, the coating has only a minor effect on the cutting forces, as it increases the cutting force on average by 6%, 7%, and 5% for CW625N, CW724R, and CW511L, respectively.

To further interpret the data, an ANOVA was performed using Minitab software. According to the results, all four factors: rake angle, feed, material, and coating, had a statistically significant impact. Additionally, the interactions between rake angle and material, feed and material, and rake angle and coating were statistically significant. The fit of model was $R^2 = 99,40\%$. Figure 2 shows

the main effect plot. A Turkey-pairwise comparison revealed that there are no significantly different means for the combinations of 0° rake angle and no coating with 0° rake angle and the coating, 8° and coated with 0° and uncoated, and 16° coated with 8° uncoated. Also, means were not significantly different for a feed of 0.2 mm/rev and CW625N compared to a feed of 0.1mm/rev and CW511L. For the combination of rake angle and material, 0° in CW724R and 8° in CW724R, 8° in CW724R and 0° in CW625N, 0° in CW625N and 16° in CW724R, and 24° in CW724R and 16° in CW625N showed no significantly different means. The results show that CW625N should be cut with a high rake angle and a low feed rate to achieve the lowest possible cutting force. On the contrary, cutting CW511L at a high feed rate and a low rake angle leads to the highest cutting forces. The coating condition has only a minor influence on the cutting force.

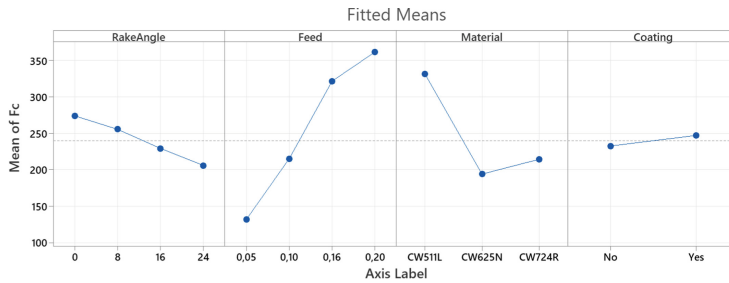


Fig. 2. Main effects plot for F_c .

The cutting forces are measured in machine coordinates. To calculate the forces parallel and normal to the rake face, the machine coordinates must be rotated with the rake angle. Thus, the friction force F and the normal force N to the friction force can be calculated from the measured cutting and feed force. These two components are often used to calculate a friction coefficient. That does not seem to reflect reality but rather a force ratio $k = F/N$, which nevertheless depicts the friction conditions [1,6]. When considering tool edge geometry, Albrecht concluded that the coefficient of friction is no longer increasing with the rake angle [1]. However, the force ratios for the different materials and tools are plotted against the feed in Fig. 3. As a general trend, it is noticeable that the force ratios are highest in CW511L and lowest for CW625N. A possible explanation is differences in the chemical composition and the microstructure of the alloys. In CW625N, the lead might act as an internal lubricant in the cutting zone and reduces friction [6]. Although in CW724R there is brittle κ -phase present, which increases the breakability of the chip and reduces the adhesion to the tool, CW511L consists mainly of soft α -phase and therefore shows the highest cutting force ratios, and thus the highest friction in the cutting zone [6]. Surprisingly, the force ratios increased for the coated tools compared to the uncoated tools. In turning tests in wet conditions, Klocke, Nobel, and Veselovac measured slightly decreased force ratios [6]. That might be due to the influence

of the cutting fluid used. However, due to the increased hardness of the coating, lower force ratios and lower friction also are expected in dry conditions. That is supported by Nobel et al., who performed friction tests in dry conditions with uncoated and TiAlN coated tungsten carbide on CW511L and observed a reduction in friction with the application of the coating [9]. A possible explanation for the higher force ratios measured in this study is the two to four times higher roughness values for the coated tools compared to the uncoated tools; see Table 2.

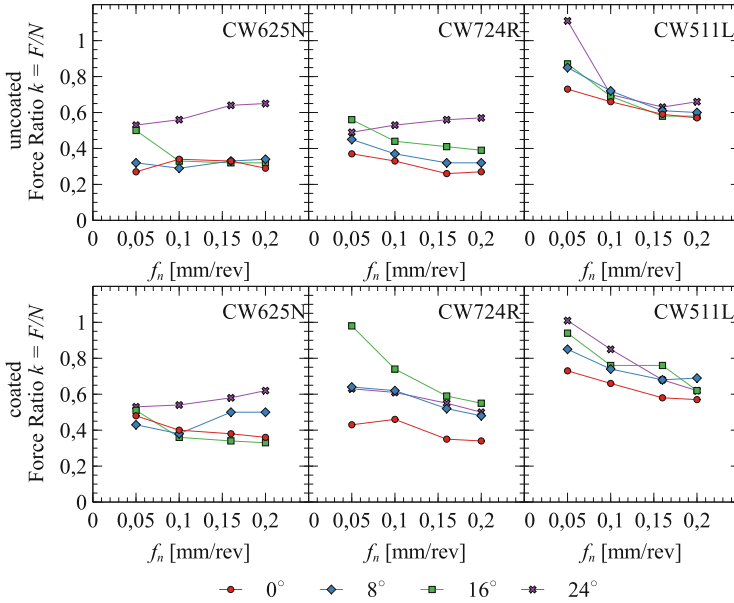


Fig. 3. Cutting force ratio k for different tools and materials.

The shape and length of the chips have an impact on the stability and reliability of the process, especially in automated machining. Long, unbroken chips can wrap around the tool or workpiece and damage the newly generated surface. On the contrary, extremely small chips can damage the machine tool by clogging the filter system for the cooling lubricant. For the transport of the chips, they must be neither too long nor too short. In general, chip forms like ark chips, elemental chips, or short tubular and helical chips are favorable, while long spiral or helical chips, snarled chips, and needle chips, are unfavorable. The chip form can be influenced by several factors, such as the geometry of the tool, the cutting parameters, or the use of cooling lubricant and their combined effects [2]. The chips produced during this investigation were spiral, needle, loose arc or elemental, and snarled chips. Table 3 shows the chips formed for each alloy, tool, and feed tested. For the CW625N alloy, the chips will become shorter at lower rake angles. The coating appears to increase chip breakability at lower rake angles,

while decreasing it at higher rake angles. For the uncoated tool, 8° at feed rates of 0.16 and 0.2 mm/rev or 16° and 24° at feed rates of 0.05 and 0.1 mm/rev seem favorable regarding chip breakability. Chip formers or cooling lubricants might enhance the chip breakability at high rake angles. Taking into account the slightly increased cutting forces and predominantly unfavorable chip forms, the use of AlTiN to cut CW625N cannot be recommended. Alloy CW724R shows good chip breakability for both tools, but the coating leads to unfavorable needle chips at a rake angle of 0°, and the three highest feeds tested. Overall, CW511L exhibited the worst chip breakability. The uncoated tools with the two lower rake angles exhibited acceptable chip breakability at low feed rates, while the two higher rake angles produced only snarled chips. The AlTiN coating appears to increase chip breakability, so the coating may be beneficial for the CW511L cutting process, although a slight increase in cutting force was measurable compared to the uncoated tools.

Table 3. Chip forms for different alloys, feeds, and rake angles. ×: Spiral chips, +: Loose/Elemental chips, o: Needle chips, -: Snarled chips.

		CW625N				CW724R				CW511L				
		α in [°]												
		0	8	16	24	0	8	16	24	0	8	16	24	
uncoated	f_n in [mm/rev]	0.05	×	o	+	+	+	×	×	×	+	+	-	-
		0.1	o	o	+	+	+	+	+	+	-	-	-	-
		0.16	o	+	×	×	+	+	+	+	×	-	-	-
		0.2	o	+	×	×	+	+	+	+	×	×	-	-
coated	f_n in [mm/rev]	0.05	o	+	×	×	+	×	×	×	+	×	-	-
		0.1	o	×	×	×	o	+	+	+	+	+	+	-
		0.16	o	o	×	×	o	+	+	+	+	×	-	×
		0.2	o	o	×	×	o	+	+	+	+	×	-	-

4 Conclusion

A larger rake angle reduces the cutting forces but can have a negative effect on the chip form. This study showed that an AlTiN tool coating slightly increases the cutting forces compared to an uncoated tool. This could be due to increased friction in the cutting zone due to the higher roughness of the coated tools. However, this is contrary to studies by Nobel et al., who demonstrated slightly reduced friction when cutting the alloys CW724R and CW511L with an AlTiN-coated tool [9]. In future investigations on the rake angle and the tool coating, the impact on tool life should be considered. An increased rake angle will reduce the edge angle and potentially weaken the tool, so the tool wears out faster. On

the other hand, the decrease in cutting forces could be more eminent than a slightly reduced tool life. To improve the chip breakability, especially at higher rake angles, the use of a chip breaking geometry or high-pressure cooling should be investigated. The influence of the rake angle on the residual stresses should be investigated in further research.

Acknowledgements. The authors thank the Research Council of Norway for supporting this work through the research project *LOBUS - Low Lead Brass for Sustainable Community Development*.

References

1. Albrecht, P.: New developments in the theory of the metal-cutting process: Part I. the ploughing process in metal cutting. *J. Manufact. Sci. Eng. Trans. ASME* **82**(4), 348–356 (1960). <https://doi.org/10.1115/1.3664242>, http://asmedigitalcollection.asme.org/manufacturingscience/article-pdf/82/4/348/6494579/348_1.pdf
2. Carmignato, S.: Chip-forms, chip breakability, and chip control. In: Laperrière, L., Reinhart, G. (eds.) *CIRP Encyclopedia of Production Engineering*, pp. 245–260. Springer, Cham (2019). https://doi.org/10.1007/978-3-662-53120-4_6394, https://link.springer.com/referenceworkentry/10.1007/978-3-662-53120-4_6394
3. Davis, J.R.: *ASM International Handbook Committee: Copper and Copper Alloys*. ASM International (2001)
4. Estelle, A.A.: Drinking water lead regulations: impact on the brass value chain (2016). <https://doi.org/10.1080/02670836.2016.1220906>
5. Johansson, J., Alm, P., M'Saoubi, R., Malmberg, P., Ståhl, J.E., Bushlya, V.: On the function of lead (Pb) in machining brass alloys. *Int. J. Adv. Manufact. Technol.* (2022). <https://doi.org/10.1007/s00170-022-09205-0>
6. Klocke, F., Nobel, C., Veselovac, D.: Influence of tool coating, tool material, and cutting speed on the machinability of low-leaded brass alloys in turning. *Mater. Manufact. Process.* **31**(14), 1895–1903 (2016). <https://doi.org/10.1080/10426914.2015.1127944>, <http://www.tandfonline.com/doi/full/10.1080/10426914.2015.1127944>
7. Kuyucak, S., Sahoo, M.: A review of the machinability of copper-base alloys. *Can. Metall. Q.* **35**(1), 1–15 (1996). [https://doi.org/10.1016/0008-4433\(95\)00023-2](https://doi.org/10.1016/0008-4433(95)00023-2)
8. Nobel, C., Hofmann, U., Klocke, F., Veselovac, D.: Experimental investigation of chip formation, flow, and breakage in free orthogonal cutting of copper-zinc alloys. *Int. J. Adv. Manufact. Technol.* **84**(5), 1127–1140 (2015). <https://doi.org/10.1007/s00170-015-7749-z>
9. Nobel, C., Hofmann, U., Klocke, F., Veselovac, D., Puls, H.: Application of a new, severe-condition friction test method to understand the machining characteristics of Cu-Zn alloys using coated cutting tools. *Wear* **344–345**, 58–68 (2015). <https://doi.org/10.1016/j.wear.2015.10.016>
10. Nobel, C., Klocke, F., Lung, D., Wolf, S.: Machinability enhancement of lead-free brass alloys. *Procedia CIRP* **14**, 95–100 (2014). <https://doi.org/10.1016/j.procir.2014.03.018>

Open Access This chapter is licensed under the terms of the Creative Commons Attribution 4.0 International License (<http://creativecommons.org/licenses/by/4.0/>), which permits use, sharing, adaptation, distribution and reproduction in any medium or format, as long as you give appropriate credit to the original author(s) and the source, provide a link to the Creative Commons license and indicate if changes were made.

The images or other third party material in this chapter are included in the chapter's Creative Commons license, unless indicated otherwise in a credit line to the material. If material is not included in the chapter's Creative Commons license and your intended use is not permitted by statutory regulation or exceeds the permitted use, you will need to obtain permission directly from the copyright holder.



Paper IV

Müller, M. S., Brans, K., Meurer, M., Sørby, K., & Bergs, T. (2023). The effect of high-pressure cutting fluid supply on the chip breakability of lead-free brass alloys. *The International Journal of Advanced Manufacturing Technology*. <https://doi.org/10.1007/s00170-023-12440-8>

This paper was written during a research stay at RWTH Aachen University, Laboratory for Machine Tools and Production Engineering. It is published in The International Journal of Advanced Manufacturing Technology.

To improve machinability and in particular chip breakability, brass alloys are usually alloyed with small quantities of lead. Due to environmental and health concerns, the use of lead has been restricted in the last years. As lead-free brass alloys are progressively implemented in the industry, challenges arise due to their differing properties from traditional leaded brass alloys. One of the main challenges in automated continuous cutting processes is the worse chip breakability of lead-free brass alloys leading to longer and tangled chips. Hence, the impact of a high-pressure cutting fluid supply, as well as the impact of a chip-breaking geometry and the combined effect of both, has been investigated at different feeds. The three brass alloys CuZn37 (CW508L), CuZn38As (CW511L), and CuZn42 (CW510L) were studied at varying cutting fluid supply pressure levels and feed rates in a radial cutting operation. Cutting forces were measured, and chips were analyzed. No overall systematic impact of the cutting fluid supply pressure on the cutting forces was observed. In conclusion, increased pressure levels, a chip-breaking geometry, and an increased feed rate enhance the chip breakability of the investigated alloys.



The effect of high-pressure cutting fluid supply on the chip breakability of lead-free brass alloys

Magdalena Susanne Müller¹ · Kilian Brans² · Markus Meurer² · Knut Sørby¹ · Thomas Bergs^{2,3}

Received: 23 June 2023 / Accepted: 1 October 2023
© The Author(s) 2023

Abstract

To improve machinability and in particular chip breakability, brass alloys are usually alloyed with small quantities of lead. Due to environmental and health concerns, the use of lead has been restricted in the last years. As lead-free brass alloys are progressively implemented in the industry, challenges arise due to their differing properties from traditional leaded brass alloys. One of the main challenges in automated continuous cutting processes is the worse chip breakability of lead-free brass alloys leading to longer and tangled chips. Hence, the impact of a high-pressure cutting fluid supply, as well as the impact of a chip-breaking geometry and the combined effect of both, has been investigated at different feeds. The three brass alloys CuZn37 (CW508L), CuZn38As (CW511L), and CuZn42 (CW510L) were studied at varying cutting fluid supply pressure levels and feed rates in a radial cutting operation. Cutting forces were measured, and chips were analyzed. No overall systematic impact of the cutting fluid supply pressure on the cutting forces was observed. In conclusion, increased pressure levels, a chip-breaking geometry, and an increased feed rate enhance the chip breakability of the investigated alloys.

Keywords Lead-free brass · High-pressure cutting fluid supply · Machining · Chip breakability · Chip breaking geometry

Nomenclature

Symbol	Unit	Meaning
A	[%]	Elongation after fracture
a_e	[mm]	Width of cut
a_p	[mm]	Depth of cut
d	[mm]	Diameter
F	[N]	Friction force
F_c	[N]	Main cutting force
F_f	[N]	Feed force
F_N	[N]	Normal force to friction force
f	[mm/r]	Feed
p	[bar]	Pressure
Ra	[μm]	Arithmetic mean surface roughness
R_m	[MPa]	Tensile strength
$R_{p0.2}$	[MPa]	Yield strength
Rz	[μm]	Maximum height of profile
r	[μm]	Cutting edge radius
v_c	[mm/min]	Cutting speed
α	[°]	Clearance angle
β	[°]	Wedge angle
γ	[°]	Rake angle
λ_h	[—]	Chip thickness ratio

Magdalena Susanne Müller
magdalena.s.muller@ntnu.no

Extended author information available on the last page of the article

1 Introduction

Brass is an engineering material alloyed from copper and zinc. Due to its favorable properties, such as being non-magnetic and having good heat and electrical conductivity, it is widely used in various industries, e.g., sanitary, electrical, and automotive. One of the main manufacturing processes for brass components is machining. Due to the advantages of cutting over alternative technologies which often only cover a part of the manufacturing process [1], it is likely to remain a relevant manufacturing technique for components from brass. Small quantities of lead in brass improve the machinability of these alloys by decreasing cutting forces and tool wear and provoking shorter chips [2, 3]. On the other hand, the EU and other authorities restrict the use of lead due to environmental and health concerns. Therefore, several low-lead and lead-free brass alloys have been developed during the last years [4]. To compensate for the disadvantages of machining lead-free and low-lead brass alloys, machining processes need to be reconsidered, by optimizing process parameters and tool geometries.

Johansson et al. [3] investigated the influence of lead in brass alloys on machinability using an orthogonal turning process and an orthogonal planing process. Since lead is non-

soluble in brass, it segregates as small globules around the grain boundaries [3]. They drew the conclusion that during the cutting process, the globules will elongate to form flake-like structures that act as crack initiation points. That led to shorter chips and a shorter tool-chip contact. Additionally, the development of a stable chip-tool contact area was inhibited by the above-described mechanism, and therefore cutting forces and friction were lower in the leaded brass alloy [3]. Machining of lead-free or low-lead brass generally results in increased cutting forces and, in some cases, long snarled chips [2, 3]. Tools with a positive rake angle might reduce the cutting forces, but this tends to result in longer chips [5, 6]. A suitable chip-breaking geometry on the tool rake face or a high-pressure cooling supply can counteract this [7].

High-pressure cooling supply is beneficial regarding chip breakability [8]. Different studies using several workpiece materials achieved varying results regarding the influence of a high-pressure cutting fluid supply on the cutting force [9–12]. The length of the tool-chip contact on the rake face decreases due to the high-pressure cutting fluid supply and might contribute to lower cutting forces, while the pressure applied has an impact on the grade of chip segmentation [13]. There is a variety of studies investigating solely the impact of the high-pressure cutting fluid on the chip breaking using flat cutting inserts [14–16]. A combination of both, chip breaking geometry and high-pressure cutting fluid supply usually enhances the chip breakability. On the other hand, conventional chip-breaking geometries can interact with the high-pressure cutting fluid supply and deflect the high-pressure beam. Hence, mainly plane face tools are used in high-pressure cutting fluid supply [17].

Various papers concerning the machinability of lead-free brass alloys using either dry-cutting conditions or conventional cooling have been published in recent years. Klocke et al. [18] found higher chip segmentation, lower chip compression, lower process forces, and better surface quality in the form of fewer burrs when machining CuZn42 compared to CuZn38As when using a conventional cutting fluid supply. On the contrary, Toulfatzis et al. [19] found CuZn38As to show a better result in terms of surface roughness compared to CuZn42 when applying dry-cutting conditions. These conflictive results could be explained by the difference in cutting fluid supply and by the different cutting parameters applied. Additionally, CuZn38As showed low abrasive tool wear but strong adhesions in the study by Klocke et al. [18], while the study by Toulfatzis et al. [19] did not consider tool wear. In friction tests performed by Nobel et al. [20], CuZn38As showed higher tangential forces and coefficients of friction as compared to CuZn42. This was explained by the homogeneous microstructure, strong adhesion, and high plastic strain capacity of CuZn38As. Thus, CuZn42 showed lower coefficients of friction due to the inhomogeneous microstructure with around 50% β -phase present. This led to the conclusion

that worse chip breakability is to be expected when comparing CuZn38As to CuZn42 [20]. A better chip morphology with an increased percentage of β -phase was also reported by Toulfatzis et al. [21] after machining differently heat-treated brass alloys. On the other hand, an increased percentage of β -phase will decrease the corrosion resistance of brass alloys and increase the likelihood of dezincification [22], which is especially unfavorable in plumbing installations.

Toulfatzis et al. [23] concluded that in lead-free alloys chip size and morphology are mainly influenced by the β -phase fraction since it acts as a microcrack initiator and influences the shear band formation. In investigations by [24], no chip breakage occurred when cutting CuZn38As and CuZn41.5 with a lower β -phase fraction with a flat carbide tool. Chip-breaking properties could be increased by using groove-shaped chip-breaking geometries [24]. CuZn37 is a brass alloy used for cold-formed parts mainly in the electronics industry. CuZn37 has high formability and consists similarly to CuZn38As mainly of α -phase. Due to its similar mechanical properties, microstructure, and chemical composition, similar machining behavior is expected [25].

When cutting lead-free brass alloys, chip breakability seems to be the most critical topic. Long, unbroken chips can tangle around the workpiece or the tool, are more difficult to remove, and may lead to extended downtimes in automated cutting processes. Furthermore, lead-free brass alloys show higher cutting forces when compared to lead-alloyed brass alloys. A high-pressure cutting fluid supply might be beneficial to address the aforementioned aspects, as it is known to reduce the chip length. On the other hand, the impact of high-pressure cutting fluid supply on cutting forces is unclear in literature, especially for low-lead brass alloys. In this study, the effects of high-pressure cutting fluid supply on cutting the lead-free brass alloys CuZn37, CuZn38As, and CuZn42 are evaluated. Tools with a flat rake face and tools with a chip-breaking geometry are utilized to investigate the effects of chip-breaking geometry and high-pressure cutting fluid supply. Cutting forces are measured, and chips are evaluated. The following chapters will give an overview of the materials and methods used in this study, the results, and a discussion of the results, as well as a conclusion.

2 Materials and methods

2.1 Brass alloys used in this study

In this study, the three lead-free brass alloys CuZn38As (CW511L), CuZn42 (CW510L), and CuZn37 (CW508L) were investigated. While CuZn42 is a dual-phase brass alloy, containing α and β -phase, CuZn38As, and CuZn37 are nearly single α -phase brass alloys, containing only trace amounts of β -phase in the microstructure. Both phases show

different lattice structures, which are associated with different properties. The lattice structure of the α -phase is face-centered cubic, which leads to lower hardness and higher ductility. On the other hand, the lattice structure of the β -phase is a body-centered cubic, which typically shows lower cold formability and higher hardness. Usually, dual-phase brasses will show shorter chips and lower chip thickness ratios compared to single-phase brass alloys due to their inhomogeneous microstructure. Nevertheless, this paper aims to investigate the potential of high-pressure cooling supply on chip breaking in both single and dual-phase brass alloys.

All materials were supplied as extruded rods. CuZn37 and CuZn42 were provided with a diameter of $d = 40$ mm, while CuZn38As was supplied with a diameter of $d = 32$ mm. For good comparability, all materials were cut to a diameter of $d = 31.5$ mm in the preparations of the tests.

Before carrying out the machining tests, samples of all materials were prepared for metallurgical investigations by wet grinding and polishing followed by color etching using Klemm II reagent. The micrographs are shown in Fig. 1. CuZn37 shows an almost pure α -phase microstructure. Some trace amounts of β -phase present as small precipitations around the grain boundaries of the α -grains, see Fig. 1 a). CuZn38As is presented as single α -phase brass as well, as shown in Fig. 1 b). CuZn38As contains arsenic, which acts as a corrosion inhibitor, Table 1. CuZn42 shows a dual phase α and β microstructure with a phase distribution of approx. 50% α -phase and 50% β -phase, see Fig. 1 c). The α -phase appears as bright-colored, elongated grains, while the darker grains are β -phase. There are some minor lead-precipitations present around the grain boundaries in all three alloys, which corresponds to the chemical compositions as given in Table 1.

Table 2 gives an overview of the mechanical properties of the materials. The hardness was measured at multiple points along the cross-section of the rod. A hardness gradient was observed across the cross-section. The hardness was highest in the subsurface area and decreased towards the center of the rods.

2.2 Cutting inserts

To evaluate both the effect of the high-pressure cutting fluid and the combined effect of high-pressure cutting fluid and a chip breaking geometry on chip breakability, two different types of inserts were used in a radial cutting operation. First, a regular insert of type ISCAR, GIPA 4.00-0.40, grade IC20, as shown in Fig. 2, was used. IC20 is an uncoated cemented carbide grade, which is suitable for brass alloys. The GIPA 4.00-0.40 insert has a chip-breaking geometry. To further investigate the effect of the high-pressure cutting fluid supply on the chip breakability, some of the inserts were ground to

get a flat rake face, while the rake angle and clearance angle were kept like the original geometry.

Prior to machining, all inserts were analyzed. First, the geometry and surface roughness of the inserts were evaluated by means of focus variation using an Alicona Infinite Focus G5 microscope, see Table 3. Additionally, to visualize the chip-breaking geometry of the original tools a topography picture was recorded using the Alicona microscope, as shown in Fig. 2. Furthermore, pictures of the tools, especially the cutting edge, were taken using a digital Keyence VHX-6000 microscope. Thus, the negative effects of chipping phenomena on the unworn cutting edge could be excluded and the tool wear during the experiments could be detected. All tools had a designation consisting of a number and a short code for the type of rake face. Tools with chip breakers are called CB and tools with a flat rake face are called F. Numbers from #1 to #3 are assigned as shown in Table 3. Tools with #1 were used for tests with CuZn37, tools with #2 were used for CuZn42, and tools with #3 were used for CuZn38As, respectively.

2.3 Machine tool and test setup

The machining tests in this study were performed on a DMG Mori NZX 1500-ST3 lathe with an integrated high-pressure cooling supply aggregate. The aggregate can achieve pressures of up to $p = 72$ bar, which can be varied in eight predefined steps. The mineral oil-based Blasomill GT20 by Blaser Swisslube was used as cutting oil. The cutting inserts were inserted into a GHDR 20-3-JHP holder by ISCAR. This holder has internal cutting fluid supply channels and is suitable for the high-pressure cutting fluid supply of up to $p = 340$ bar. The holder had two nozzles with a diameter of 1.8 mm each. One nozzle was placed above the insert in a way that the cutting fluid impact point was on the rake face, while the second nozzle was placed below the insert so the cutting fluid impact point was on the clearance face. The rods were clamped in the lathe with a collet chuck.

To prepare the brass, all rods were turned to a diameter of $d = 31.5$ mm. To minimize the influence of the edges of the tool, grooves were cut in the rods. Each groove had a width of 3 mm and a depth of 9 mm. During the tests, the remaining discs between the grooves were cut with the inserts described. The geometry of the discs led to a width of cut of $a_e = 3$ mm and a depth of cut of $a_p = 7$ mm to prevent the tool from hitting the core of the rod. The test setup is shown in Fig. 3. Table 4 gives an overview of the cutting parameters applied in this study. A fully factorial test series was performed, where each set of parameters was repeated three times to get a statistically valid result. Cutting forces were measured during each cut utilizing a Kistler Dynamometer type 9119AA2. The dynamometer measures cutting forces in the directions indicated in Fig. 3 and additionally the passive force, which

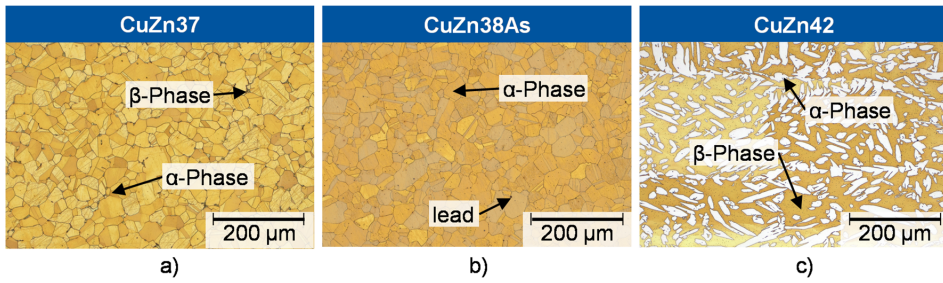


Fig. 1 Optical micrographs of the brass alloys CuZn37 (a), CuZn38As (b), and CuZn42(c)

Table 1 Composition of the Brass Alloys CuZn37, CuZn38As, and CuZn42

Material	Cu	Zn	Pb	Sn	P	Fe	Ni	As
CuZn37	64.3	35.67	0.034	-	-	0.099	0.0015	-
CuZn38As	63.2	36.6	0.04	0.01	-	0.07	0.01	0.02
CuZn42	56.73	42.36	0.086	-	0.011	0.256	0.266	-

Table 2 Mechanical properties of the brass alloys CuZn37, CuZn38As, and CuZn42

Material	Tensile Strength R_m [MPa]	Yield Strength $R_{p0.2}$ [MPa]	Elongation after Fracture A [%]	Hardness HBW
CuZn37	348	206	43.5	82
CuZn38As	354	296	56	91
CuZn42	506	406	34	110

Fig. 2 Natural image and topographical image of the chip-breaking geometry of the CB cutting insert

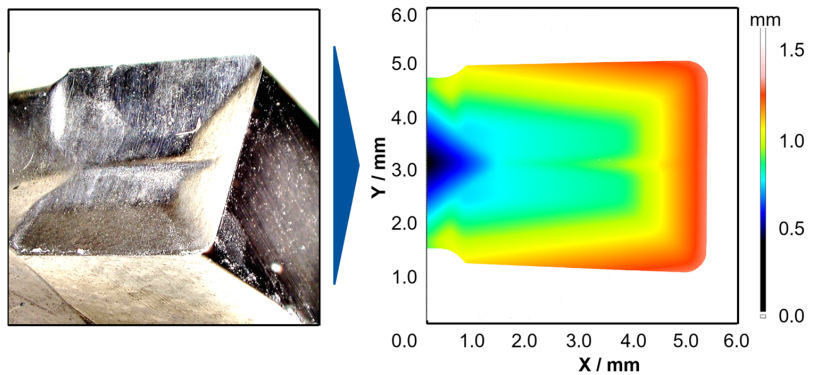
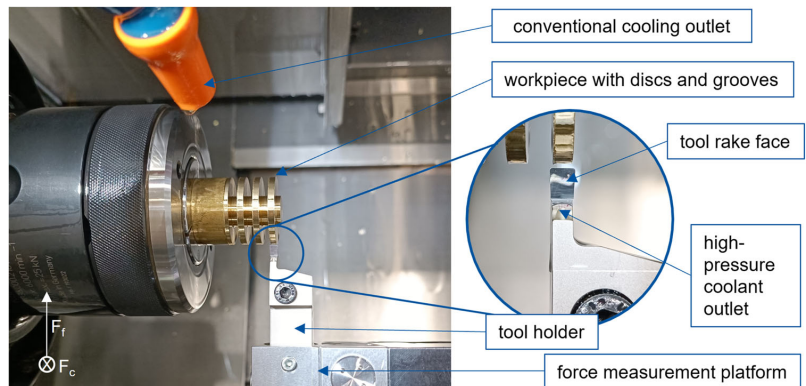


Table 3 Geometrical measurements of the cutting inserts used in the experiments

Tool	Rake face	Cutting edge radius r [μm]	Clearance angle α [$^\circ$]	Wedge angle β [$^\circ$]	Rake angle γ [$^\circ$]	Roughness R_a [μm]	Roughness R_z [μm]
CB #1	Chip breaker	3.6	7.1	67.6	15.3	0.5	2.2
CB #2	Chip breaker	5.5	7.0	67.0	16.0	0.7	3.5
CB #3	Chip breaker	4.3	7.0	66.9	16.1	0.5	2.8
F #1	Flat	12.3	7.7	68.7	13.7	0.6	3.4
F #2	Flat	13.0	7.4	69.1	13.5	1.0	4.1
F #3	Flat	12.0	7.5	69.1	13.4	0.5	2.8

Fig. 3 Experimental setup



is not indicated in the figure and not analyzed any further as it is reduced to almost 0 N due to the preparation of the rod. Before starting the measurement, the sensors were reset after the tool was positioned close to the rod, and the rotation of the rod and the cutting fluid supply were started. This was done to prevent the pressure of the cutting fluid supply from interacting with the cutting force measurement. After each set of parameters, the chips were collected.

2.4 Roughness measurements

The arithmetic mean roughness Ra of the machined surface was measured after the experiments. The surface roughness was measured perpendicular to the direction of the speed. To measure the roughness, a MarSurf LD 260 device by Mahr with the corresponding software MarWin was used. The measured profile length was $l = 2\text{ mm}$, and an S-filter was used. The scanning velocity was set to $v_s = 0.5\text{ mm/sec}$. The roughness was measured once per cut and three times per set of parameters.

2.5 Chip analysis

Overview pictures of all collected chips for each set of cutting parameters were taken with a digital camera. Afterward, the chip thickness of up to five randomly selected chips was measured at several points by means of a KEYENCE digital microscope. For each material and tool, one to two chips from the pressure levels $p = 3\text{ bar}$ and $p = 72\text{ bar}$, and a feed of $f = 0.15\text{ mm/r}$ were selected and prepared for metallographic investigations by grinding, polishing, and etching using Klemm II reagent for 45 to 60sec. With these samples, the chip segmentation was analyzed by measuring the thickness of the chips at valleys (h'_{min}) and peaks (h'_{max}) utilizing a KEYENCE digital microscope.

3 Results and discussion

3.1 Cutting forces

Prior to and after the cutting tests, the cutting inserts were examined with a digital microscope to evaluate tool wear. None of the inserts exhibited noticeable tool wear, even though small workpiece material adhesions were detected, as to be expected in the cutting of low-lead brass alloys [18, 24]. As a result, tool wear is neglected in further analysis.

First, average values of the main cutting force were calculated for the three repetitive tests, as shown in Figs. 4, 5, and 6. The cutting forces were measured in the machine coordinate system. The force vector consisting of the main cutting force F_c and the feed force F_f was rotated by the rake angle γ to calculate the forces in the tool coordinate system using the formula:

$$\begin{pmatrix} F \\ F_N \end{pmatrix} = \begin{pmatrix} \cos \gamma & \sin \gamma \\ -\sin \gamma & \cos \gamma \end{pmatrix} \begin{pmatrix} F_f \\ F_c \end{pmatrix} \quad (1)$$

resulting in a force vector containing the friction force F and the normal force F_N . The ratio of these forces is not equivalent to Coulomb's coefficient of friction but indicates the friction conditions. Therefore, it is called force ratio, rather than coefficient of friction [18, 26]. Nevertheless, the force ratio indicates the friction conditions [18, 26]. Therefore, the term force ratio is rather used than the coefficient of friction in this paper. As the normal force F_N is highly impacted by the cutting edge radius, a direct comparison of force ratios calculated from forces measured with different tools is not reasonable.

For all materials, the cutting forces increased when increasing the feed. The pressure of the cutting fluid seems to have only a minor influence, as the average difference between the highest and lowest average cutting force measured at one feed rate was 3%. This is in good accordance

Table 4 Test parameters

Insert	Feed f [mm/r]	Pressure p [bar]	Volumetric Flow Rate [L/min]	Material	Cutting speed v_c [mm/min]	Depth of cut a_p [mm]	Width of cut a_e [mm]
original ground		3	0.016				
	0.1	24	0.085	CuZn42			
	0.15	55	0.125	CuZn38As	150	7	3
	0.2	72	0.167	CuZn37			
		8 (conv. cooling)	0.4				

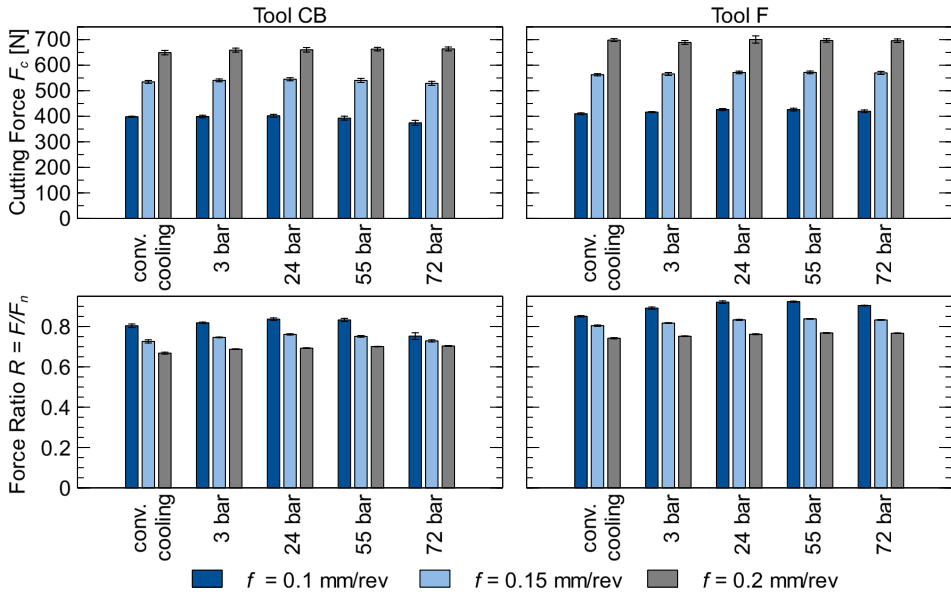


Fig. 4 Cutting forces and force ratios for CuZn37. The error bars show the standard deviation

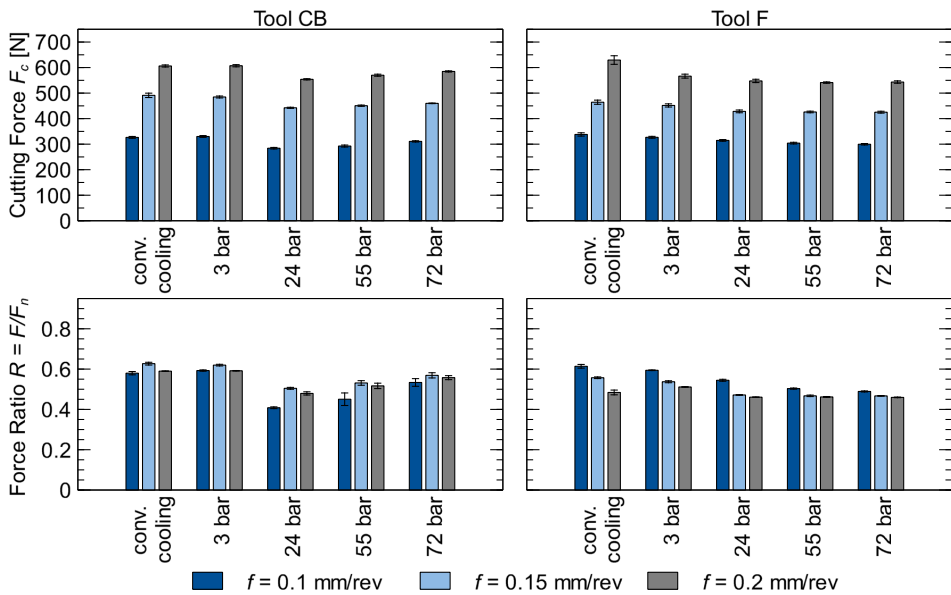


Fig. 5 Cutting forces and force ratios for CuZn38As. The error bars show the standard deviation

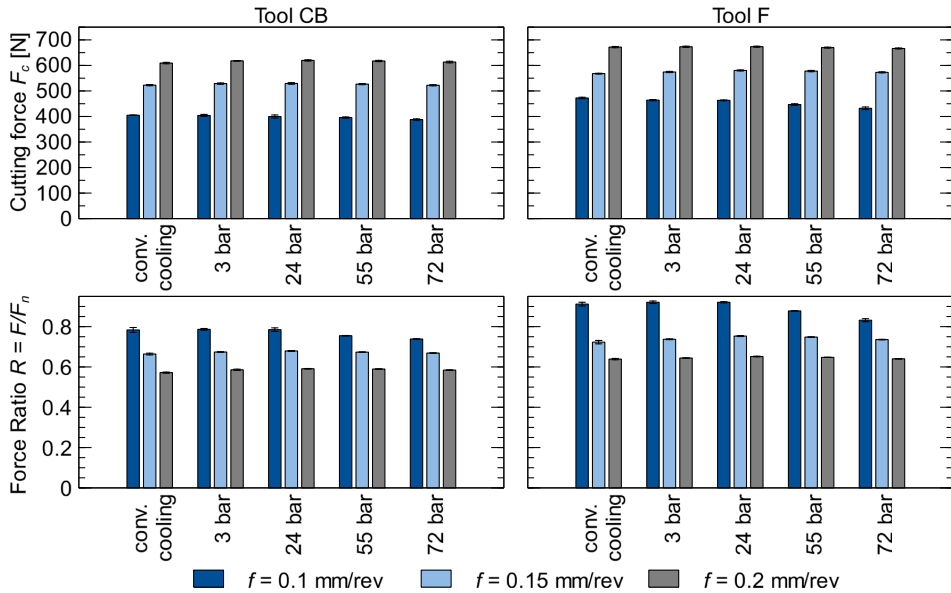


Fig. 6 Cutting forces and force ratios for CuZn42. The error bars show the standard deviation

with Craford et al. [10] and Machado and Wallbank who could not find significant changes in the measured cutting force due to a high-pressure cutting fluid supply investigating steel and titanium. Craford et al. explained this by the cutting fluid not penetrating deep enough into the cutting zone to impact the friction conditions at pressures below 1000 bar. On the other hand, there are some studies showing an impact on the cutting force [11–13]. For CuZn38As, the impact of the pressure was slightly higher. For CuZn38As, the highest cutting forces were measured when applying conventional cooling, while the forces decreased at the higher cutting fluid pressures. The force ratio, and the cutting force, showed a minimum at a pressure level of $p = 24$ bar when cutting with tool CB. For the feed level of $f_n = 0.1$ mm/r the cutting force was about 14% higher for the pressure level of 3 bar and about 3% and 9% higher for 55 bar and 72 bar when compared to 24 bar. At the higher feed levels, these differences decreased. They were 9%, 2%, and 4% for $f_n = 0.15$ mm/r and 9%, 3%, and 5% for $f_n = 0.2$ mm/r. Lower temperatures while cutting CuZn38As could lead to a higher strain-hardening effect as described by Laakso et al. [27]. Due to more cutting fluid entering the tool-chip contact at pressure levels above $p = 24$ bar, see Table 4, better cooling might have been achieved, leading to a lower temperature in the cutting zone and a higher strain hardening effect. Therefore, cutting forces increased. A similar result is described for titanium, austenitic steel, or nickel alloys. On the contrary, cutting forces did not increase at higher pressure levels

when using tool F. This might be explained by the absence of a chip-breaking geometry and, therefore, an increased contact area and increased cutting temperature compared to tool CB [27]. This interdependency needs further investigation as cutting temperature was not measured during this study.

For CuZn37 and CuZn42 the cutting forces increased when changing to tool F, which can be explained by a slightly lower rake angle, a higher cutting edge radius, and a potentially longer tool-chip contact [5, 6, 28]. Additionally, the cutting forces of CuZn38As were overall lower than in the two other materials. This can be explained by the higher friction represented by a higher force ratio in cutting CuZn37 and the higher tensile strength of CuZn42.

To further interpret and analyze the results a multivariate analysis of variances (MANOVA) was conducted using Minitab software. As response variables, the feed force and the cutting force were used. Alloy, tool, feed rate, and cutting fluid supply pressure as well as their interactions were used as factors. The coefficient of determination was $R^2 = 99.70\%$ for the feed force and $R^2 = 99.69\%$ for the cutting force, respectively. A confidence level of $\alpha = 0.05$ was used. For both responses, all terms can be considered to have a statistically significant impact.

According to the main effects plot, as shown in Fig. 7, the cutting force is mostly impacted by the alloy and the feed, while the tool and pressure levels only showed a minor impact. For the feed force, as shown in Fig. 8, the pressure level had the lowest impact, while the impact of the

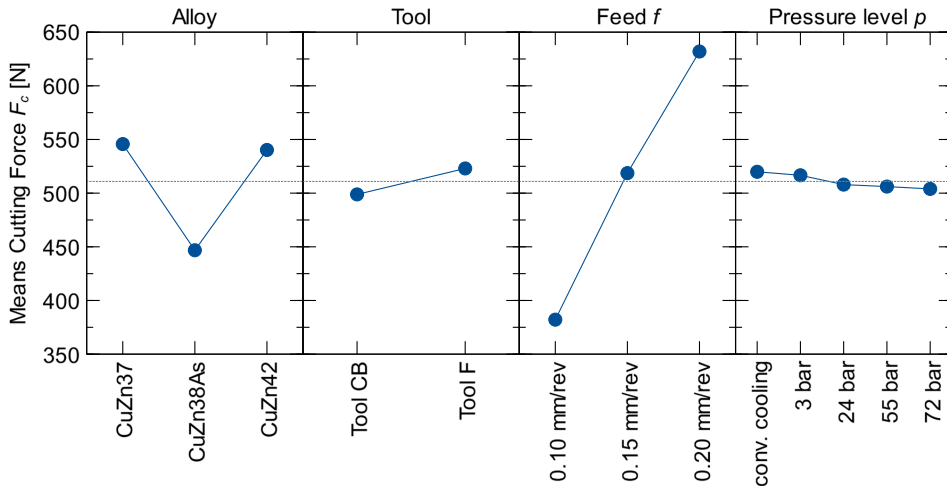


Fig. 7 Main effects plot for cutting force F_c

tool and feed was the highest. The results of the statistical analysis support the conclusions drawn from the force measurements.

A higher feed usually leads to a lower force ratio; the only exemption is CuZn38As when cutting with tool CB. Here the force ratio was the highest for a feed of $f = 0.15$ mm/r. A higher feed led to a higher chip thickness. An increased chip thickness makes the chip more rigid and thereby changes the chip up-curl radius. A different chip up-curl radius changes how the chip flows over the rake face and interacts with the chip-breaking geometry. Therefore, tool-chip contact length

and consequently the friction conditions might have changed depending on the feed. Further investigations are necessary to explore this. On the other hand, the force ratio seemed to be more impacted by the pressure of the cutting fluid than the cutting force. The minimum force ratio was in most cases reached at the highest pressure level. An exemption was CuZn38As cut with tool CB. Here, the minimum was at $p = 24$ bar, similar to the force minimum, see Fig. 5. Moreover, CuZn38As showed lower force ratios compared to the literature where an emulsion and conventional cooling were investigated [18]. This might be explained by the

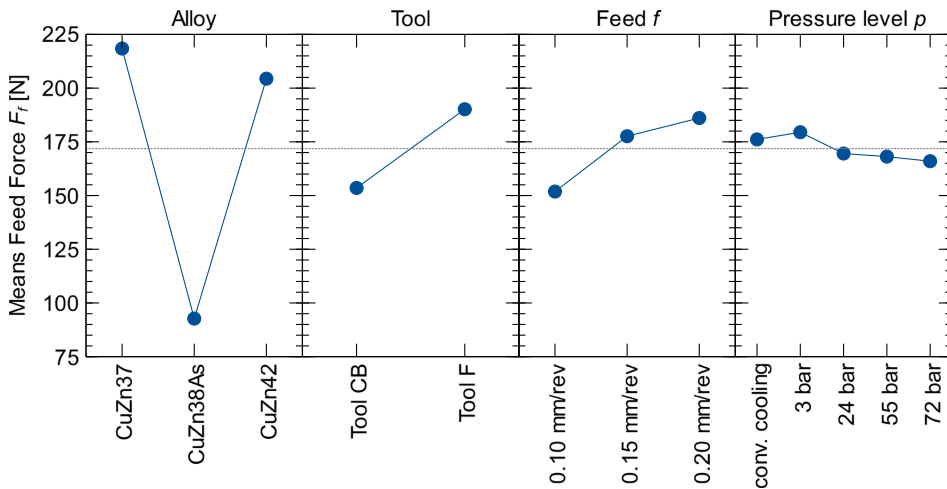


Fig. 8 Main effects plot for cutting force F_f

cutting fluid penetrating the gap between the chip's backside and rake face better due to high-pressure supply and thereby decreasing the adhesion between tool and chip or by the different properties of oil compared to emulsion. Different tool geometries, especially the cutting edge radius, might influence the force ratio and F_N . A higher pressure meant more cutting fluid penetrating the contact zone, which seemed to help reduce the force ratio, especially for tool F, see Table 4. The force ratio in CuZn42 was similar to that found in the literature, even though different cutting fluids and supply strategies were used [18]. Due to the increased β -phase content of CuZn42 a lower adhesion was expected compared to CuZn38As and CuZn37. For CuZn37, the cutting fluid did not seem to impact the force ratio, despite the similar microstructure to CuZn38As.

3.2 Chip form, chip thickness ratio, and degree of chip segmentation








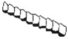






Pictures of the chips from every set of parameters were taken. To give a brief overview, chips produced at pressure levels $p = 3$ bar and $p = 72$ bar and at a feed of $f = 0.15$ mm/r are presented in Fig. 9.

The chips produced when cutting **CuZn37** at a feed of $f = 0.10$ mm/r were long with only some slightly shorter per cut. At the highest pressure level, the chips were still long and unbroken, even though they were slightly smaller than for the lower pressure levels. For cutting CuZn37 at $f = 0.10$ mm/r with tool F, there was already a difference visible when changing from conventional cooling to high-pressure cooling with a pressure of $p = 3$ bar. Long tubular chips, some shorter tubular chips, and flat spiral chips were produced at conventional cooling, while only short tubular chips and flat spiral chips were produced at a pressure level of $p = 3$ bar. With further increase of the pressure level, only spiral chips were present. When increasing the feed to $f = 0.15$ mm/r the chips, as shown in Fig. 9, became shorter independent of the cutting fluid supply pressure level. For tool CB at pressure levels of $p = 24$ bar, $p = 55$ bar, and $p = 77$ bar only short tubular chips were present, for tool F only flat spiral chips were produced. Macroscopically no difference between the different pressure levels was visible. At a feed of $f = 0.2$ mm/r, there was macroscopically no difference visible at different pressure levels. When using tool CB short tubular chips and some conical spiral chips were produced, while only flat spiral chips were produced when using tool F. Table 5 gives an overview and examples



Fig. 9 Overview of chips produced in the cutting of the three workpiece materials at $f = 0.15$ mm/r

Table 5 Explanation of chip forms detected while cutting the three different alloys at different feeds and cutting fluid supply pressures

Chip form according to ISO 3685	Number according to ISO 3685	Characteristics	Example	Pictogram
Flat spiral chips	3.1	<ul style="list-style-type: none"> • Varied in diameter • Varied in number of windings 		
Conical spiral chips	3.2	<ul style="list-style-type: none"> • Varied in diameter • Varied in number of windings 		
Long washer-type helical chips	4.2	<ul style="list-style-type: none"> • Long unbroken type • Loosely coiled 		
Long conical helical chips	5.1	<ul style="list-style-type: none"> • Long unbroken type • Tightly coiled 		
Short conical helical chips	5.2	<ul style="list-style-type: none"> • Shorter, tightly coiled 		
Snarled conical helical	5.3	<ul style="list-style-type: none"> • Long, curled and snarled 		
Loose ark chips	6.2	<ul style="list-style-type: none"> • Shortly broken chip fragments 		

of all chip forms according to ISO 3685 detected during the cutting experiments. Based on this systematic chip forms were evaluated and overviews with pictograms were created. The drawings of the chips are not true to scale. It is visible from Table 6 how chip forms change with increasing cutting fluid supply pressure level and feed, as described above. Chip

forms are overall more favorable using tool CB. While the chips at low feed and pressure levels are mainly long conical helical chips, chips at higher feed and pressure level turn into short conical helical chips and flat or conical spiral chips. Tool F seems to produce more spiral chips, while tool CB produces more conical helical chips. That can be explained

Table 6 Overview of chip forms produced in CuZn37 according to ISO 3685































Cutting fluid pressure level		Conventional Cooling		3 bar		24 bar		55 bar		72 bar	
		Tool CB	Tool F	Tool CB	Tool F	Tool CB	Tool F	Tool CB	Tool F	Tool CB	Tool F
<i>f</i> [mm/r]	0.10										
	0.15										
	0.20										

Table 7 Overview of chip forms produced in CuZn38As according to ISO 3685

Cutting fluid pressure level		Conventional Cooling		3 bar		24 bar		55 bar		72 bar		
		Tool	CB	F	CB	F	CB	F	CB	F	CB	F
<i>f</i> [mm/r]	0.10											
	0.15											
	0.20											

by the chip-breaking geometry, forcing the chip to flow in a certain direction.

In **CuZn38As** regardless of the feed and tool only a slight impact of pressures above $p = 55$ bar was visible by some shorter chips, but mainly long tubular chips were produced, as shown in Fig. 9 for a feed of $f = 0.15$ mm/r. Table 7 gives a schematic overview of all chip forms produced. Similar to Table 6, chip forms are determined according to ISO 3685 and Table 5. In CuZn38As predominantly long helical chips were produced regardless of tool type, feed, or cutting fluid supply pressure level. At a feed of $f = 0.10$ mm/r at a pressure of $p = 55$ bar for both tools and at a pressure of $p = 24$ bar for tool CB snarled conical helical chips were produced. Furthermore, at a feed of $f = 0.15$ mm/r and pressure of $p = 72$ bar tool CB produced only short conical helical chips, which was overall the best result regarding chip form for CuZn38As.

For **CuZn42**, cut with a feed of $f = 0.1$ mm/r, the chips became smaller when cutting with tool CB. For tool F and for a pressure of $p \leq 24$ bar no chip breakage occurred, while at $p = 55$ bar and $p = 72$ bar chip breakage occurred and chips at $p = 72$ bar were visible shorter than at $p = 55$ bar. At a feed of $f = 0.15$ mm/r chip breakage occurred at all pressure levels. At higher pressure levels and for tool CB the chips became shorter, similar to the feed of $f = 0.2$ mm/r.

A schematic overview of chip forms for all pressure levels and feed rates is given in Table 8. Here, the aforementioned effects are visible. Additionally, it is shown, that tool F only produced flat spiral chips, when chip breakage occurred. A similar trend was seen in Table 6 for CuZn37. Since CuZn42 shows flat spiral chips for both tools, this behavior might be explained by the microstructure rather than the different tool geometries.

In summary, for cutting CuZn42 with tool CB and at higher feeds, a high-pressure cooling supply seems to be not necessary to achieve chip breakage. When cutting CuZn37 or CuZn38As probably a combination of high pressure, chip-breaking geometry, and high feed will lead to better chip breakage. The positive effect of high-pressure cutting fluid supply on the chip breakability is already well documented in the literature for various materials, for example for hardened and alloyed steel [14–16], where usually higher pressure levels are used.

The chip thickness ratio λ_h describes the ratio between the chip thickness h' and the undeformed chip thickness h . It can be calculated by the formula

$$\lambda_h = h'/h. \tag{2}$$

The undeformed chip thickness h in radial cutting operations equals the feed f . A higher chip thickness ratio means

Table 8 Overview of chip forms produced in CuZn42 according to ISO 3685

Cutting fluid pressure level		Conventional Cooling		3 bar		24 bar		55 bar		72 bar		
		Tool	CB	F	CB	F	CB	F	CB	F	CB	F
<i>f</i> [mm/r]	0.10											
	0.15											
	0.20											

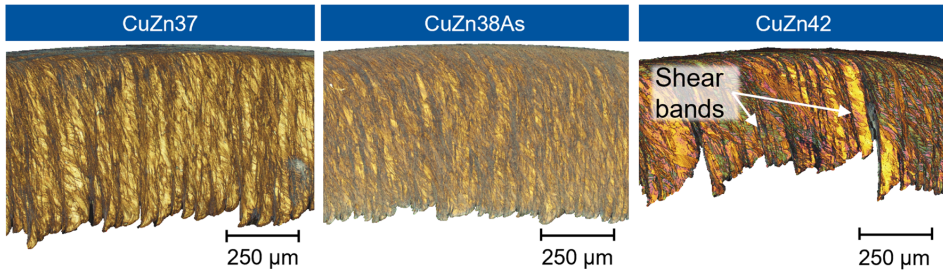


Fig. 10 Optical Micrographs of the Chips for $f = 0.15 \text{ mm/r}$; $p = 72 \text{ bar}$; Tool CB for the brass alloys CuZn37 (a), CuZn38As (b), and CuZn42 (c)

more deformation of the chip happens during the cutting process. This can indicate higher friction in the secondary shear zone due to less thermal softening effects [24]. The chip thickness ratio was measured by means of a microscope as described above.

In **CuZn37**, tool F showed a slightly higher chip thickness ratio. For both tools, a higher feed led to a lower chip thickness ratio. Based on the expectation that more cutting fluid reaches the tool-chip contact at a higher cutting fluid supply pressure, better cooling of the tool-chip contact was expected. This would lead to a lower degree of thermal softening and more work hardening. Therefore, it was expected to see higher chip thickness compression ratios at higher cutting fluid supply pressures. On the contrary, for most of the feed and tool combinations, the chip thickness ratio decreased with increasing cutting fluid pressure. This might be explained by lower friction in the secondary shear zone due to better lubrication by the cutting fluid penetrating the secondary shear zone better when applied with higher pressure levels thereby removing the chip earlier from the tool-chip interface. However, the calculated force ratio does not confirm this explanation. For tool CB, the force ratio was lowest at conventional cooling and pressure of $p = 72 \text{ bar}$, while it was slightly higher for all other pressure levels. For tool F, the force ratio increased slightly with the cutting fluid supply pressure. The force ratio only gives an indication of the friction conditions in the cutting zone. A measurement of the friction by a dedicated method, for example, described in Nobel et al. [20] could be used to investigate this phenomenon further.

In **CuZn38As** the chip thickness ratio was lower for tool CB. This can be explained by the higher cutting edge radius and the slightly decreased rake angle of tool F. Here, for none of the tools a general trend regarding the feed or the pressure of cutting fluid supply was visible. For **CuZn42**, the chip thickness ratio was higher for tool F. Here, similar to CuZn37, the chip thickness ratio decreased when increasing the feed.

Overall, chip thickness ratios for CuZn37 and CuZn38As were comparable, ranging between $1.6 < \lambda_h < 2.5$ and

$1.5 < \lambda_h < 2.75$, respectively, while chip thickness ratios for CuZn42 measured with the light microscope ranged between $1.25 < \lambda_h < 2.25$. The homogenous and highly ductile face-centered cubic (fcc) α -phase microstructure of CuZn37 and CuZn38As led most likely to higher friction in the secondary shear zone, while CuZn42 contains more of the harder body-centered cubic (bcc) β -phase, reducing the friction and thereby the chip thickness ratio. Similar behavior was reported by Nobel et al. [24] for CuZn38As and CuZn41.5 with varying lead contents. However, the force ratio for CuZn38As was lower than for CuZn37 and CuZn42. The force ratio is not only dependent on the friction in the cutting zone but also on the geometry of the cutting edge. As the cutting edge radius varies between the different tools, a direct comparison is not reasonable. Further investigations are necessary to fully interpret these results.

Figure 10 displays longitudinal microsections of each material to analyze the chip shape and chip segmentation in detail. The chips shown were produced using the tool with chip-breaking geometry, a feed rate of $f = 0.15 \text{ mm/r}$, and maximum cutting fluid supply pressure of $p = 72 \text{ bar}$. The degree of chip G_s segmentation was calculated by the formula

$$G_s = \frac{h'_{max} - h'_{min}}{h'_{max}}, \tag{3}$$

where h'_{max} is the thickness of the chip at a peak and h'_{min} is the chip thickness at a valley as shown in Fig. 11. Figure 12 shows considerable differences among the materials regarding the degree of chip segmentation. As previously

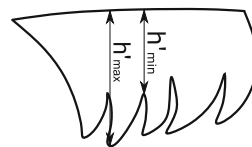


Fig. 11 Visualization of the measurement of h'_{max} and h'_{min}

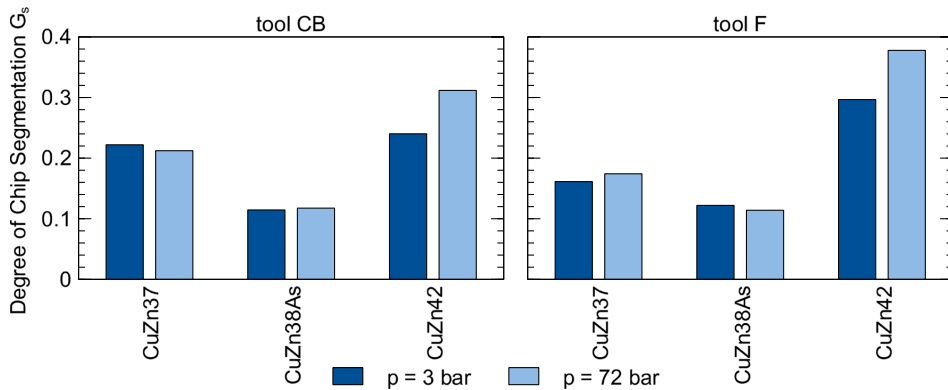


Fig. 12 Degree of chip segmentation for the highest and lowest pressure level in all materials and with both tools for a feed of $f = 0.15$ mm/r measured in the prepared microsections of the chips

determined by the light microscope investigations, the chip thickness ratio for CuZn42 was lower than for CuZn37 and CuZn38As. Regardless of the cutting fluid supply pressure and tools used, the degree of chip segmentation G_s was highest for CuZn42 and varied in the $0.24 < G_s < 0.38$ range for the parameter combinations studied. This was clearly visible by distinct shear bands through the whole thickness of the chip, as indicated in Fig. 10. For CuZn37, the degree of chip segmentation was in the range of $0.16 < G_s < 0.22$. Here, shear bands were less distinct but still visible. The chips of CuZn38As had the lowest degree of segmentation in the range of $0.11 < G_s < 0.12$. The less distinct shear bands in the micrograph of the chips from CuZn38As support that. These differences can be primarily explained by the differences in the elongation after the fracture of the three test materials, Table 2. With increasing elongation after fracture, the material can withstand higher degrees of deformation before a fracture occurs. As a result, the material with higher elongation after fracture is more resistant to cracks in the chip or chip segmentation during the chip formation process. This explanation is supported by comparing the elongation after the fracture of the materials, given in Table 2, with the degrees of chip segmentation G_s , shown in Fig. 12. Only minor material-specific differences are noticeable when analyzing the influence of cutting fluid supply pressure and tool geometry. The impact of these two factors is negligible for the alloys CuZn37 and CuZn38As with a low degree of chip segmentation. For CuZn42 with an overall higher degree of segmentation, the degree of chip segmentation G_s increases with higher cutting fluid supply pressure and when using the tool CB. These results can be attributed to a higher degree of deformation on the chip at a higher pressure and when interacting with the chip groove. In summary, it seems like the chip formation was only to a minor extent influenced by the pressure of the cutting fluid supply and the geometry of

the cutting tool. Nevertheless, the high-pressure cutting fluid as well as the chip-breaking geometry of tool CB showed a macroscopic effect leading to shorter chips.

3.3 Surface roughness

The surface roughness was $Ra = 0.27\mu\text{m}$ ($\sigma = 0.009$) for CuZn37 with tool CB and $Ra = 0.19\mu\text{m}$ ($\sigma = 0.006$) for tool F. For CuZn38As, the surface roughness was $Ra = 0.25\mu\text{m}$ ($\sigma = 0.015$) and $Ra = 0.35\mu\text{m}$ ($\sigma = 0.020$), respectively. For CuZn42 it was measured $Ra = 0.29\mu\text{m}$ ($\sigma = 0.027$) for tool F and $Ra = 0.4\mu\text{m}$ ($\sigma = 0.044$) for tool CB. The measurements were similar for each material, and tool, and across all pressure levels and feeds. There are no systematic impacts by the feed or the pressure visible. This can be explained by the geometry and conditions of the radial cutting process, where the cutting edge is not moved parallel to the workpiece's axis of rotation. The surface roughness was evaluated parallel to the axis of rotation. Presumably, micro defects of the cutting edge determined the roughness, rather than process conditions. This is supported by the roughness profiles recorded, which had similar shapes for the same tool despite different cutting parameters applied. Furthermore, the influence of the alloy can neither be confirmed nor denied, since every alloy was cut with a new tool with unique micro defects at the cutting edge. Therefore, it was decided to not analyze the surface roughness further in this paper.

4 Conclusion

The impact of high-pressure cutting fluid supply and tool geometry on the machinability of the lead-free brass alloys CuZn37, CuZn38As, and CuZn42 was investigated.

First, the cutting forces and force ratios were analyzed. The feed had the highest impact on the cutting forces, while the impact of the pressure was low for CuZn38As and neglectable for CuZn42 and CuZn37.

The cutting forces were the lowest in CuZn38As. CuZn38As showed a minimum cutting force at a cutting fluid supply pressure level of $p = 24$ bar, likely due to a combination of strain hardening and thermal softening effects. Further investigation is needed to verify this explanation. Both CuZn37 and CuZn42 showed increased cutting forces when changing from tool CB to tool F. The increase was explained by the different tool geometries. The MANOVA supports the result that mainly the alloy and the feed will influence the cutting force. Future research should take the interaction of the chip-breaking geometry with the feed level into consideration.

Force ratios in CuZn38As were lower compared to values reported in the literature when using a conventional cutting supply strategy. The high-pressure cutting fluid supply likely lowered the adhesion tendency of the alloy described in the literature. However, CuZn42 showed similar force ratios as compared to the literature. Here, the adhesion tendency of the alloy is lower due to the beta-phase, which might lower the impact of the cutting fluid supply strategy on the force ratio. For CuZn37, the pressure level seems to have a negligible influence on the force ratio.

The chip forms produced varied depending on the alloy, the feed, the tool, and the pressure level. In CuZn37, a higher feed led to shorter chips. The impact of the pressure level was more predominant with tool F and at lower feed levels as chips became shorter with increasing pressure. In CuZn38As, predominantly long tubular chips were produced regardless of tool, pressure, or feed. The shortest chips were produced when using a feed of $f = 0.15$ mm/r, a pressure of $p = 72$ bar and tool CB. However, cutting forces were lowest at a pressure level of $p = 24$ bar for tool CB and CuZn38As. In CuZn42, tool CB led to better results, especially at a feed of $f = 0.10$ mm/r. Chips became shorter when increasing the pressure and at a feed of $f = 0.20$ mm/r loose arc hips were produced when using tool CB and pressures $p \geq 24$ bar. In summary, CuZn38As and CuZn37 should be cut using tool CB, a high feed, and a high pressure regarding chip breakability. In CuZn42 a high feed and tool CB can already lead to an acceptable result. Taking into account the results from chip thickness ratio and degree of chip segmentation investigations, only minimal effects of the tool geometry and the pressure level were visible. Regarding the surface roughness, no conclusion could be drawn.

Increased pressure levels seem to be most beneficial when aiming for short chips. On the contrary, a high-pressure cutting fluid supply requires more energy the higher the pressure is. Additional effects, as visible in CuZn38As for tool CB, lead to increased cutting forces when the tool-chip contact is

cooled too much. A medium-high cutting fluid supply pressure at $p = 24$ bar with an adapted chip-breaking geometry for high-pressure cutting fluid supply and brass alloys might be optimal. Further research is needed to fully understand the effects acting in the alloy during high-pressure cutting fluid supply and optimize the chip breakability. Additionally, varying the size of the nozzle diameter and the point of impact on the cutting insert could be interesting to optimize the effect of high-pressure cutting fluid supply.

Acknowledgements Magdalena S. Müller and Knut Sørby thank the Research Council of Norway for support through the research project LOBUS - Low Lead Brass for Sustainable Community Development (RCN Project. No. 296054).

Author Contributions This work is the result of a cooperation between the Department of Mechanical and Industrial Engineering (MTP) at NTNU and the Laboratory for Machine Tools and Production Engineering (WZL) of RWTH Aachen University. The experimental work was conducted at WZL during a four-month research stay of Magdalena S. Müller. All authors contributed to the study's conception and design. Material preparation, data collection, and analysis were performed by Magdalena S. Müller and Kilian Brans. The first draft of the manuscript was written by Magdalena S. Müller and all authors commented on previous versions of the manuscript. All authors read and approved the final manuscript.

Funding Open access funding provided by NTNU Norwegian University of Science and Technology (incl. St. Olavs Hospital - Trondheim University Hospital). Magdalena S. Müller and Knut Sørby received financial research support from the Research Council of Norway for support through the research project LOBUS - Low Lead Brass for Sustainable Community Development (RCN Project. No. 296054).

Open Access This article is licensed under a Creative Commons Attribution 4.0 International License, which permits use, sharing, adaptation, distribution and reproduction in any medium or format, as long as you give appropriate credit to the original author(s) and the source, provide a link to the Creative Commons licence, and indicate if changes were made. The images or other third party material in this article are included in the article's Creative Commons licence, unless indicated otherwise in a credit line to the material. If material is not included in the article's Creative Commons licence and your intended use is not permitted by statutory regulation or exceeds the permitted use, you will need to obtain permission directly from the copyright holder. To view a copy of this licence, visit <http://creativecommons.org/licenses/by/4.0/>.

References

1. Wegener K, Kuster F, Weikert S, Weiss L, Stirnimann J (2016) Success story cutting. *Procedia CIRP* 46:512–524. <https://doi.org/10.1016/j.procir.2016.04.110>
2. Nobel C, Klocke F, Lung D, Wolf S (2014) Machinability Enhancement of Lead-free Brass Alloys. *Procedia CIRP* 14:95–100. <https://doi.org/10.1016/j.procir.2014.03.018>
3. Johansson J et al (2022) On the function of lead (Pb) in machining brass alloys. *Int J Adv Manuf Technol*. <https://doi.org/10.1007/s00170-022-09205-0>
4. Estelle AA (2016) Drinking water lead regulations: impact on the brass value chain. *Mater Sci Technol* 32:1763–1770. <https://doi.org/10.1080/02670836.2016.1220906>

5. Saglam H, Unsacar F, Yaldiz S (2006) Investigation of the effect of rake angle and approaching angle on main cutting force and tool tip temperature. *Int J Mach Tools Manuf* 46:132–141. <https://doi.org/10.1016/j.ijmactools.2005.05.002>
6. Duan C, Zhang L (2013) A reliable method for predicting serrated chip formation in high-speed cutting: analysis and experimental verification. *Int J Adv Manuf Technol* 64:1587–1597. <https://doi.org/10.1007/s00170-012-4125-0>
7. Puls H, Klocke F, Lung D (2012) A new experimental methodology to analyse the friction behaviour at the tool-chip interface in metal cutting. *Prod Eng Res Devel* 6:349–354. <https://doi.org/10.1007/s11740-012-0386-6>
8. Krolczyk GM et al (2019) Ecological trends in machining as a key factor in sustainable production - A review. *J Clean Prod* 218:601–615. <https://doi.org/10.1016/j.jclepro.2019.02.017>
9. Machado AR, Wallbank J (1994) The Effects of a High-Pressure Coolant Jet on Machining. *Proc Inst Mech Eng B J Eng Manuf* 208:29–38. https://doi.org/10.1243/PIME_PROC_1994_208_057_02
10. Crafoord R, Kaminski J, Lagerberg S, Ljungkrona O, Wretland A (1999) Chip control in tube turning using a high-pressure water jet. *Proc Inst Mech Eng B J Eng Manuf* 213:761–767. <https://doi.org/10.1243/0954405991517191>
11. Courbon C et al (2009) Investigation of machining performance in high-pressure jet assisted turning of Inconel 718: An experimental study. *Int J Mach Tools Manuf* 49:1114–1125. <https://doi.org/10.1016/j.ijmactools.2009.07.010>
12. Braham-Bouchnak T, Germain G, Morel A, Furet B (2015) Influence of high-pressure coolant assistance on the machinability of the titanium alloy Ti555-3. *Mach Sci Technol* 19:134–151. <https://doi.org/10.1080/10910344.2014.991029>
13. Sharma VS, Dogra M, Suri NM (2009). Cooling techniques for improved productivity in turning. <https://doi.org/10.1016/j.ijmactools.2008.12.010>
14. Kramar D, Krajnik P, Kopac J (2010) Capability of high pressure cooling in the turning of surface hardened piston rods. *J Mater Process Technol* 210:212–218. <https://doi.org/10.1016/j.jmatprotec.2009.09.002>
15. Klocke F, Lung D, Krämer A, Cayli T (2013) Sangermann, H?: Potential of modern lubricoolant strategies on cutting performance. *Key Eng Mater* 554–557:2062–2071. <https://doi.org/10.4028/www.scientific.net/KEM.554-557.2062>
16. Globočki Lakić G, Sredanović B, Kramar D, Kopač J (2017) Possibilities of application of high pressure jet assisted machining in hard turning with carbide tools. *Tribol Indust* 39:238–247 <https://doi.org/10.24874/ti.2017.39.02.11>
17. Sangermann H (2013) Hochdruck-Kühlschmierstoffzufuhr in der Zerspanung. Ph.D. thesis. RWTH Aachen University. <http://publications.rwth-aachen.de/record/229480?ln=de>
18. Klocke F, Nobel C, Veselovac D (2016) Influence of tool coating, tool material, and cutting speed on the machinability of low-lead brass alloys in turning. *Mater Manuf Processes* 31:1895–1903. <https://doi.org/10.1080/10426914.2015.1127944>
19. Toulfatzis A, Pantazopoulos G, David C, Sagris D, Paipetis A (2018) Machinability of eco-friendly lead-free brassalloys: cutting-force and surface-roughness optimization. *Metals* 8:250. <https://doi.org/10.3390/met8040250>
20. Nobel C, Hofmann U, Klocke F, Veselovac D, Puls H (2015) Application of a new, severe-condition friction test method to understand the machining characteristics of Cu-Zn alloys using coated cutting tools. *Wear* 344–345:58–68. <https://doi.org/10.1016/j.wear.2015.10.016>
21. Toulfatzis A, Pantazopoulos G, David C, Sagris D, Paipetis A (2018) Final heat treatment as a possible solution for the improvement of machinability of Pb-free brass alloys. *Metals* 8:575. <https://doi.org/10.3390/met8080575>
22. Moriarty M, Wu Y, Murray T, Hutchinson C (2021) The effect of phase fraction, size and shape on the dezincification of duplex brasses. *Corros Sci* 184:109366. <https://doi.org/10.1016/j.corsci.2021.109366>
23. Toulfatzis AI, Pantazopoulos GA, Besseres GJ, Paipetis A (2016) S: Machinability evaluation and screening of leaded and lead-free brasses using a non-linear robust multifactorial profiler. *Int J Adv Manuf Technol* 86:3241–3254. <https://doi.org/10.1007/s00170-016-8435-5>
24. Nobel C, Hofmann U, Klocke F, Veselovac D (2015) Experimental investigation of chip formation, flow, and breakage in free orthogonal cutting of copper-zinc alloys. *Int J Adv Manuf Technol* 84:1127–1140. <https://doi.org/10.1007/s00170-015-7749-z>
25. Lung D, Nobel C, Klocke F (2013) Entwicklung einer Hochleistungserspanung für schwererspanbare bleifreie Kupferknet- und -gusslegierungen : Schlussbericht der Forschungsstelle(n) Nr. 1, Werkzeugmaschinenlabor (WZL) der RWTH Aachen zu dem über die AiF im Rahmen des Programms zur Förderung der Industriellen Gemeinschaftsforschung und -entwicklung (IGF) vom Bundesministerium für Wirtschaft und Technologie aufgrund eines Beschlusses des Deutschen Bundestages geförderten Vorhaben IGF16867 N ; (Bewilligungszeitraum: 01.01.2011). Tech. Rep Werkzeugmaschinenlabor der RWTH Aachen, Aachen <http://publications.rwth-aachen.de/record/230384/files/4856.pdf>
26. Albrecht P (1960) New developments in the theory of the metal-cutting process: part I. The Ploughing Process in Metal Cutting. *J Eng Industry* 82:348–357. <https://doi.org/10.1115/1.3664242>
27. Laakso SV, Hokka M, Niemi E, Kuokkala V-T (2013) Investigation of the effect of different cutting parameters on chip formation of low-lead brass with experiments and simulations. *Proc Inst Mech Eng B J Eng Manuf* 227:1620–1634. <https://doi.org/10.1177/0954405413492732>
28. Zoghiipour N, Tascioglu E, Celik F (2022) Kaynak, Y The influence of edge radius and lead content on machining performance of brass alloys. *Procedia CIRP* 112:274–279. <https://doi.org/10.1016/j.procir.2022.09.084>

Publisher's Note Springer Nature remains neutral with regard to jurisdictional claims in published maps and institutional affiliations.

Authors and Affiliations

Magdalena Susanne Müller¹  · Kilian Brans² · Markus Meurer² · Knut Sørby¹ · Thomas Bergs^{2,3}

Kilian Brans
k.brans@wzl.rwth-aachen.de

Markus Meurer
m.meurer@wzl.rwth-aachen.de

Knut Sørby
knut.sorby@ntnu.no

Thomas Bergs
t.bergs@wzl.rwth-aachen.de

¹ Department of Mechanical and Industrial Engineering,
Norwegian University of Science and Technology, Richard
Birkelands vei 2B, 7491 Trondheim, Norway

² Laboratory of Machine Tools and Production Engineering
(WZL), RWTH Aachen University, Campus-Boulevard 30,
52074 Aachen, Germany

³ Fraunhofer Institute for Production Technology IPT,
Steinbachstr. 17, 52074 Aachen, Germany

Paper V

Müller, M. S., & Sørby, K. (2023a). Investigation on chip breakability in lead-free brass alloy CW511L using different chip breaking geometries. *Intelligent Computation in Manufacturing Engineering-CIRP ICME'23 (in press) Procedia CIRP*

This paper was presented at the CIRP ICME '23 in Naples, Italy. It is accepted for publication in Procedia CIRP

Components manufactured from brass alloys are widely used in plumbing systems. Traditionally, lead is added to the alloy to improve the machinability. In recent years, the use of lead has been restricted due to health and environmental concerns. New lead-free and low-lead alloys were developed. These alloys usually show a higher cutting force compared to traditional lead-containing brasses. This paper investigates the influence of different rake angles and tool coating on cutting force and chip formation. The two lead-free brass alloys, CW511L and CW724R, are compared to the low-lead brass CW625N.

17th CIRP Conference on Intelligent Computation in Manufacturing Engineering

Investigations on chip breakability in lead-free brass alloy CW511L using different chip breaking geometries

Magdalena Susanne Müller^a, Knut Sørby^{a*}

^aDepartment of Mechanical and Industrial Engineering, Norwegian University of Science and Technology, Richard Birkelands vei 2B, 7491-Trondheim, Norway

* Corresponding author. E-mail address: knut.sorby@ntnu.no

Abstract

Brass is an alloy of copper and zinc, commonly alloyed with lead. Due to legal restrictions, the lead-content is decreasing nowadays. This leads to higher cutting forces and worse chip breakability. To face these challenges, adapted tool geometries were investigated. To decrease cutting forces, positive rake angles can be utilized. On the other hand, this will lead to worse chip breakability in single phase lead-free brass alloys. Therefore, chip breaking geometries are necessary. This paper investigates and compares different forms of chip breaking geometries to improve chip breakability when using highly positive rake angles in lead free brass alloy CW511L.

© 2023 The Authors. Published by ELSEVIER B.V. This is an open access article under the CC BY-NC-ND license (<https://creativecommons.org/licenses/by-nc-nd/4.0>)

Peer-review under responsibility of the scientific committee of the 17th CIRP Conference on Intelligent Computation in Manufacturing Engineering, 12-14 July, Gulf of Naples, Italy

Keywords: lead-free brass, machining, chip breaking geometry

1. Introduction

Copper-zinc alloys were traditionally alloyed with lead to improve the machinability. Due to new legal restrictions, the permitted amount of lead in brass decreased to date and is likely to decline even further. Since then, lead-free, and low-lead brass alloys are being developed and analyzed. Usually, these alloys show lower machinability, indicated by higher cutting forces, increased tool wear, and worse chip breakability.

One of these alloys is CW511L (CuZn38As) which is characterized by almost pure α -phase microstructure. It usually shows high cutting forces compared to leaded brass alloys, longer chips with higher chip compression and lower segmentation, higher cutting temperatures, higher abrasive and adhesive tool wear, and worse workpiece quality due to burrs and breakouts of the workpiece material due to adhesion to the

tool. These phenomena can be explained by increased ductility and the pure α -phase microstructure. [1], [2].

Research on how lead improves machinability has shown that the tool-chip contact length and the friction coefficient in leaded brass are lower than lead-free brass alloys. Usually, lead is segregated as globules around the grain boundaries in the microstructure of brasses. While cutting, the globules elongate to a flake-like structure and act as crack initiation points. Therefore, Johansson et al. suggest focusing on chip formation over tribological properties in the research of brass alloys [3].

An increased rake angle will minimize cutting forces in turning processes, but on the other hand, it will increase the chip length [4], [5].

Nobel et al. found that CW511L does not show chip breakage when cutting with a flat carbide tool. Due to the high chip compression and chip upward curl radius Nobel et al. recommended using a high chip breaker land width and a lower

back angle. The tools used in the study by Nobel et al. had a groove type chip former [6].

In chip breakers of the groove type it is crucial that the chip-breaker land width l is shorter than the chip tool contact. If so, the chip will flow in the groove and will be deformed by the chip breaker. The groove radius r needs to have a suitable size. If it is too small, the chip will not follow the curvature [7].

This paper compares the influence of four different groove-type chip-breaking geometries to a tool with a flat rake face on the cutting of CW511L alloy. All tools had a rake angle of 20° , while the chip-breaker land width and the groove radius were varied. Cutting forces and chips were investigated.

2. Materials and methods

The brass alloy used in this study is CW511L. The chemical composition and mechanical properties can be found in Table 1 and Table 2, respectively. The material was supplied as extruded rods and had a diameter of 32 mm. The microstructure presents as an almost pure α -phase, as shown in Figure 1.

Table 1 Chemical composition of CW511L alloy.

Element	Cu	Zn	Pb	Sn	Fe	Ni	As
Percentage	63.2	36.6	0.04	0.01	0.07	0.01	0.02

Table 2 Mechanical Properties of CW511L alloy.

Tensile Strength R_m [MPa]	Yield Strength $R_{p0.2}$ [MPa]	Elongation to Break A [%]	Brinell Hardness [HBW]
354	296	56	82.6

All rods were turned to a diameter of 31.5 mm in preparation for the experiments. Then grooves of 5 mm in width and 9 mm in depth were cut into the bars. This preparation left 4 mm wide discs. The discs were cut in a radial grooving operation during the tests. This principle was used to minimize the influence of the tool edges and get a process closer to orthogonal cutting. A Kistler dynamometer (type 9257B) was used on a Weiler Commodor 230 VCD conventional lathe to measure the cutting forces. Table 3 gives an overview of the cutting parameters in this study. The experiments were performed fully factorial.

Table 3 Cutting parameters used.

Cutting speed v_c [m/min]	Feed f_n [mm/rev]	Cutting width a_p [mm]
150	0.05	3
	0.10	
	0.16	

The cutting inserts were custom ground N123H2-0520-0002-BG H13A blanks by Sandvik Coromant. All inserts were ground to have a rake angle of 20° . One insert had a flat rake face for comparison, while the other had a groove-shaped chip breaker. The groove radius r and the chip-breaker land width l formed the chip breakers. The groove radius and the land width were varied for different inserts, as shown in Figure 2 and

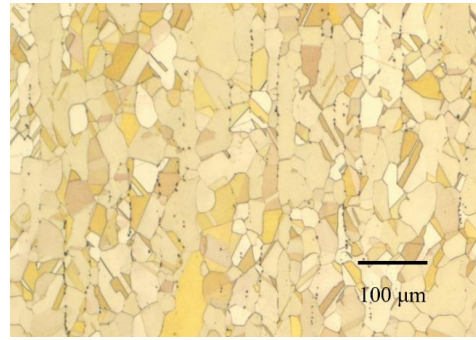


Figure 1 Microstructure of CW511L alloy used in this study.

Table 4. The inserts were evaluated with an Alicona microscope using focus variation and scanning the actual geometry and the cutting edge quality. For results of the measurements of the tools, see Table 5. Tool #4 did not fulfill the requirement of a rake angle of 20° . However, it was included in the tests to additionally study the impact of the rake angle on the chip breakability and the cutting forces. After each cutting experiment, the chips were collected for further evaluation. An ANOVA was performed using Minitab software.

Table 4 Parameters used for chip formers.

Insert Number	l [mm]	r_G [mm]
1	4.0	0.0
2	0.5	4.0
3	1.0	3.0
4	1.5	2.0
5	2.0	1.5

Table 5 Geometrical specifications of the cutting inserts measured with the ALICONA microscope.

Insert Number	Rake angle γ [°]	l [mm]	r [mm]	Cutting edge radius [μm]
1	20.6	1.8	2.5	58
2	20.4	1.1	3.1	34
3	20.2	0.7	3.5	31
4	11.8	-	5.7	14
5	20.8	3.5	0.6	18

3. Results and discussion

After the tests, the average main cutting forces were calculated from the three repetitive measurements. Figure 3 gives an overview of these average main cutting forces. Additionally, the force ratio was calculated. The force ratio is the ratio between the force parallel to the rake face F and the force normal to the rake face F_N . The measured cutting force F_c

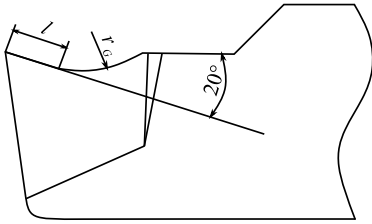


Figure 2 Schematic drawing of the insert with the groove shaped chip former characterized by the chip-breaker land width l and the groove radius r .

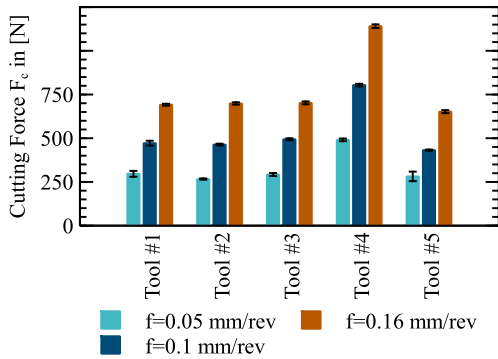


Figure 1 Cutting forces measured during machining of CW511L with the different tools.

and feed forces F_f were rotated with the measured rake angle of the tool used to calculate these forces. This calculation was done by the expression

$$\begin{pmatrix} F \\ F_N \end{pmatrix} = \begin{bmatrix} \cos \gamma & \sin \gamma \\ -\sin \gamma & \cos \gamma \end{bmatrix} \cdot \begin{pmatrix} F_f \\ F_c \end{pmatrix} \quad (1)$$

where γ is the rake angle. The force ratio indicates the friction conditions in the cutting zone. However, it is not the same as the coefficient of friction [1], [8]. The force ratio is plotted in Figure 4.

The measured cutting forces were similar for tools #1, #2 and #3. Tool #4 showed a remarkably higher main cutting force which can be explained by the lower rake angle. On the other hand, tool #5 showed a slightly lower main cutting force which can be attributed to the lower cutting edge radius [9] compared to tools #1, #2, and #3, see Table 5. The force ratios overall showed a behavior like the cutting forces, as the force ratios were highest for tool #4 and similar for tools #1, #2, and #3, while the reference tool #5 showed slightly lower force ratios. Nevertheless, the force ratios typically decreased with an increase in the feed. That might be attributed to better chip breakability at higher feed rates and shorter tool-chip contact lengths.

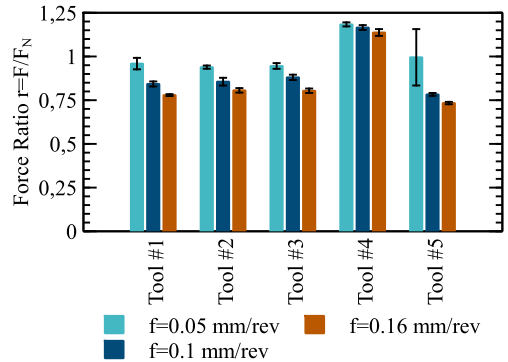


Figure 4 Force ratios calculated from cutting forces measured during cutting of CW511L.

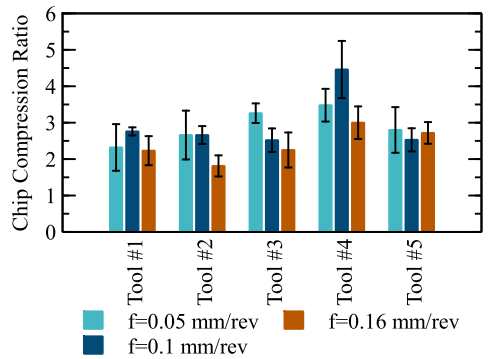


Figure 5 Chip compression ratios of CW511L using different tools.

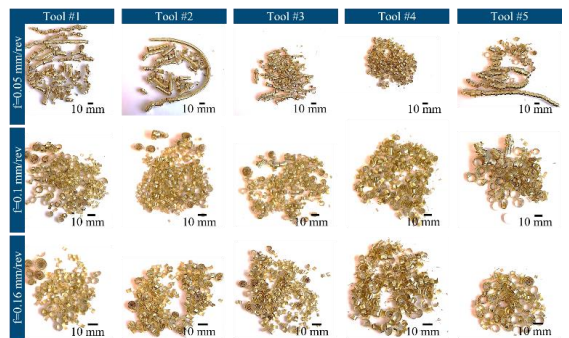


Figure 2 Overview of chips produced during cutting of CW511L with the different tools.

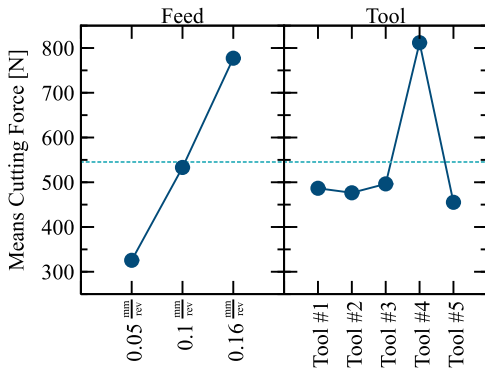


Figure 3 Main effects plot for the main cutting force.

Figure 5 shows the chip compression ratios calculated from the measurements of the chip thickness in the microscope. The values of the chip compression ratio deviate, which is due to the varying chip thickness. Nevertheless, the chip compression ratio is usually the smallest for the highest feed. Tool #4 shows the highest chip compression ratio for each feed rate, which can be explained by the increased rake angle of this tool. The chip compression ratio indicates the degree of plastic deformation of the chip [10]. For example, Tool #3 shows slightly higher chip compression ratios than the other tools. Additionally, the cutting forces measured with Tool #3 are marginally higher than for tools #1 and #2. More energy used to deform the chip can explain that. A more deformed chip will usually be more brittle and break more easily. Most likely, the radius of the chip-breaking geometry groove of tool #3 is big enough, while the groove of tools #1 and #2 are too small, which leads to the chip not following the chip breaker contour [7].

Figure 6 presents an overview of the chips produced during machining with the different tools. It is noticeable that a higher feed leads to shorter chips. Solely tool #4 shows very short chips at the lowest feed of $f_n = 0.05$ mm/rev. That can be attributed to the lower rake angle and higher deformation induced into the chip. Of the other tools, Tool #3 showed the shortest chips at a feed of $f_n = 0.05$ mm/rev. At higher feed rates, the differences become harder to detect, but it is visible that the chip curl radii vary with the tool geometry. Reference Tool #5, for example, shows high chip curl radii, which can be attributed to the missing chip forming geometry and less deformation induced in the chip.

An ANOVA was performed with the measurements of the main cutting force as response variable and tool, feed, and the combination of both as input variables. According to the analyses, all variables lead to statistically significantly different results. The model fit R^2 was 99.78%. The main effects plot is shown in Figure 7. The strong dependence of the main cutting force on the feed becomes visible, as well as the impact of the lower rake angle in Tool #4.

A Tukey pairwise comparison with a confidence level of 95% revealed that the means of all feed values were significantly different, as shown in Table 6. Regarding the tool,

it was shown that tool #4 and #5 were statistically significant different from all other tools, while tool #3 and #1 and tool #1 and #2 were not statistically significant different. Seven statistically significant different groups were found for the combination of the two feed and tool. It is noticeable that Tool#4 has its own groups for feeds of $f_n = 0.16$ mm/rev and 0.1 mm/rev, and the $f_n = 0.05$ mm/rev is in a group with other tools using a feed of $f_n = 0.1$ mm/rev. That clearly can be attributed to the lower rake angle of Tool#4. Especially at a feed of $f_n = 0.16$ mm/rev, there was no statistically significant difference in the cutting force between tools #1, #2, and #3. As there is additionally no macroscopic difference visible in the chips produced with these parameters, see Figure 6, it can be concluded that at higher feeds, the difference between the chip-breaking geometries used in this study is neglectable. At a feed of $f_n = 0.05$ mm/rev and $f_n = 0.1$ mm/rev, tools #1, #2, #3, and #5 are in one group, so there is no statistically significant difference regarding the main cutting force for these parameters. For a feed of $f_n = 0.05$ mm/rev, as shown in Figure 6, the chip length, and the chip compression ratios, see Figure 5, were visibly different. Tool#3 showed the shortest chips and a slightly higher chip compression ratio when compared to the other combinations in this group. For the feed of $f_n = 0.1$ mm/rev, there is hardly any difference visible between tools #1, #2, #3, and the reference tool #5 when considering the chip form as shown in Figure 6, and the chip compression ratio in Figure 5.

To sum it up, as there is no statistically significant difference when it comes to the main cutting force and the combinations of tools #1, #2, and #3 with the three different feed levels used in this study, the macroscopic chip form and the chip compression ratio should be taken into consideration. On the macroscopic scale, the chips produced with tools #1, #2, and #3 at the two higher feed levels did not present visibly different. There are differences noticeable considering the chips produced at a feed of $f_n = 0.05$ mm/rev. Tools #1 and #2 gave overall some longer chips, but additionally some shorter chips. For tool #3, the chips were shorter, and the length was more evenly distributed. The chip compression ratios of tool #3 were slightly higher than those of tools #2 and #3. That means that more energy was used to deform the chip, which could explain the slightly higher mean of the main cutting force for tool #3, see Figure 3. On the other hand, a higher deformation of the chip most likely contributed to the better chip breakability noticed at the lowest feed for tool #3.

Even though none of the presented tool geometries lead to sufficient chip breaking, i.e., comma-shaped chips, tool #3 can be considered the best option when using a rake angle of 20° and aiming to minimize cutting forces.

Table 6 Grouping information using Tukey Post hoc test with a confidence level of 95% for the factors, feed, tool, and feed*tool.

Feed f	0.05		0.1		0.16		
	Tool#4		Tool#3 Tool#1		Tool#1 Tool#2		Tool#5
Feed f * Tool	0.16* Tool#4	0.1* Tool#4	0.16* Tool#3, 0.16* Tool#2, 0.16* Tool#1	0.16* Tool#1, 0.16* Tool#5	0.1* Tool#3, 0.05* Tool#4, 0.1* Tool#1, 0.1* Tool#2	0.1* Tool#1, 0.1* Tool#2, 0.1* Tool#5	0.05* Tool#1, 0.05* Tool#2, 0.05* Tool#3, 0.05* Tool#5

4. Conclusion

A chip-breaking geometry can help with chip breaking in CW511L, while it does not have a significant impact on the main cutting force or force ratio. At lower feed ratios, none of the supposed geometries showed sufficient chip-breaking capabilities, as all chips produced were conical helical, long tubular, or spiral chips. At higher feed ratios, the main effect of the chip-breaking geometries was to form different chip curl radii. The chip-breaking behavior was highly dependent on the feed ratio for all tools.

Tool #3 showed the best chip-breaking capabilities at the lowest feed rate. On the other hand, the average main cutting force and the chip compression ratio were slightly higher for this tool. Tool #4, having a lower rake angle, showed better chip-breaking capabilities at the lowest feed rate, but additionally remarkably higher cutting forces. When increasing the feed rate, the positive effect of the lower rake angle on the chip breakability was minimized, while the average main cutting force still was significantly higher. More research regarding appropriate chip-breaking geometries in the machining of lead-free brass is necessary.

Acknowledgements

The authors thank the Research Council of Norway for supporting this work through the research project LOBUS – Low Lead Brass for Sustainable Community Development (RCN Project. No. 296054).

References

- [1] F. Klocke, C. Nobel, and D. Veselovac, "Influence of Tool Coating, Tool Material, and Cutting Speed on the Machinability of Low-Leaded Brass Alloys in Turning," *Mater. Manuf. Process.*, vol. 31, no. 14, pp. 1895–1903, Oct. 2016, doi: 10.1080/10426914.2015.1127944.
- [2] C. Nobel, F. Klocke, D. Lung, and S. Wolf, "Machinability enhancement of lead-free brass alloys," in *Procedia CIRP*, Jan. 2014, vol. 14, pp. 95–100, doi: 10.1016/j.procir.2014.03.018.
- [3] J. Johansson, P. Alm, R. M'Saoubi, P. Malmberg, J.-E. Ståhl, and V. Bushlya, "On the function of lead (Pb) in machining brass alloys," *Int. J. Adv. Manuf. Technol.*, Apr. 2022, doi: 10.1007/s00170-022-09205-0.
- [4] H. Saglam, F. Unsacar, and S. Yaldiz, "Investigation of the effect of rake angle and approaching angle on main cutting force and tool tip temperature," *Int. J. Mach. Tools Manuf.*, vol. 46, no. 2, pp. 132–141, Feb. 2006, doi: 10.1016/J.IJMACHTOOLS.2005.05.002.
- [5] C. Duan and L. Zhang, "A reliable method for predicting serrated chip formation in high-speed cutting: analysis and experimental verification," *Int. J. Adv. Manuf. Technol.*, vol. 64, no. 9–12, pp. 1587–1597, Feb. 2013, doi: 10.1007/s00170-012-4125-0.
- [6] C. Nobel, U. Hofmann, F. Klocke, and D. Veselovac, "Experimental investigation of chip formation, flow, and breakage in free orthogonal cutting of copper-zinc alloys," *Int. J. Adv. Manuf. Technol.*, vol. 84, no. 5, pp. 1127–1140, Sep. 2015, doi: 10.1007/s00170-015-7749-z.
- [7] G. Boothroyd and W. A. Knight, *Fundamentals of Machining and Machine Tools*, Second Edition, vol. 28. mdi Dekker, 1988.
- [8] P. Albrecht, "New developments in the theory of the metal-cutting process: Part I. the ploughing process in metal cutting," *J. Manuf. Sci. Eng. Trans. ASME*, vol. 82, no. 4, pp. 348–356, Nov. 1960, doi: 10.1115/1.3664242.
- [9] N. Zoghypour, E. Tascioglu, F. Celik, and Y. Kaynak, "The influence of edge radius and lead content on machining performance of brass alloys," in *Procedia CIRP*, 2022, vol. 112, pp. 274–279, doi: 10.1016/j.procir.2022.09.084.
- [10] D. G. Thakur, B. Ramamoorthy, and L. Vijayaraghavan, "Machinability investigation of Inconel 718 in high-speed turning," *Int. J. Adv. Manuf. Technol.*, vol. 45, no. 5–6, pp. 421–429, Nov. 2009, doi: 10.1007/s00170-009-1987-x.

Paper VI

Müller, M. S., & Sørby, K. (2023c). The Effect of Tool Geometry on Chip Formation and Chip Morphology of Lead-Free Brass Alloy CW511L. *Submitted to: Advances in Manufacturing*. <https://doi.org/https://doi.org/10.21203/rs.3.rs-3423897/v1>

This paper is submitted to *Advances in Manufacturing*.

Lead as an alloying element in brass is legally restricted. Investigations to adapt to the properties of lead-free brass alloys in machining are necessary. The main problems in machining lead-free brass alloys are increased cutting forces and long snarled chips. This paper investigates the impact of the rake angle and different chip-breaking geometries on the chip breakability of the lead-free brass alloy CW511L (CuZn38As). Orthogonal cutting tests were conducted on a lathe. Cutting force measurements, chip analysis, and high-speed camera recordings were performed to analyze the cutting process. The camera recordings were used to analyze the chip formation process with tools with varying chip-breaking geometries. Chips were investigated in microscopic studies. An increased rake angle led to increased chip length but decreased cutting forces. A chip-breaking geometry with a restricted contact length could help to counteract the negative impact of a positive rake angle on the chip breakability with only a marginal effect on the cutting forces. It is crucial to choose a chip-breaking geometry following the cutting parameters. Out of the investigated tools, a tool with a chip breaker land width of 0.7 mm and a groove radius of 3.5 mm was the most beneficial regarding the chip breakability.

The Effect of Tool Geometry on Chip Formation and Chip Morphology of Lead-Free Brass Alloy CW511L

Magdalena Susanne Müller^{1*} and Knut Sørby¹

^{1*}Department of Mechanical and Industrial Engineering, Norwegian University of Science and Technology, Richard Birkelands vei 2B, Trondheim, 7491, Norway.

*Corresponding author(s). E-mail(s): magdalena.s.muller@ntnu.no;
Contributing authors: knut.sorby@ntnu.no;

Abstract

Lead as an alloying element in brass is legally restricted. Investigations to adapt to the properties of lead-free brass alloys in machining are necessary. The main problems in machining lead-free brass alloys are increased cutting forces and long snarled chips. This paper investigates the impact of the rake angle and different chip-breaking geometries on the chip breakability of the lead-free brass alloy CW511L (CuZn38As). Orthogonal cutting tests were conducted on a lathe. Cutting force measurements, chip analysis, and high-speed camera recordings were performed to analyze the cutting process. The camera recordings were used to analyze the chip formation process with tools with varying chip-breaking geometries. Chips were investigated in microscopic studies. An increased rake angle led to increased chip length but decreased cutting forces. A chip-breaking geometry with a restricted contact length could help to counteract the negative impact of a positive rake angle on the chip breakability with only a marginal effect on the cutting forces. It is crucial to choose a chip-breaking geometry following the cutting parameters. Out of the investigated tools, a tool with a chip breaker land width of 0.7 mm and a groove radius of 3.5 mm was the most beneficial regarding the chip breakability.

Keywords: lead-free brass, chip formation, chip breaking geometry, rake angle, cutting forces, chip morphology

Acknowledgement

The authors thank the Research Council of Norway for supporting this work through the research project LOBUS – Low Lead Brass for Sustainable Community Development (RCN Project. No. 296054). The authors report there are no competing interests to declare.

1 Introduction

Copper-zinc alloys are commonly alloyed with lead to enhance their machinability. However, new

regulatory standards reduce the permissible lead content for materials used in drinking water systems and other applications. Consequently, the industry has turned its attention to the development and analysis of lead-free and low-lead brass alloys. These alloys exhibit lower machinability compared to their lead-containing counterparts, with higher cutting forces, increased tool wear, and less effective chip breakage [1].

One of these alloys is CW511L (CuZn38As), which is characterized by an almost pure α -phase microstructure. Compared to leaded brass alloys it shows higher cutting forces, longer chips

with higher chip compression and lower segmentation, higher cutting temperatures, and a larger tendency to burr formation. Also, the abrasive and adhesive tool wear is relatively high. These phenomena are explained by the increased ductility and pure face-centered cubic (fcc) α -phase microstructure [2, 3].

Lead brass exhibits a reduced contact length between the tool and chip, along with a lower coefficient of friction, compared to lead-free brass alloys. Lead is present in the form of globules concentrated around grain boundaries. During machining, these globules undergo elongation, forming a flake-like structure that serves as initiation points for cracks. Therefore, Johansson et al. [4] propose that future research on brass alloys should prioritize investigating chip formation rather than focusing solely on tribological properties.

The rake angle is one of the most impactful factors on the tool-chip contact area. Increasing the rake angle minimizes the cutting forces in turning operations. However, it also increases the chip length [5, 6]. There is an optimum value of the rake angle. At this optimum, the tool-chip contact length is reduced, leading to lower cutting forces. Overall, a better surface quality can be expected, using an optimum rake angle. Above the optimum value accelerated tool wear will appear, leading to higher cutting forces, and the tool is weakened when increasing the rake angle [5].

Nobel et al. [7] found that CW511L exhibited no chip breakage when using a carbide tool with a flat rake face. Therefore, they investigated groove-type chip breakers. Due to the high chip compression and upward chip curl radius, Nobel et al. [7] recommended the use of a high chip breaker land width and a lower back angle.

In the case of groove-type chip breakers, the chip breaker land width must be shorter than the chip tool contact. If this is the case, the chip will flow into the groove and be deformed by the chip breaker. The groove radius must be of a suitable size. If it is too small, the chip will not follow the curve [8].

Chip control and efficient chip breaking play a critical role in machining, particularly in turning processes. Effective chip breaking ensures process reliability, high productivity, and operational safety. Long, unbroken chips have the potential to

damage the tool, the machine tool, and the workpiece, or even pose risks to machine operators, resulting in additional costs to the production process. The chip breakability is influenced by various factors, including chip-breaker design, properties of the work material, tool material, tool geometry, process variations, machine tool and operation type, cutting conditions, and the potential use of cutting fluids. Given the complexity of the interactions between these factors, there is still a need for fundamental knowledge in this area [9]. Three basic chip types are continuous, segmented, and elemental chips. Intermediate forms, such as wavy chips, exist. Continuous chips can cause problems with disposal and evacuation from the cutting zone. Intermediate and segmented chips tend to cause fewer issues in this regard [10].

Jawahir and Fang [11] examined tools with varying chip breaker land widths, three different chip groove radii, groove styles, and nose radii, while cutting low, medium, and high carbon steels. Their investigation demonstrated that selecting the appropriate chip-breaking geometry resulted in minimal power consumption. Specifically, shorter land widths, lower grooves, a raised back wall, and a sharp tool consistently yielded the best outcomes in terms of chip breakability.

This paper presents two test series aimed at examining the cutting forces and chip breakability of CW511L. All cutting tests were conducted using radial turning operations to closely approximate orthogonal turning conditions. In the first series, the rake angle was systematically varied, with all tools featuring a flat rake face. In the second test series, the rake angle was held constant while the chip-breaking geometry in the form of groove styles was altered. The chip formation process was analyzed by use of high-speed camera recordings. Both test series involved investigations into cutting forces and chip characteristics.

2 Materials and Methods

2.1 Experimental setup

This study aims to investigate the influence of the tool design on the chip formation process in lead-free brass alloy CW511L (CuZn38As). Orthogonal cutting tests were performed under dry-cutting conditions using a Weiler Commodor 230 VDC conventional lathe. Cutting forces were measured

Table 1 Chemical Composition of CW511L.

Material	Cu	Zn	Pb	Sn	Fe	Ni	As
CW511L	63.2	36.6	0.04	0.01	0.07	0.01	0.02

Table 2 Mechanical Properties of CW511L.

Material	Tensile Strength R_m [MPa]	Yield Strength $R_{p0,2}$ [MPa]	Elongation to Break A [%]	Hardness HB
CW511L	354	296	56	82.6

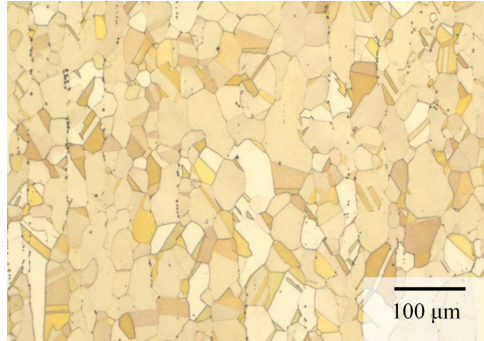
using a Kistler 9257B dynamometer. The chip formation was recorded using a FASTCAM SA3 model 60K-M1 high-speed camera with a frame rate of 4000 fps. The material used for the tests was an extruded rod with a diameter of $d = 32$ mm. Prior to the experiments, the rods were turned to a radial diameter of $d = 31.5$ mm, and grooves were cut into them to produce the disk-shaped elements used in the machining tests. A disk width of 2 mm was used in test series 1, and a disk width of 3 mm was used in test series 2. During the machining tests, a cutting operation similar to a parting-off operation was used on the disks.

2.2 Materials

In all tests, the workpiece material utilized was the lead-free brass alloy CW511L (CuZn38As). The chemical composition of the alloy is provided in Table 1, while Table 2 presents an overview of its mechanical properties. The microstructure of CW511L is depicted in Figure 1, revealing a predominantly face-centered cubic (fcc) α -phase with trace amounts of β -phase and lead. The alloy composition imparts high ductility and low hardness. The only active addition to CW511L alloy is arsenic to improve the dezincification resistance. This alloy has been heat treated to achieve the predominantly α -phase microstructure and make it dezincification resistant.

2.3 Experimental Design

An overview of the experimental design and the machining parameters is given in Table 3. In this study, two series of tests were conducted. In the first series of tests, the rake angle was varied to investigate the influence on the chip formation

**Fig. 1** Microstructure of CW511L Alloy.

process and the cutting forces. The cutting inserts were based on LG123L1-0600-BG H13A uncoated carbide blanks manufactured by Sandvik Coromant. The blanks were ground to different rake angles of 0° , 8° , 16° , and 24° , while the clearance angle was kept constant at 7° . Both uncoated and coated tools were prepared for tests. The coated tools featured a commercial AlTiN-based coating called FerroCon, provided by CemeCon. The general tool geometry of these tools is shown in Table 4. A detailed analysis of the tool geometry is presented by Müller and Sørby [12].

In the second part of this study, custom-ground cutting inserts based on N123H2-0520-0002-BG H13A blanks were investigated. The rake angle on all tools was 20° , but various groove-type chip-breaking geometries were ground in the blanks. The chip breaker land width, l , was varied from 0.7 to 1.8 mm, and the groove radius r_G was varied from 2.5 to 3.5 mm. Additionally, a reference geometry with a chip breaker land width of 3.5 mm and only a very small radius was used. Table 4 shows the combinations that were tested. The tool geometries were verified by using an ALICONA infinite focus microscope using focus variation [13].

The cutting speed v_c was kept constant at $v_c = 150$ mm for all tests in both series. The feed was varied from $f_n = 0.05$ to 0.2 mm/r for test series 1 and from $f_n = 0.05$ to 0.16 mm/r for test series 2. Chips were collected after each cut. Representative chips from the tests were mounted in epoxy and metallographically polished. The chip thickness was measured at several points of these chips

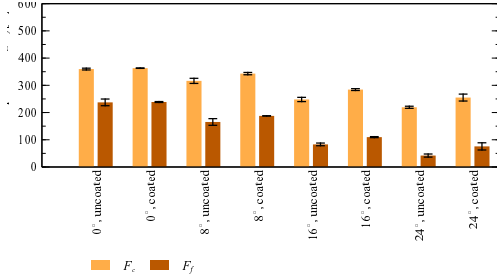


Fig. 2 Cutting Force Components for Tools with Varying Rake Angles and Coating Conditions.

using a light microscope, and the chip thickness ratio and the degree of chip segmentation were calculated.

3 Results and Discussion

3.1 Impact of the Rake Angle on the Cutting Forces and the Force Ratio

Figure 2 shows the cutting force F_c and the feed force F_f for the feed value $f_n = 0.1$ mm/r. The force ratio is the ratio between the force component parallel to the tool's rake face F and the component normal to the tool's rake face F_N and indicates the friction conditions in the cutting zone [3, 14].

When increasing the rake angle, the cutting force and the feed force decreased, particularly for the uncoated tools. Additionally, the cutting forces and the force ratio were overall higher for the coated tools. The roughness of the coated tools was around $0.05 \mu\text{m}$, while the roughness of the uncoated tools was around $0.01 \mu\text{m}$, which could have led to the increase in cutting force components and friction in the cutting zone [12]. The coating is in the literature described to reduce friction in brass [15]. Overall, the cutting force F_c was reduced by 39% in uncoated and by 30% in coated tools when comparing the rake angles of 0° and 24° . The result of decreased cutting forces at increased rake angles was in accordance with the literature [5, 6]. Similar trends were visible at the other investigated feed levels.

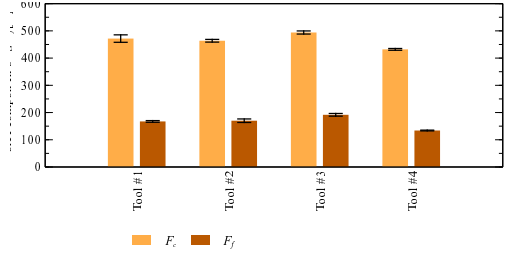


Fig. 3 Cutting Force Components for Tools with Varying Chip Breaking Geometries.

3.2 Impact of the Different Chip-Breaking Geometries on the Cutting Forces

Figure 3 shows the results of the cutting force measurements in series 2 for tools with various chip-breaking geometries and a fixed 20° rake angle. There was only a small variation in the cutting forces visible for the different chip-breaking geometries. Solely the reference geometry without a chip breaker, tool #4, shows a slightly lower main cutting force, feed force, and force ratio.

Overall, the cutting forces in series 2 were increased compared to series 1. Primarily, this is due to the increased depth of cut in test series 2. Additionally, the different tool blank geometries and cutting edge radii might have had a minor impact on the difference in the cutting force components measured. The different geometries of the blanks should be considered. Due to the L-shape of the blanks used in test series 1, the chip could flow free across the rake face as the tool had no tool back behind the tool chip contact. The more standard geometry of the blanks used in series 2 combined with the groove-type chip-breaking geometries might have led to the chip hitting the tool back and increasing the cutting forces. The tool back geometry was present in all tools of test series 2, including reference tool #4.

3.3 Chip Formation

The collected chips were visually categorized into chip forms according to ISO 3685. Additionally, the length and size of the chips were visually compared.

The chip formation was analyzed by means of

Table 3 Overview of the Experimental Design



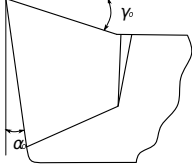
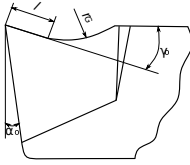




Test series	1	2
Characteristic	Varying rake angle	Varying chip-breaking geometry
Example pictures of the tool geometries		
Schematic drawing of tool geometry		
Rake angle γ_0	$0^\circ, 8^\circ, 16^\circ, 24^\circ$	20°
Clearance angle α_0	7°	7°
Tool material	Uncoated tungsten carbide, AlTiN-coated tungsten carbide	Uncoated tungsten carbide
Cutting speed v_c	150 m/min	150 m/min
Feed f_n	0.05, 0.1, 0.16, 0.2 mm/r	0.05, 0.1, 0.16 mm/r
Depth of cut a_p	2 mm	3 mm

Table 4 Tool Geometries Used in Test Series 2.

Tool	Groove radius r_G [mm]	Land width l [mm]	Cutting edge radius r_{ce} [μ m]	Sketch of the cutting edge
#1	2.5	1.8	58	
#2	3.1	1.1	34	
#3	3.5	0.7	31	
#4 (Reference)	0.6	3.5	18	

embedded, ground, polished, and etched chip sections in an optical microscope. The chip thickness was measured at different points of the chip, and the shape of the chips was analyzed. Figure 4 shows an example of macroscopic chips and embedded and polished chips. In Figure 5 examples of the different microscopical chip forms produced during this study are shown. The produced chips were either segmented, continuous, or intermediate. Some chips contained both, segmented and intermediate parts, as shown in Figure 5 c.

For series 2, additional videos with a high-speed

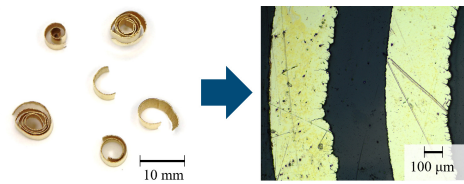


Fig. 4 Macroscopic and Microscopic Picture of the Chips Formed with Tool #3 at a Feed of $f = 0.1$ mm/r.

camera were recorded and analyzed to get a deeper understanding of the chip flow behavior. Chip up-curl radii were measured. In addition, the tool chip contact length in reference tool #4 was measured.

3.3.1 Impact of the Rake Angle on the Chip Formation

The overall macroscopic chip length increased with increasing rake angles and decreasing feeds. Overall, the chips were slightly shorter in the coated tools. In the uncoated tools, short ribbon and flat spiral chips were formed with the 0° tool. With the 8° tool, additionally, conical spiral chips were formed at the highest feed. With the 16° and 24° tools, only snarled chips were formed. With the coated tool loose arc and flat spiral, chips were formed at 0° and 8° , while snarled chips and flat spiral chips were formed at 16° and 24° .

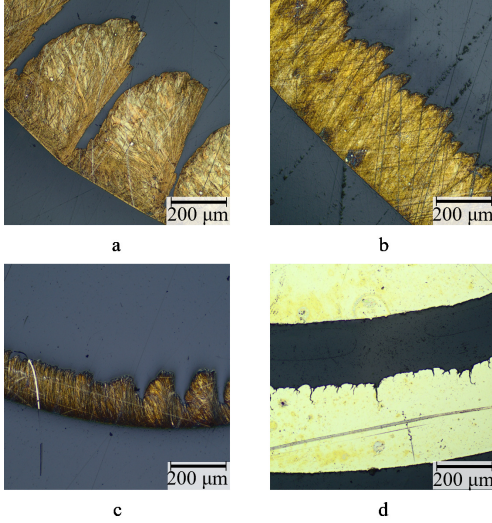


Fig. 5 Examples of different microscopic chip forms present in this study: a) segmented type, b) intermediate type, c) chip changing from segmented to intermediate type, d) continuous type.

Considering the chip shape visible in the microscope, the coated and uncoated 0° tool produced sawtooth-shaped chips. The 8° uncoated tool produced mixed chips, consisting of sawtooth and ribbon-like patterns, while the coated tool still produced sawtooth chips. Like the uncoated 8° tool, the uncoated 16° tool produced mixed type chips. The coated 16° tool produced ribbon chips. For the 24° tools, the uncoated one produced ribbon chips, while the coated tool produced mixed-type chips. Two parameters associated with chip formation are the chip thickness ratio and the degree of chip segmentation. The chip thickness ratio λ_h is the ratio between the chip thickness after the cut h' and the uncut chip thickness h . In radial cutting operations, the undeformed chip thickness h equals the feed f_n . The chip thickness was measured across multiple sections of different chips, and an average value was calculated. The chip thickness ratio was calculated from these results. A higher chip thickness ratio indicates a higher degree of deformation in the chip. This can be explained by increased friction in the secondary shear zone [7]. The degree of chip segmentation G_s indicates the ratio between the height of the

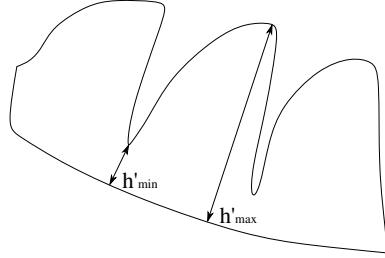


Fig. 6 Schematic drawing of a chip segment showing examples of the measurements of h'_{min} and h'_{max} .

peaks h'_{max} and valleys h'_{min} of a chip. Figure 6 shows schematically how h'_{max} and h'_{min} have been measured. The degree of chip segmentation can be calculated by the formula

$$G_s = \frac{h'_{max} - h'_{min}}{h'_{max}}. \quad (1)$$

The degree of chip segmentation can take values between 0 and 1. A degree of chip segmentation closer to 1 is associated with a more sawtooth-shaped chip, while a degree of chip segmentation closer to 0 is typically associated with a continuous ribbon chip. Additionally, a higher degree of chip segmentation will, like a higher chip thickness ratio, indicate higher chip deformation. Especially for the mixed-type chips, the degree of chip segmentation will highly depend on the chip segment analyzed.

Figure 7 gives an overview of measured chip thicknesses, the chip thickness ratio, and the degree of chip segmentation calculated from the chip thicknesses. The chip thickness ratio and degree of chip segmentation decreased when the rake angle increased. In the coated tools, the chip thickness ratio was slightly higher than in the corresponding uncoated tools, except for the 8° tool. The degree of chip segmentation was the highest for the coated 8° tool. Under the microscope, chips from this tool showed a sawtooth geometry with considerably low valleys, as indicated by h'_{min} in Figure 7, which led to those results. The otherwise higher chip thickness ratio in coated tools compared to uncoated tools could be explained by the higher roughness of the coated tools.

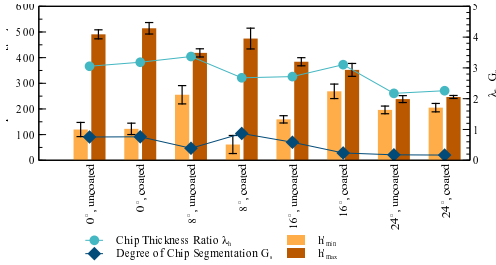


Fig. 7 Chip Thickness, Chip Thickness Ratio and Degree of Chip Segmentation for Tools with Varying Rake Angles and Coating Condition.

In summary, increased rake angles in cutting CW511L led to longer chips with a lower chip thickness ratio and lower chip segmentation. It seems like the coating increased the friction in the cutting zone slightly, in accordance with the results discussed earlier regarding the cutting forces. A higher rake angle induced less deformation into the chips, leading to continuous ribbon chips. Due to the tendency of ribbon chips to be longer, they are undesirable in automated cutting processes. To utilize the lower cutting forces generated by a higher rake angle, measures to counteract long chips must be investigated.

3.3.2 Impact of the Different Chip Breaking Geometries on the Chip Formation

Macroscopically, the chips produced in test series 2 had a similar appearance regardless of the tool used at feed levels of $f_n = 0.1$ and 0.15 mm/r. All chips are classified as flat spiral chips, varying slightly in size. At the lowest tested feed level of $f_n = 0.05$ mm/r, differences were more visible, as tools #1, #2, and #4 produced both long and short tubular chips and tool #3 only produced short tubular chips. These observations make tool #3 the most suitable for cutting CW511L at the given parameters and the lowest feed of $f_n = 0.05$ mm/r regarding the chip breakability. Like test series 1, chips from test series 2 were embedded, ground, and polished to analyze further in the microscope. Figure 8 shows the results of the chip thickness measurement, the calculated chip thickness ratio, and the degree of chip segmentation. The chip thickness ratio is around

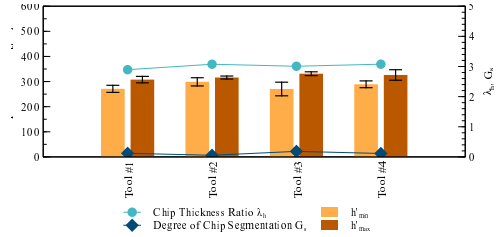


Fig. 8 Chip Thickness, Chip Thickness Ratio and Degree of Chip Segmentation for Tools with Varying Chip Breaking Geometries.

$\lambda_h = 3$ for all tools, being the lowest for tool #1 and the highest for tools #2 and #3. The differences are, however, too small to be significant. Overall, the degree of chip segmentation was low, around $G_s = 0.12$ for tool #1, 0.05 for tool #2, 0.18 for tool #3, and 0.11 for tool #4. All chips had a ribbon-like appearance in the microscope, which explains the low degree of chip segmentation. The chip segmentation in tool #3 was the highest, in good accordance with the macroscopically shortest chips in tool #3 discussed above.

High-speed videos were recorded and analyzed to further interpret the chip-breaking process in test series 2. Figure 9 shows an example picture of a recording. From the video clips, chip up-curl radii for all tools and tool-chip contact lengths for reference tool #4 were measured. For all tools, chip breakage usually occurs when the chip collides with the workpiece. Figure 10 gives an overview of the chip up-curl radii, and Table 5 displays the tool-chip contact lengths. Chip up-curl radii were the highest for reference tool #4, at around $r_{ch} = 5.0$ mm for $f_n = 0.05$ and 0.1 millim/r and around $r_{ch} = 4.6$ mm for a feed of $f_n = 0.16$ mm/r. Tool #3 showed overall the lowest up-curl radii. When cutting with tools #1 and #2, the chips flew over the chip-breaking geometry but did not follow the curvature completely. A gap was visible between the tool and chip at the chip-breaking geometry leading to less deformation by the chip-breaking geometry and higher chip up-curl radii. For tool #3, no such gap was visible. With reference-tool #4, the chip did not follow the tool's contour either. The chip, however, would usually hit the back wall. The natural tool-chip contact length was analyzed

Table 5 Tool-Chip Contact Lengths Measured with High-Speed Camera on Reference Tool#4.

Feed f_n [mm/rev]	Tool-chip contact length [mm]	Standard deviation [mm]
0.05	1.1	0.13
0.10	1.3	0.15
0.16	1.5	0.20

with tool #4 since the initial tool-chip contact length was not restricted or changed by the tool geometry in this tool. The tool-chip contact length increased with the feed and varied between 1.1 and 1.5 mm, as shown in Table 5. Considering these results and the measurements of the tool geometry, only tool #3 had a land width l shorter than the natural contact length. Accordingly, only tool #3 had a restricted contact length for all investigated feed levels, with $l = 0.7$ mm, and should therefore lead to the best results regarding chip breaking. A restricted contact length leads to the utilization of the whole chip-breaking geometry by the chip and leads to smaller up-curl radii and tighter chips as described in Jawahir and Fang [11]. The radius of the chip-breaking geometry of tool #3 was the largest of the three tools #1 – 3, measuring 3.5 mm. However, it was not small enough to efficiently deform the chips and led to significantly smaller up-curl radii and reasonably enhanced chip breakability. Yet, the chip up-curl radius was decreased in tool #3 compared to tools #1 and #2, as the chip-breaking geometry was utilized the best in this tool due to a restricted contact length. A chip-breaking geometry with an even smaller chip breaker land width and smaller groove radius than tool #3 might increase the chip breakability, especially at low feed levels. A decreased groove radius might improve chip breakability at higher feed levels. The chip up-curl radius seems to have a higher impact on the chip length and is more sensitive to the chip-breaking geometry. On the other hand, the chip thickness ratio is less impacted by the chip-breaking geometry and does not impact the chip length as much as the chip up-curl radius. Further research with adapted geometries is therefore needed to investigate this.

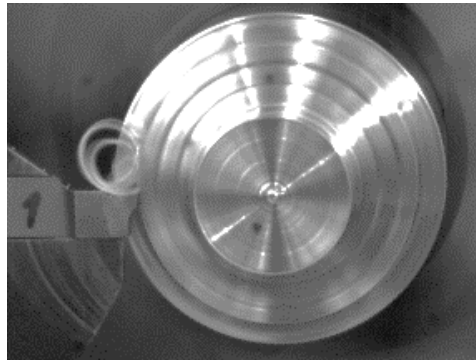


Fig. 9 Screenshot Taken from a Video with the High-Speed Camera of Cutting CW511L with Tool #1.

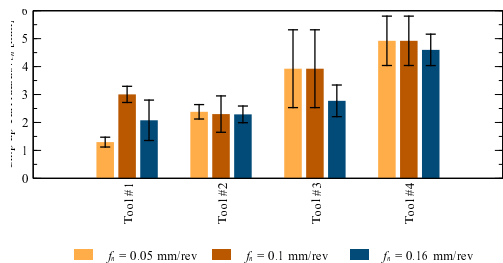


Fig. 10 Chip up-curl Radii for the Different Feeds Measured from the High-Speed Videos.

4 Conclusion

This study investigated the influence of the rake angle and different chip-breaking geometries on cutting forces and chip breakability in lead-free brass alloy CW511L. Cutting forces decreased significantly when increasing the rake angle from 0° to 24° . A TiAlN-based coating did not influence the cutting forces or force ratios remarkably. The chip-breaking geometry had a marginal impact on the measured cutting forces and force ratio. With increasing rake angles, the chip breakability decreased, leading to long and tangled chips. The chip thickness ratio and chip segmentation decreased, and the chips changed from sawtooth to ribbon chips as less deformation was applied to the chip by the tools with increased rake angles. If the lower cutting forces reachable by

a high positive rake angle are utilized in automated cutting, the use of chip-breaking geometries is advisable to reach better chip breakability. The chip-breaking geometries with varying chip breaker land widths and groove radii impacted the chip forms. The chip up-curl radii could be reduced to varying extents by the chip-breaking geometries which lead to higher deformation of the chip and enhanced chip breakability. Tool #3 performed best in this series of tests. However, the chip-breaking performance could be improved by decreasing the chip breaker land width, especially for higher feed levels, and decreasing the radius of the groove. The chip-breaking geometry should be designed considering the exact cutting parameters, as the feed will influence the tool-chip contact length, which will influence which chip breaker land width is efficient. An increased back wall could help to enhance chip breakability.

References

- [1] Estelle, A. A. Drinking water lead regulations: impact on the brass value chain. *Materials Science and Technology (United Kingdom)* **32**, 1763–1770 (2016). URL <https://doi.org/10.1080/02670836.2016.1220906>.
- [2] Nobel, C., Klocke, F., Lung, D. & Wolf, S. Machinability Enhancement of Lead-free Brass Alloys. *Procedia CIRP* **14**, 95–100 (2014). URL <https://doi.org/10.1016/j.procir.2014.03.018>.
- [3] Klocke, F., Nobel, C. & Veselovac, D. Influence of Tool Coating, Tool Material, and Cutting Speed on the Machinability of Low-Leaded Brass Alloys in Turning. *Materials and Manufacturing Processes* **31**, 1895–1903 (2016). URL <https://doi.org/10.1080/10426914.2015.1127944>.
- [4] Johansson, J. *et al.* On the function of lead (Pb) in machining brass alloys. *The International Journal of Advanced Manufacturing Technology* (2022). URL <https://doi.org/10.1007/s00170-022-09205-0>.
- [5] Saglam, H., Unsacar, F. & Yaldiz, S. Investigation of the effect of rake angle and approaching angle on main cutting force and tool tip temperature. *International Journal of Machine Tools and Manufacture* **46**, 132–141 (2006). URL <https://doi.org/10.1016/j.ijmachtools.2005.05.002>.
- [6] Duan, C. & Zhang, L. A reliable method for predicting serrated chip formation in high-speed cutting: analysis and experimental verification. *The International Journal of Advanced Manufacturing Technology* **64**, 1587–1597 (2013). URL <https://doi.org/10.1007/s00170-012-4125-0>.
- [7] Nobel, C., Hofmann, U., Klocke, F. & Veselovac, D. Experimental investigation of chip formation, flow, and breakage in free orthogonal cutting of copper-zinc alloys. *The International Journal of Advanced Manufacturing Technology* **84**, 1127–1140 (2015). URL <https://doi.org/10.1007/s00170-015-7749-z>.
- [8] Boothroyd, G. *Fundamentals of metal machining and machine tools* Vol. 28 (Crc Press, 1988).
- [9] Jawahir, I. Chip-forms, chip breakability and chip control. *CIRP Encyclopedia of Production Engineering; Laperrière, L., Reinhart, G., Eds* 178–194 (2014).
- [10] Jawahir, I. & Van Luttervelt, C. Recent developments in chip control research and applications. *CIRP annals* **42**, 659–693 (1993).
- [11] Jawahir, I. & Fang, X. A knowledge-based approach for designing effective grooved chip breakers—2d and 3d chip flow, chip curl and chip breaking. *The International Journal of Advanced Manufacturing Technology* **10**, 225–239 (1995).
- [12] Müller, M. S. & Sørby, K. The influence of the rake angle on the cutting of low-lead and lead-free brass alloys. *Manufacturing Driving Circular Economy. Proceedings of the 18th Global Conference on Sustainable Manufacturing, October 5-7, 2022, Berlin. Lecture Notes in Mechanical Engineering* (2023).
- [13] Müller, M. S. & Sørby, K. Investigation on chip breakability in lead-free brass alloy

cw5111 using different chip breaking geometries. *Intelligent Computation in Manufacturing Engineering - CIRP ICME'23*, (in press) *Procedia CIRP* (2023).

- [14] Albrecht, P. New Developments in the Theory of the Metal-Cutting Process: Part I. The Ploughing Process in Metal Cutting. *Journal of Engineering for Industry* **82**, 348–357 (1960). URL <https://doi.org/10.1115/1.3664242>.
- [15] Nobel, C., Hofmann, U., Klocke, F., Veselovac, D. & Puls, H. Application of a new, severe-condition friction test method to understand the machining characteristics of Cu–Zn alloys using coated cutting tools. *Wear* **344-345**, 58–68 (2015). URL <https://doi.org/10.1016/j.wear.2015.10.016>.

Statements and Declarations

Funding

Magdalena S. Müller and Knut Sørby received financial research support from the Research Council of Norway for support through the research project LOBUS – Low Lead Brass for Sustainable Community Development (RCN Project. No. 296054).

Competing Interests

The authors have no relevant financial or non-financial interests to disclose.

Author Contributions

All authors contributed to the study's conception and design. Material preparation, data collection, and analysis were performed by Magdalena S. Müller. The first draft of the manuscript was written by Magdalena S. Müller and all authors commented on previous versions of the manuscript. All authors read and approved the final manuscript.

ISBN 978-82-326-7666-8 (printed ver.)
ISBN 978-82-326-7665-1 (electronic ver.)
ISSN 1503-8181 (printed ver.)
ISSN 2703-8084 (online ver.)



NTNU

Norwegian University of
Science and Technology